



January 2012

Multiphysics Modeling And Simulation Process To Develop Thin Piezoelectric Film Sensors To Measure The Vibration Of Structures With Complex Shapes And Boundary Conditions.

Md. Razib Rahim

Follow this and additional works at: <https://commons.und.edu/theses>

Recommended Citation

Rahim, Md. Razib, "Multiphysics Modeling And Simulation Process To Develop Thin Piezoelectric Film Sensors To Measure The Vibration Of Structures With Complex Shapes And Boundary Conditions." (2012). *Theses and Dissertations*. 1371.
<https://commons.und.edu/theses/1371>

This Thesis is brought to you for free and open access by the Theses, Dissertations, and Senior Projects at UND Scholarly Commons. It has been accepted for inclusion in Theses and Dissertations by an authorized administrator of UND Scholarly Commons. For more information, please contact zeinebyousif@library.und.edu.

MULTIPHYSICS MODELING AND SIMULATION PROCESS TO DEVELOP THIN
PIEZOELECTRIC FILM SENSORS TO MEASURE THE VIBRATION OF
STRUCTURES WITH COMPLEX SHAPES AND BOUNDARY CONDITIONS.

by

Md. Razib Rahim

Bachelor of Science, Bangladesh University of Engineering & Technology, Bangladesh

A Thesis

Submitted to the Graduate Faculty

of the

University of North Dakota

in the fulfillment of the requirements

for the degree of

Master of Science in Mechanical Engineering

Grand Forks, North Dakota

December

2012

Copyright 2012 Md. Razib Rahim

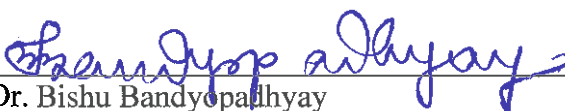
This thesis, submitted by Md. Razib Rahim in partial fulfillment of the requirements for the Degree of Master of Science from the University of North Dakota, has been read by the Faculty Advisory Committee under whom the work has been done and is hereby approved.



Dr. Marcellin Zahui, Chairperson

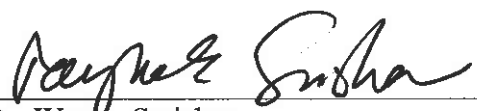


Dr. George Bibel

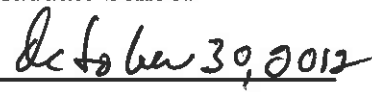


Dr. Bishu Bandyopadhyay

This thesis meets the standards for appearance, conforms to the style and format requirements of the Graduate School of the University of North Dakota, and is hereby approved.



Dr. Wayne Swisher
Dean of the Graduate School

10/30/2012 

Date

PERMISSION

Title Multiphysics Modeling and Simulation Process to Develop Thin
Piezoelectric Film Sensors to Measure the Vibration of Structures with
Complex Shapes and Boundary Conditions.

Department Mechanical Engineering

Degree Master of Science

In presenting this thesis in fulfillment of the requirements for a graduate degree from the University of North Dakota, I agree that the library of this University shall make it freely available for inspection. I further agree that permission for extensive copying for scholarly purposes may be granted by the professor who supervised my thesis work or, in his absence, by the chairperson of the department or the dean of the Graduate School. It is understood that any copying or publication or other use of this thesis or part thereof for financial gain shall not be allowed without my written permission. It is also understood that due recognition shall be given to me and to the University of North Dakota in any scholarly use which may be made of any material in my thesis.

Md. Razib Rahim

10/31/2012

TABLE OF CONTENTS

LIST OF FIGURES.....	vii
LIST OF TABLES.....	ix
ACKNOWLEDGEMENTS.....	x
ABSTRACT.....	xi
CHAPTER	
I. INTRODUCTION.....	1
II. LITERATURE REVIEW.....	7
III. INTRODUCTION TO MULTIPHYSICS MODELING METHODS AND ANSYS ELEMENTS USED.....	20
3.1 Multiphysics Modeling Methods.....	20
3.2 Direct Method Procedure.....	21
3.3 ANSYS Element Characteristics.....	22
3.4 Piezoelectric Elements.....	25
3.5 Contact Elements.....	32
3.6 Structural Elements.....	41
IV. ANALYSES FORMULATION.....	45
4.1 Piezoelectric Analysis.....	47
4.2 Mode Frequency Analysis.....	51
4.3 Spectrum Analysis.....	53

4.4 Harmonic Response Analysis.....	58
V. PVDF CONSTITUTIVE PROPERTY	66
5.1 Piezoelectricity.....	66
5.2 PolyVinylidene Fluoride (PVDF).....	69
5.3 PVDF Constitutive Matrices.....	73
VI. MULTIPHYSICS MODELING & SIMULATION AND EXPERIMENTAL RESULTS.....	75
6.1 ANSYS Parametric Design Language (APDL).....	76
6.2 Multiphysics Modeling.....	76
6.3 Contact Generation.....	80
6.4 Multiphysics Simulation.....	83
6.5 Graphs, Results & Figures.....	86
6.6 Experimental Setup, Procedures & Results.....	93
6.7 Conclusion & Future Scope.....	103
APPENDICES.....	104
APPENDIX A.....	105
APPENDIX B	143
APPENDIX C	164
REFERENCES.....	168

LIST OF FIGURES

Figure	Page
3.1: SOLID227 Element Geometry	26
3.2: PLANE223 Element Geometry	30
3.3: CONTA174 Element Geometry	32
3.4: TARGE170 Element Geometry	37
3.5: TARGE170 3D Segment Types	38
3.6: SHELL63 Element Geometry	41
3.7: Stress Output of SHELL63	43
4.1: Harmonic Frequency Response Plot	65
5.1: Structure of PVDF	69
6.1: Sensor Shape MATLAB Plot [Solid Line (Desired Shape) Star (Actual Shape)]	77
6.2: Keypoint Creation Using APDL Code	78
6.3: Line Plot Using APDL Code	78
6.4: Sensor Area Creation in ANSYS	78
6.5: 50 μ m Thick Sensor Volume	78
6.6: Meshed Sensor Volume	79
6.7: Meshed Aluminum Beam and Sensor Volume	80
6.8: Shell-Solid Bonded Contact Assembly	82
6.9: Cantilevered Aluminum Beam With Bonded Sensor	83
6.10: First Two Mode Shapes of the Bonded Structure	84

6.11: Frequency Response of Beam vs. Generic Sensor Output Charge	90
6.12: Frequency Response of Plate vs. Generic Sensor Output Charge	90
6.13: Frequency Response of Shell vs. Generic Sensor Output Charge	91
6.14: Frequency Response of Beam vs. Shaped Sensor Output Charge	91
6.15: Frequency Response of Plate vs. Shaped Sensor Output Charge	92
6.16: Frequency Response of Shell vs. Shaped Sensor Output Charge	92
6.17: Side View of the Cantilevered Beam Setup	93
6.18: The Experimental Setup for the Beam with Sensor on Top	94
6.19: The Experimental Setup for the All End Fixed Plate	95
6.20: Top View of the Experimental Setup of the Cantilevered Pipe	95
6.21: The Experimental Setup for the Pipe with Sensor on Top	96
6.22: The Block Diagram for Getting the Results with Accelerometer	98
6.23: The Block Diagram for Getting the Results with PVDF	99
6.24: Accelerometer Reading for the Cantilevered Beam with Sensor on Top	101
6.25: PVDF Reading for the Cantilevered Beam with Sensor Bonded on Top	101
6.26: Accelerometer Reading for the Cantilevered Shell with Sensor on Top	102
6.27: PVDF Reading for the Cantilevered Shell with Sensor Bonded on Top	102

LIST OF TABLES

Table	Page
3.1: Coupling Methods in Direct Method Approach	22
3.2: Coupled Degree of Freedom Set	27
3.3: SOLID227 Material Properties	28
3.4 Coupled Degree of Freedom Set	31
3.5: PLANE223 Material Properties	31
3.6: Real Constants for CONTA174	34
3.7: KEYOPT Options for CONTA174 Element	35
3.8: TARGET170 KEYOPT Options	40
3.9: SHELL63 Real Constants	42
3.10: KEYOPT Options for SHELL63	43
4.1: ANSYS Elements for Piezoelectric Analysis	47
5.1: Physical Constants for the PVDF Film	73
6.1: Geometrical and Material Properties for Aluminum Beam	79
6.2: The Value of the first 6 Modes in ANSYS	84

ACKNOWLEDGEMENTS

This work would not have been possible without the support from my advisor Dr. Zahui. With the direction provided by Dr. Zahui, I learned a great deal about FEA, Vibrations and Active Noise Control. I am deeply indebted to my advisory committee for their confidence, tolerance and support during last two years. I would also like to thank the Mechanical Engineering Department at the University of North Dakota for providing the space and means to complete this research. Finally, I would like to thank my family members and friends for their support during this project. Their understanding and support has been a great placate.

ABSTRACT

Piezoelectricity was discovered in 1880 by Jacques and Pierre Curie. Its application has since been extended to actuators and sensors, widely used in industry, automotive, and aerospace applications. The last two decades have seen intensive research in piezoelectric theory in an effort to effectively capture and control the distinctive coupling of electricity and elasticity. However, due to the complexity of the theory involved, finite element and numerical methods are often used in the process. Limited analytical exact solutions are also found in literature. The objective of this work is to devise a multiphysics modeling and simulation process to develop thin piezoelectric film sensors to measure the vibration of structures with complex shapes and boundary conditions. First, the output charge of generic piezoelectric films, respectively attached to a beam and a plate, is modeled using ANSYS and experimentally verified. Second, the modeling method is extended to a cylindrical shell followed by experimental verifications. Appropriate material properties obtained from past researches were incorporated as required. Finally, shaped sensors for the measurement of specific dynamic characteristics of a beam, plate and cylindrical shell respectively, are developed and experimentally validated. The results show that Multiphysics modeling can be an efficient design tool and be effectively used to simulate complex systems. This tool can be also used to detect or simulate design flaws and errors.

CHAPTER I

INTRODUCTION

The objective of this work is to devise a multiphysics modeling and simulation process to develop thin piezoelectric film sensors to measure the vibration of structures with complex shapes such as beam, plate and cylindrical pipe with various boundary conditions. First, the output charge of generic piezoelectric films, respectively attached to a beam and a plate, is modeled using ANSYS and experimentally verified. Second, the modeling method is extended to a cylindrical shell followed by experimental verifications. Finally, shaped sensors for the measurement of specific dynamic characteristics of a beam, plate and cylindrical shell respectively, are developed and experimentally validated. A powerful finite element tool, ANSYS is used for the multiphysics modeling and simulation in this research work. At first the models of the structures were created with specific dimensions and were meshed. The sensors were introduced afterwards and placed on the top surfaces of the structures and were also meshed. Two types of polyvinylidene fluoride (PVDF) sensors were used: generic and shaped film. The generic film one covered the whole top surface of the structures and the shaped one had a parabolic shape. Power spectrum analysis was performed to determine the response of the beam and the sensor and the analysis seemed pretty consistent with each other. The results of ANSYS were taken into Matlab for further processing. It was

noted from the results that the values were very congruous to each other. The results were also validated theoretically and experimentally in the lab. Some of the most important things which are really crucial for our research are discussed in the later portion of this chapter.

PVDF which has been very famous among all the piezoelectric polymers these days due to its exclusive characteristics has played an important role in our research. It is a new generation of so-called “smart” materials that has emerged to detect changes in the loading or environmental conditions, can select rationally among a set of respective responses, as a result can also carry out these actions in a controlled manner. A broad range of applications utilizing such functions includes active vibration damping, acoustic suppression, damage detection, position and shape control of compliant structures, and self-inspection of structural integrity. As an integral part of the “smart” materials group, PVDF exhibit a type of behavior that is often compared with biological reactions involving transformations of the sensed information into the desired response [1]. Due to such special qualities, PVDF have been increasingly used in a rapidly expanding range of applications such as electromechanical transducers, position sensors and vibration control actuators. Many synthetic polymers, including polypropylene, polystyrene and poly(methyl methacrylate); semi-crystalline polyamides and amorphous polymers such as vinyl acetate have also demonstrated piezoelectric properties. However, piezoelectric effects in these materials are relatively weak, often unstable and, therefore, are of limited

practical significance. Strong and stable piezoelectric properties have only been observed in the synthetic polymer PVDF or PVF2 and PVDF copolymers [1]. It has become popular in recent years because some of its unique advantages such as: i) Flexibility (possibility of application on non-level surfaces), ii) High mechanical strength, iii) Dimensional stability, iv) Balanced piezoelectric activity in the plane of the film, v) High and stable piezoelectric coefficients over time up to approximately 90°C, vi) Characteristic chemical inertness, vii) Continuous polarization for great length spooled onto drums, viii) Thickness between 9 μ m and 1mm [1], ix) Acoustic impedance close to that of water with a flat response curve etc. A thin layer of nickel, copper or aluminum is deposited on both surfaces of the material in order to provide electrical conductivity for applying an electrical field, on the other hand to allow measurements of the charge induced by mechanical deformations.

The piezoelectric material described above was used in this work to model vibration sensors using Multiphysics methods. Multiphysics treats simulations that involve multiple physical models or multiple simultaneous physical phenomena. Multiphysics analysis is a combination of analyses from various fields of sciences and engineering. For example, mixing chemical kinetics and fluid mechanics or combining finite elements with molecular dynamics. It usually involves solving coupled systems of partial differential equations. Almost any physical simulation involves coupled systems, like electric and magnetic fields for electromagnetism or pressure and velocity for sound. Another situation is the mean field approximation for the electronic structure of atoms, where the electric field and the electron wave functions are fused. There are lots of

different commercially available software packages for simulating multiphysics models. These software packages mainly depend on the Finite Element Method or similar commonplace numerical methods for simulating coupled physics: thermal stress, electromechanical interaction, fluid structure interaction (FSI), fluid flow with heat transport and chemical reactions, electromagnetic fluids (magnetohydrodynamics or plasma), electromagnetically induced heating. In many cases, to get accurate results, it is momentous to include mutual dependencies where the material properties significant for one field (such as the electric field) vary with the value of another field (such as temperature) and vice versa. Multiphysics analysis is a powerful approach that is becoming easier to use due to recent progress in desktop computing. Improved software environment makes it possible to model and simulate complex systems. Almost every kind of design industries like automobile, airplane, piping etc. uses such software for their versatility of solving problems. However the application of this technique is still in its infancy. The work presented here is using finite element to simulate the response of PolyVinylidene Fluoride (PVDF) film bonded to vibrating beam, plate or cylindrical shell. This is a coupled fields' analysis, in which the output of the electric field depends on the output of the mechanical field.

The simulation process is based on the use of PSD. In statistical signal processing and physics, PSD is a positive real function of a frequency variable affiliated with a stationary stochastic process, or a deterministic function of time, which has dimensions of power per hertz (Hz). It is often called simply the spectrum of the signal. Intuitively, the spectral density measures the frequency content of a stochastic process and helps analyze

periodicities. In physics, the signal is usually a wave, such as an electromagnetic wave, random vibration, or an acoustic wave. The spectral density of the wave, when multiplied by an appropriate factor, will give the power carried by the wave, per unit frequency, known as the power PSD of the signal. It displays the strength of the variations as a function of frequency. In other words, it exhibits at which frequencies variations are strong and at which frequencies variations are weak. It is possible to obtain energy within a specific frequency range by integrating PSD within that frequency range. It describes how the power of a signal or time series is distributed with frequency. Here power can be the actual physical power, or more often, for convenience with abstract signals, can be defined as the squared value of the signal, that is, as the real power dissipated in a purely resistive load if the signal were a voltage applied across it. The power spectral density of a signal abides if the signal is a wide-sense stationary process. If the signal is not wide-sense stationary, subsequently the autocorrelation function must be a function of two variables. It is a very useful tool to identify oscillatory signals in the time series data and to determine the amplitude. It is still useful even if data do not contain any purely oscillatory signals. In some cases, such as wide-sense cyclostationary processes, a PSD may still exist. More generally, similar techniques may be used to approximate a time-varying spectral density. If two signals both obtains power spectra (the correct terminology), then a cross-power spectrum can be calculated by using their cross-correlation function. Computation of PSD is carried out directly by the method called FFT or computing autocorrelation function and then transforming it. Most of the time it is computed and plotted to get a "feel" of data at an early stage of time series analysis. Looking at PSD is like looking at simple time series plot except the time series as a

function of frequency instead of time. Frequency is a transformation of time and looking at variations in frequency domain is just another way to see at variations of time series data.

The following chapters discuss in detail the modeling process and results. Chapter II of this dissertation introduces the literature review. Chapter III describes Multiphysics Modeling and Analysis methods. Also, ANSYS elements used in this research work are presented. ANSYS analysis procedures and formulations are presented in Chapter IV of this dissertation and followed by the detailed PVDF piezoelectricity in Chapter V. In Chapter VI, the shaped PVDF sensor bonded on aluminum beam, plate and cylindrical pipe is modeled and simulated using ANSYS. A random excitation force is applied to the structure and the finite element output voltage of the piezoelectric film and the nodal displacements of the structure are exported to MATLAB[®] for additional analysis as stated above. Finally, the displacement of the structure is calculated and compared to the output voltage of the PVDF. This work shows that multiphysics modeling can be effectively used. Finally the modeling and results of a beam, plate and cylindrical pipe with bonded PVDF film are presented.

CHAPTER II

LITERATURE REVIEW

There are plenty of different researches going on based on PVDF sensors. Some of them are described briefly here. Probe with PVDF sensor can be made for energy measurements of Optical Radiation. In 1969, Kawai [4] discovered strong piezoelectricity in such polymers as polyvinylidene fluoride (PVDF). This material also shows substantial pyroelectric properties. The first pyroelectric films were commercially available in 1981. The adoption of polyvinylidene fluoride films (PVDF) as pyroelectric sensors for oscillated or chopped optical radiation has been repeatedly reported during the last two decades. The main advantages of PVDF sensors are large integrating area, low thermal mass and very low cost. The growth of low-cost pyroelectric polymer sensors has gained a great deal of interest due to the large number of applications.

Robotic tactile sensor can be also fabricated from piezoelectric PVDF films. Traditionally, robots are used in very controlled and defined environments. However, in future military and industrial applications, robots "should be able to adapt to any work environment because it is often not practical to adapt the environment to them". The two most important senses a robot should possess are vision and touch. In fact, developing the tactile sense for robots is one of NASA's highest priorities. Several approaches have been

investigated to implement tactile sensing. Among these is a tactile sensor based on the piezoelectric effect observed in poled PVDF. Capt Pirolo [5] investigated the response of several sensor array electrode configurations fabricated from PVDF film. This work can be extended by reducing the overall size of the sensor arrays to approximate that of the adult fingertip, enhancing the sensor's spatial resolution, and increasing the sensor's sensitivity by integrating the PVDF film with the gate electrode contact of a metal-oxide-semiconductor field effect transistor (MOSFET).

PVDF films has been used as sensors for the experimental modal analysis of structures. Piezoelectric materials have attracted much research such as on active structural vibration and acoustic control. The rectangular shape of a PVDF film was introduced by Hubbard (1987) [6] for the application to vibration control of beam structures as the sensor. Lee and Moon (1990) [6] and Collins et al (1992) [6] developed a special shape of PVDF film to sense the specific vibration modal response as known modal sensors. Galea et al (1993) [6] applied the PVDF film as sensor to structural fault diagnosis and health monitoring. Collet and Jezequel (1994) [6] and Tanaka et al (1996) [6] utilized similar configurations of PVDF film as modal filters for vibration control.

A PVDF sensor with printed electrodes has been made for normal and shear stress measurements on sole [7]. Test has been done to find a method of printing electrodes on the unmetalled PVDF material to construct a matrix version of a sensor for normal and shear stress measurements on sole. A commercial PVDF material with silver ink metallization has previously been used to synthesize a single sensor prototype. With the

metal-coated PVDF material, a matrix sensor is challenging to construct; the metallization should be expunged from the certain areas of the material to form an electrode grid pattern or a number of tantamount separate sensors should be cut off from the material sheet. Hence, a new method is explored. The sensor is manufactured from unmetalled PVDF material and an array of electrodes with coveted size and shape is printed on the material surface. The study concentrates on the characteristics of single sensors manufactured with the method. Based on the results, the subtlety seems to be decreased due to the thermal stress caused by the electrode printing process. In the normal force direction the sensor sensitivity was found to be about fifth and in shear force directions about tenth of the conforming values measured with the sensor with commercial electrodes. The sensitivity, however, is still adequate for stress measurements on sole.

Low Cost PVDF Sensor Casing has been made for Ultrasound Power Measurement [8]. Ultrasound machine is extensively used in industrial and medical institutions as one of its capability to visualize the image inside the object non-invasively. In the medical sector, any over access of ultrasound wave can account heating which may be harmful to the human skin. In order to avoid the unwanted power exposed to human, ultrasound power meter is required. The existing ultrasound power meter, however is high cost, heavy and only for therapy machine. Since few years ago, polymer sensor (PVDF) has been traversed to be a potential candidate for ultrasound sensor. This sensor has excellent bandwidth and acoustic coupling. In order to empower the PVDF sensor for low cost ultrasound power meter, a robust low cost casing has been developed. The casing has

been designed to endow the optimum capturing ultrasound power from therapeutic and diagnostic ultrasound machine, minimize interference effect and noise as well as poise mechanical construction of sensor. Test result shows unobjectionable correlation between ultrasound intensity and sensor's generated voltage. Hence, the design can be calibrated and collaborated with processing devices in order to complete the low cost ultrasound power measurement system. Ultrasound is one of the most prominent and productive non-invasive therapeutic and diagnostic modality. The most frequencies used for the diagnostic and therapeutic propositions are about 1-10 MHz. Higher frequency of the ultrasound will give pleasant resolution of image. However, high frequency and high power ultrasound may cause injurious to the human soft tissues but it is not as peril as magnetic resonance imaging (MRI) and Computed Tomography (CT). PVDF is a thin film that is strong and tough as reflected by its tensile properties and impact strength. Some advantages of the PVDF are staunch to UV and the effect of weather, low smoke generation, also excellent transmittance of solar energy, excellent dielectric strength, high heat resistance and sterling physical and mechanical properties for a fluoropolymer. However, peppy casing of PVDF sensor for well functioned ultrasound application is not yet well defined. In order to enable the exertion of PVDF sensor for ultrasound power measurement, a sturdy casing has been designed and implemented using low cost material. The casing is built from plastic material. There are two PVDF film attached inside the tank-type casing. The size of the casing can be assorted and depends on the size of therapeutic or diagnostic ultrasound probe. The work was also to scout a low cost appropriate material that can absorb the ultrasound wave. This material or absorber is salient to reduce the reflection of ultrasound wave inside the receiver. In order to rebate

the current leakage and protect the signal from external noise, a special connector between sensor and electronic circuit also fostered. For testing purpose, 1 MHz frequency from ultrasound therapy machine was used. The ultrasound probe area is 5 cm². De-gassed water was used as ultrasound wave propagation medium.

Investigation of the Transient Behavior of a Cantilever Beam has been done using PVDF sensors [9]. A PVDF film sensor was used to stroke the transient responses of a cantilever beam subjected to an impact loading. The measurement capability of a PVDF sensor was affected by the area of the PVDF film sensor and the signal conditioner (charge amplifier). The influences of these effects on the experimental measurements were investigated. The transient responses for the dynamic strain of the beam were squared simultaneously by the PVDF sensor and a conventional strain gauge. The resonant frequencies of the beam were determined by applying the Fast Fourier Transform on ephemeral results in the time domain of the PVDF sensor and the strain gauge. The experimentally reckoned resonant frequencies from the PVDF sensor and the strain gauge were compared with those predicted from theoretical and FEM numerical calculations. Based on the comparison of the results measured for these two sensors, the PVDF film sensor proved capable of measuring transient responses for dynamic strain, and its sensitivity was better than that of the strain gauge. Furthermore, almost all the resonant frequencies can be salvaged from the results of transient responses for PVDF film.

PVDF Strain Sensors has been used for Health Monitoring of Bonded Composite Patches to detect the damage [10]. These sensors offer the leverage of requiring no power to

function and the sensors may be manufactured to suit any size and geometry. PVDF sensors were bonded to a specimen representative of the F-111 wing pivot fitting doubler and substantiated under hot/wet conditions for a series of load cases. The output of the PVDF sensors was espied to vary linearly with applied load but a dependence on loading frequency was observed. Damage growth within the specimen was detected by PVDF sensors. Identical trends in damage growth were observed by the sensor. The environmental durability of the PVDF sensors was found to be very good, although care needed to be taken whilst fondling the sensors to avoid physically damaging them. For economic reasons there is a rampant trend to operate military aircraft well past their original design life. However, this results in a rapidly supplementing number of airframe structural defects and gives rise to the urgent need for cost effective, efficient repair procedures. This situation is extremely relevant to the RAAF where many aircraft types, such as the F-111, P3C, Macchi and the F/A-18 will have surmounted their design life well before they can be replaced. The application of bonded composite patches to repair or prop up defective metallic structures is becoming recognized as a very effective and versatile procedure for many types of problems. The goal for very demanding repair applications is to incorporate sensors, actuators and electronics in repair systems - smart repair systems - to monitor and report on the health of the overhaul and the repaired structure, as well as to actuate in order to preclude damage or failure of the repaired structure. Current research in this area is mainly pinpointed on developing on-line health monitoring techniques for safety-critical bonded repairs. This will allow the operator to move away from costly time-based maintenance procedures toward real-time health condition counseling of the bonded repair and the repaired structure and will allow timely

decisions on preventative and registered maintenance before failure of the repair or repaired structure. Sensors used for the health monitoring of bonded patches need to be robust, resistant to the service environment, accurate and reliable. It is also enticing to have sensors which require low operating power levels especially when used with 'stand-alone' in-situ data acquisition instrumentation. Piezoelectric polymer sensors, such as PVDF has been used to fulfill the purpose. These types of sensors produce a voltage, due to the piezoelectric effect, when stretched or compressed, and therefore require no power to operate. the use of PVDF sensors to measure the health of a bonded repair representative of the F-111 doubler under manifold loading conditions in a hot/wet environment. An peerless correlation was found between the conventional electrical resistance strain gauges and the PVDF sensors, indicating the materiality of the PVDF sensors for patch health monitoring. By percolating continuously and reliably in extreme hot/wet environments these sensors exhibited excellent durability. However, further work is required to revamp sensor bonding techniques and improve sensor robustness in order to reduce the risk of physical damage.

Fabricated PVDF Acoustic Emission Sensors are used for Lubricated Bearing Monitoring [11]. A fabricated Acoustic Emission (AE) sensor using PVDF film and its application for lubricated bearing monitoring on a rotodynamic machine has been found. The advantages of a PVDF sensor are not only flexibility in terms of complex shapes but also low acoustic impedance leading to efficient energy coupling and broad frequency range. The calibrated resonance frequency of the sensor is 38 kHz using an artificial AE source (number E976-84) obtained from American Standard Testing Materials (ASTM). The

experiment on a rotodynamic test rig at different machine conditions showed that the fabricated AE sensor can identify different machine operating conditions. Therefore, the fabricated AE sensor offers a potential alternative as a non-destructive monitor lubricated bearings. AE is typically a transient elastic wave generated by sudden released energy in materials under stress. Such AE can be naturally generated by, for example, mechanical stress, pressurization, acoustic fields, etc. Recently, the use of AE has been of much interest for its potential in material testing processes. It may be particularly useful in Non-Destructive Testing (NDT) in which damage zones could be easily detected through fabricated AE sensors without damaging the tested materials. NDT consequently offers not only real time monitoring and overall structural performance checking but also a low cost process. Generally, frequency ranges of AE lie between 20 kHz to 1.2 MHz. The sensor is the equipment which is used for detection and monitoring of the AE signal. Practically, the AE sensors used in NDT utilize piezoelectric materials as a transducer with high sensitivity and a low response time. Conventional AE sensors are generally fabricated using lead zirconate titanate (PZT), a ceramic type of piezoelectric material. Although the use of PZT has shown excellent detection performance, the PZT, is physically hard and brittle. Therefore the AE sensors are not only difficult to produce in various complex shapes but also vulnerable to mechanical vibrations. In addition, the relatively high acoustic impedance of the PZT may result in a coupling mismatch leading to inefficient energy coupling. Recently, PVDF films were introduced as an alternative piezoelectric material for some applications. Unlike the existing PZT materials, PVDF films offer not only flexibility in terms of complex shapes but also low acoustic

impedance leading to efficient energy coupling without the mismatch problem. Moreover, PVDF films have a frequency response in the region of the AE signal.

Biometric Identification can be done from a Floor Based PVDF Sensor Array Using Hidden Markov Models [12]. Biometrics is a cognate field in a world of growing terrorist threats and security concerns. A floor based sensor array has been assayed as a biometric identification system. The sensor array is engrossed of strips of laminate PVDF piezoelectric material. The sensor strips are partaken by an analog to digital converter and the data is processed with Matlab. A subset of each person's footfall data was encapsulated by a characteristic hidden Markov model (HMM). To discriminate different between people, each remaining single footfall was cast into an idiosyncratic HMM. The resulting solitary models were compared to the characteristic models. Over our entire population of training data, a false positive rate of approximately 20% was achieved alongside a false negative rate of 18%. Additionally, the sensor mien was studied in an effort to relate piezoelectric signal to footfall force through strain rate. Biometric-based identification systems are of increasing importance in combating identity theft and terrorism. In particular, there is a need for unobtrusive biometric systems in high volume applications such as airport screening. A number of different biometric features have been investigated for identification, including fingerprint, voice, iris, face, and gait. Footprint-based biometric systems have, in contrast, received less attention. However, footprints are easily collected and have been shown to be capable of biometric identification. Existing footprint-based sensor systems make use of a commercial pressure-sensing mat, an optical fiber grid, a resistive grid similar to a computer

keyboard, load cells, and binary pressure sensors. These systems vary in cost, accuracy and complexity. A number of signal processing algorithms have also been investigated in footprint-based systems, such as feature identification (such as stride length and the separation between heel and toe strike), Markov Chain Monte Carlo method, and Hidden Markov Models (HMM). This system uses piezoelectric materials as sensors in the form of PVDF laminate. An advantage of this approach is that once configuration is determined, the sensor array could be printed onto large polymer sheets making this system readily scalable to large area applications. Low-frequency sampling (<50 Hz) reduces the burden on the analog to digital (A/D) conversion system. The system only requires that a compliant surface be installed as a flooring material; this surface does not need to reveal itself as a sensor, thus facilitating covert collection of data.

Film-type sensor materials has been introduced in measurement of physiological force and pressure variables. Measurement of physiological signals divulges valuable information on the physiological state of a patient [13]. New and unobtrusive ways to tailor physiological force and pressure variables with film-type sensor materials are explored. The measured variables are divided into two application areas; the first is related to cardiopulmonary variables while the second one is intensified on plantar pressure mapping. In the area of cardiopulmonary variables, the measurement of heart and respiration rates and heart sounds are studied. Pressure mapping, instead, procures information on the interface pressure distribution between a person and the surface the person is on. The plantar pressure distribution between a foot and ground or shoe is measured to find out regions of the plantar area where the pressure has lofty

values. The high pressure values are linked with pressure ulcers. The semicrystalline PVDF material has solid structure which generate a charge when they are mechanically deformed. With normal measurement arrangement, PVDF is not suitable for static measurements and only the change of an external force can be measured. Hence, the sensors made of these materials are propitious especially in the measurements of physiological pulsatile signals. The sensors are constructed manually from commercial film materials. The entire measurement process is considered; from the design and construction of the sensors and measurement devices to the analysis of the measured data with Matlab® software. In the measurements of cardiopulmonary variables, the sensor attachments are disparaged and the measurement systems are designed to be unobtrusive and comfortable for the user. The sensors utilizing the PVDF materials can be integrated into clothing or into daily life objects (e.g. a chair or a bed) to measure vital signals. This suggests that the sensor materials are suitable for such measurements even though some differences between the results obtained with the materials were found. In the area of the plantar pressure measurements, instead, a new sensor prototype for pressure measurements during gait is introduced. The developed sensor utilizes fiscal PVDF material with silver ink metallization and it simultaneously measures both normal and shear stresses. Also, a sensor predicated on unmetallized PVDF material with printed electrodes is tested. Based on the promising results obtained with these sensor prototypes, the aim is to further mellow a matrix version of the sensor for on-floor and also in-shoe plantar pressure measurements.

A piezoelectric tactile sensor with three sensing elements for robotic, endoscopic and prosthetic applications has been made [14]. A prototype tactile sensing system with only three sensing elements has been reported. The magnitude and position of the applied force is hoarded by utilizing triangulation approach combined with membrane stress. Some information about the shape of the contacted object is obtained. The PVDF sensor is designed to overcome the problems of cross talk between sensing elements and to slash the complexity associated with some PVDF tactile sensors arranged in matrix form. A theoretical analysis of the sensor is parented and compared with experimental results. The limitation of the sensor is also reported. The sensor in miniaturized form can also be integrated into an endoscopic grasper and a prosthetic finger.

Amplitude and phase of photo thermal signal in a leaf of plant “schefflera arboricola” has been measured by PVDF sensor [15]. Recently, research on photosynthesis of a plant is becoming very important one from serious problems of CO₂ increment, and food depletion crisis. This research is also very interesting one to sonic and ultrasonic investigators. Phenomena of photosynthesis must be analyzed from two aspects which are a microscopic view point and a macroscopic one. In microscopic research interaction of photon, phonon and electron in plant organization plays fundamental and important roles. On the other hand, introduction to concept of a complex system with dispersive structure may be important from a viewpoint of macroscopic approach. Studied has been done about thermal radiation for a thermal damage protection in process of photo-synthesis of plant “schefflera arboricola (hereafter called kapok)” using PVDF sensor when light of dye laser with selected wave length is irradiated locally on various positions at top of a

leaf. results of amplitude and phase of photo thermal signal (hereafter called PT signal)
from top or back of a leaf measured by PVDF sensor has been found.

CHAPTER III
INTRODUCTION TO MULTIPHYSICS MODELING METHODS AND
ANSYS ELEMENTS USED

One of the exciting areas of technology to emerge in recent years is MEMS (micro electromechanical systems) where the engineers design and build systems with physical dimension of microns. This new technology is a powerful tool because virtually all MEMS devices involve the coupling of multiple physics phenomenon, known as multiphysics. This chapter presents the finite element methods for the multiphysics analysis, elements involved which are referred in multiphysics analysis and simulation using ANSYS, a powerful finite element tool.

3.1 MULTIPHYSICS MODELING METHODS

Multiphysics modeling is a powerful approach that is becoming easier to use due to recent progress in desktop computing [16]. A multiphysics modeling is a combination of modeling from different engineering disciplines which interact to solve a global engineering problem. It is used to model and analyze complex system simulations such as active noise control systems. It is also called coupled physics analysis in which input of one field analysis depends on another analysis. The coupling between the fields can be accomplished by either matrix coupling or load vector coupling. Load transfer can take place across surfaces or volumes according to the application. Coupling across the fields

can be complicated because different fields will be running different type of analyses during the simulation. A piezoelectric analysis, for example, handles the interaction between structural and electric fields. The multiphysics analysis is specified in two distinct methods in ANSYS as “sequential method” and “direct method”. In this research direct method has been used. ANSYS also supports “reduced order modeling” and “Coupled Physics Circuit Simulation” as other miscellaneous analysis methods in multiphysics environment.

3.2 DIRECT METHOD PROCEDURE

Direct coupling is advantageous when the coupled-field interaction is highly nonlinear and is best solved in a single solution using a coupled element formulation. Examples of direct coupling include piezoelectric analysis using the PLANE223, SOLID226, or SOLID227 elements and circuit-electromagnetic analysis. Elements are specifically formulated to solve these coupled-field interactions directly. It involves just one analysis that uses a coupled-field element type containing all necessary degrees of freedom. Coupling is accomplished by calculating element matrices or element load vectors that contain all necessary terms. Coupling methods used in direct coupled field analyses are listed in Table 3.1.

Table 3.1: Coupling Methods in Direct Method Approach

Type of analysis	Coupling method	Application
Thermal-structural	Load vector	Gas Turbines
Magneto-structural	Load vector	Solenoids, Electromagnetic machines
Electro-magnetic	Matrix	Actuators
Electro-magnetic-thermal	Matrix	Induction heating, RF heating
Piezoelectric	Matrix with contact	Microphones, Sensors
Thermal-pressure	Matrix and load vector	Pressure Vessels
Pressure-structural	Matrix	Acoustics
Electrostatic-structural Analysis	Matrix / Contact	Micro-electromechanical (MEMS).

3.3 ANSYS ELEMENT CHARACTERISTICS

3.3.1 Element type

ANSYS element library consists of more than 100 different element formulations or types [17]. An element type is identified by a group name and a unique identifying number. Types of the elements involved in this simulation are piezoelectric elements, contact pair elements and structural elements as described later in this chapter.

3.3.2 Element REAL constants

Data which are required for the calculation of the element matrix, but which cannot be determined from the node locations or material properties, are input as “real constants”. Typical real constants include geometric properties e.g. area, thickness, inner diameter, outer diameter, etc. Element real constants are properties that depend on the element type.

3.3.3 Element KEYOPT options

KEYOPT are the key options or switches which are used to turn various element options on or off. These options include stiffness formulation choices, printout control and

element coordinate system choices etc. KEYOPTS are identified by number such as KEYOPT (1), KEYOPT (2), etc., with each KEYOPT able to be set to a specific value. Values for the first six KEYOPT (1) through KEYOPT (6) may be input with the **ET** or **KEYOPT** commands. Values for KEYOPT (7) or greater on any element are input with the **KEYOPT** command. The defaults for element key options are chosen to be most convenient for the ANSYS product in use, which means that some of the defaults may be different in some of the ANSYS products. These cases are clearly documented under the “Product Restrictions” section of the affected elements.

3.3.4 Element Degrees of freedom

Each element type has a degree of freedom set, which constitute the primary nodal unknowns to be determined by the analysis. They may be displacements, rotations, temperatures, pressures, voltages, etc. Derived results, such as stresses, heat flows, etc., are computed from these degree of freedom results. Degrees of freedom are not defined on the nodes explicitly, but rather are implied by the element types attached to them. Therefore the choice of element type is important in any analysis.

3.3.5 Element special features

“Special Features” list indicate that certain additional capabilities are available for the element. Most often these features make the element nonlinear and require that an iterative solution be done. The special features include plasticity, creep, swelling, large deflection, stress stiffening, adaptive descent, birth and death, hyper elasticity and viscoelasticity.

Plasticity is a nonconservative, path-dependent phenomenon i.e. the sequence in which loads are applied and in which plastic responses occur affects the final solution results.

Creep is a rate dependent material nonlinearity in which the material continues to deform under a constant load. **Swelling** is behavior in which certain materials respond to neutron flux by enlarging volumetrically. **Stress stiffening** occurs when the out-of-plane stiffness of a structure can be significantly affected by the state of in-plane stress in that structure and this coupling between in-plane stress and transverse stiffness is known as **stress stiffening**, assumes that both strains and rotations are small. If material is added to or removed from a system, certain elements in model may become “existent” or “nonexistent”. In such cases, element **birth and death** options can be employed to deactivate or reactivate selected elements, respectively. **Large strain or large deflection** assumes that the finite strains, deflections and rotations may be arbitrarily large. **Hyperelasticity** refers to materials which can experience large elastic strain that is recoverable. A material is said to be **viscoelastic** if the material has an elastic (recoverable) part as well as a viscous (nonrecoverable) part. **Adaptive descent** is a technique which switches to a “stiffer” matrix if convergence difficulties are encountered, and switches back to the full tangent as the solution converges, resulting in the desired rapid convergence rate

3.3.6 Element material properties

Various material properties are used for each element type. Typical material properties include Young's modulus, density, coefficient of thermal expansion, thermal conductivity, etc. The material properties are selected according to the analysis type chosen. Properties such as stress-strain data are called nonlinear because an analysis with these properties requires an iterative solution.

3.3.7 Surface Loads

Various element types allow surface loads. Surface loads are typically pressures for structural element types, convections or heat fluxes for thermal element types, etc. Loadings are defined to be of two types as nodal and elemental loading. Nodal loads are defined at the nodes and are not directly related to the elements. Nodal loads are associated with the degrees of freedom at the node and are typically entered with such as nodal displacement constraints and nodal force load. Element loads are surface loads, body loads, and inertia loads. Element loads are always associated with a particular element even if the input is at the nodes.

Body Loads

Various element types allow body loads. Body loads are typically temperatures for structural element types, heat generation rates for thermal element types, etc. Body loads are designated in the “Input Summary” table of each element.

3.4 PIEZOELECTRIC ELEMENTS

3.4.1 SOLID227

SOLID227 has been used as the sensor element in our research work. Solid226 which is a 3-D 20-Node Coupled-Field Solid could also be used. But due to the large number of nodes the meshing would have been way too difficult if it was used instead. Another reason of not using this is it has five degrees of freedom (DOF) per node. The additional DOF is TEMP in which we are not interested in case of our work. Solid227 is a 3D solid piezoelectric element and tetrahedral in shape and has ten nodes with four degrees of freedom per node; three structural UX, UY, UZ and VOLT as an electric degree of

freedom [18]. The element has large deflection and stiffness capabilities and it can be used for electrical, piezoresistive and piezoelectric analyses. The Fig. 3.1 below shows the geometry, node locations and the coordinate system for the element. The field keys for structural, electric conduction, electrostatic are 1, 100 and 1000 respectively. Table 3.2 shows the field keys for structural, piezoresistive and piezoelectric analysis. The reaction solution and the force label will change according to analysis type.

The SOLID227 has 10 nodes viz. I, J, K, L, M, N, O, P, Q and R. The degrees of freedom are listed in Table 3.2. No real constants are required and material properties are set as in Table 3.3. The element can be loaded using either surface loads or body loads. Pressure can be applied on each individual face of the element. Large deflection and Stress stiffening are the special features which are available for this element.

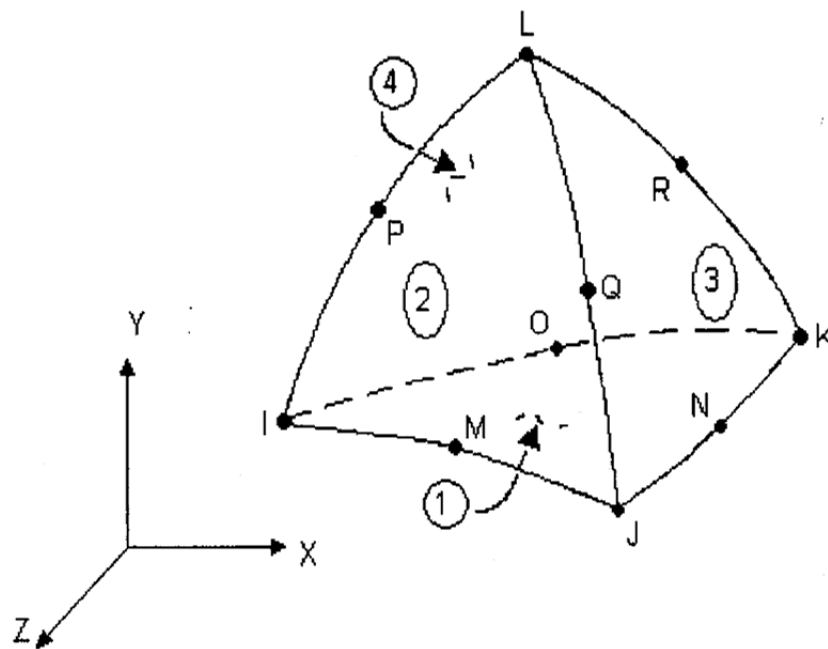


Figure 3.1: SOLID227 Element Geometry

Element output data

The element output data results include stresses, principal stresses, stress intensity, equivalent stresses, strain components, principal strains and equivalent strains.

Thermal strains, electric field and flux density components, elastic energy, dielectric energy and mutual energy. The three values of principal stresses σ_1 , σ_2 and σ_3 are

Table 3.2: Coupled Degree of Freedom Set

Analysis Type	KEYOPT (1)	DOF Label	Force Label	Reaction solution
Structural	1	UX, UY, UZ	FX, FY, FZ	Force
Piezoelectric	1001	UX, UY, UZ, VOLT	FX, FY, FZ, CHRG	Force, Electric charge (negative)
Piezoresistive	101	UX, UY, UZ, VOLT	FX, FY, FZ, AMPS	Force, Electric Current

Table 3.3: SOLID227 Material Properties

Analysis Type	KEYOPT (1)	Material Properties
Piezoelectric	1001	<p>Structural Modulus of Elasticity (X, Y and Z directions) Poisson's Ratio (X, Y and Z directions) Density Damping Thermal expansion coefficient. Anisotropic elasticity matrix (stiffness form or flexibility form)</p> <p>Electrostatic Electric permittivity in X, Y and Z directions.</p> <p>Coupling Piezoelectric matrix (strain matrix $[d]$ or stress matrix $[e]$)</p>
Piezoresistive	101	<p>Structural Modulus of Elasticity (X, Y and Z directions) Poisson's Ratio (X, Y and Z directions) Density Damping Anisotropic elastic matrix (stiffness form or flexibility form)</p> <p>Electric conduction Electric resistivity in X, Y and Z directions.</p> <p>Coupling Piezoresistive matrix (strain matrix or stress matrix)</p>

computed by using roots of the cubic equation obtained from Eq. (3.1). Where σ_x , σ_y and σ_z are the stress components in x , y and z directions. The equivalent stress or Von Mises stress can be computed from Eq. 3.2 or Eq. 3.3.

$$\begin{vmatrix} \sigma_x - \sigma & \sigma_{xy} & \sigma_{xz} \\ \sigma_{xy} & \sigma_y - \sigma & \sigma_{yz} \\ \sigma_{xz} & \sigma_{yz} & \sigma_z - \sigma \end{vmatrix} = 0 \quad (3.1)$$

$$\sigma_e = \left(\frac{1}{2} [(\sigma_1 - \sigma_2)^2 + (\sigma_2 - \sigma_3)^2 + (\sigma_3 - \sigma_1)^2] \right)^{\frac{1}{2}} \quad (3.2)$$

$$\sigma_e = \left(\frac{1}{2} [(\sigma_x - \sigma_y)^2 + (\sigma_y - \sigma_z)^2 + (\sigma_z - \sigma_x)^2 + 6(\sigma_{xy}^2 + \sigma_{yz}^2 + \sigma_{xz}^2)] \right)^{\frac{1}{2}} \quad (3.3)$$

The principal strains ε_1 , ε_2 and ε_3 are computed from the roots of the cubic equation obtained from the strain components in x , y and z directions using Eq (3.4).

$$\begin{vmatrix} \varepsilon_x - \varepsilon & \frac{1}{2} \varepsilon_{xy} & \frac{1}{2} \varepsilon_{xz} \\ \frac{1}{2} \varepsilon_{xy} & \varepsilon_y - \varepsilon & \frac{1}{2} \varepsilon_{yz} \\ \frac{1}{2} \varepsilon_{xz} & \frac{1}{2} \varepsilon_{yz} & \varepsilon_z - \varepsilon \end{vmatrix} = 0 \quad (3.4)$$

The von Mises or equivalent strain ε_e can be computed from Eqn (2.5).

$$\varepsilon_e = \frac{1}{1 + \nu^1} \left(\frac{1}{2} [(\varepsilon_1 - \varepsilon_2)^2 + (\varepsilon_2 - \varepsilon_3)^2 + (\varepsilon_3 - \varepsilon_1)^2] \right)^{\frac{1}{2}} \quad (3.5)$$

where, ν^1 is the effective Poisson's ratio. Stress intensity (SEQV) is the largest difference between the minimum and maximum principal stress. The elastic, dielectric and mutual energy densities are calculated using Eq. (3.6), (3.7) and (3.8) respectively.

$$\{U_E\} = \frac{1}{2} \{S\}^T [c] \{S\} \quad (3.6)$$

$$\{U_D\} = \frac{1}{2} \{E\}^T [\epsilon] \{E\} \quad (3.7)$$

$$\{U_M\} = -\frac{1}{2} \{S\}^T [e] \{E\} \quad (3.8)$$

where, $\{E\}$ is the electric field vector, $\{S\}$ is strain vector, $[c]$ is elasticity matrix, $[e]$ is piezoelectric stress matrix and $[\epsilon]$ is dielectric matrix. Similarly using thermal stress strain relationships and other coupled field relationships the output data is calculated.

3.4.2 PLANE223

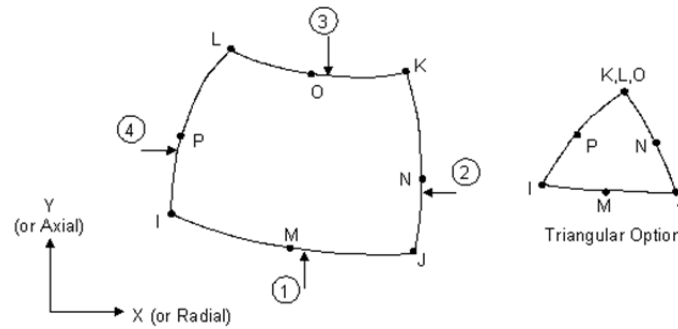


Figure 3.2: PLANE223 Element Geometry

Even though PLANE223 was not used in our research, but it could have been used as a sensor element too. It is a 2D coupled field solid element which has structural, electrical, piezoresistive, and piezoelectric capabilities. The element has eight nodes with up to three degrees of freedom per node UX, UY structural degrees of freedom and electric degree of freedom as VOLT. PLANE223 has large deflection and stress stiffening capabilities. The field keys for structural, electric conduction and electrostatic are 1, 100 and 1000 respectively. By using combination of these field keys element options can be set for following three types of analyses. KEYOPT (1) is set equal to sum of the field keys as shown in the Table 3.4. The reaction solution and the force label will change according to analysis type. The element has 8 nodes viz. I, J, K, L, M, N, O, P. The degrees of freedom are set according to Table 3.5. No real constants are required and

material properties are set according to the Table 3.5. The element can be loaded using either surface loads or body loads. Large deflection and Stress stiffening features are available for this element.

Table 3.4 Coupled Degree of Freedom Set

Analysis Type	KEYOPT (1)	DOF Label	Force Label	Reaction solution
Structural	1	UX,UY	FX, FY	Force
Piezoelectric	1001	UX, UY, VOLT	FX, FY, CHRG	Force, Electric charge (negative)
Piezoresistive	101	UX, UY, VOLT	FX, FY, AMPS	Force, Electric Current

Table 3.5: PLANE223 Material Properties

Analysis Type	KEYOPT (1)	Material Properties
Piezoelectric	1001	<p>Structural Modulus of Elasticity (X, Y and Z directions) Poisson's Ratio (X, Y and Z directions) Density Damping Thermal expansion coefficient. Anisotropic elasticity matrix (stiffness form or flexibility form)</p> <p>Electrostatic Electric permittivity in X and Y directions. Loss tangent (LSST).</p> <p>Coupling Piezoelectric matrix (strain matrix $[d]$ or stress matrix $[e]$)</p>
Piezoresistive	101	<p>Structural Modulus of Elasticity (X, Y and Z directions) Poisson's Ratio (X, Y and Z directions) Density Damping Anisotropic elasticity matrix (stiffness form or flexibility form)</p> <p>Electric conduction Electric resistivity in X and Y directions.</p> <p>Coupling Piezoresistive matrix (strain matrix or stress matrix)</p>

Additional **KEYOPT (3)** options for element behavior are set by selecting the keys 0, 1 and 2 for plane stress, axisymmetric and plane strain respectively. Element output data for this element same as output data for SOLID227 piezoelectric element.

Assumptions and restrictions

This element assumes unit thickness. It uses 2×2 or 3 point integration rules to calculate the element matrices and load vectors for the quad and triangle geometries, respectively. In a piezoelectric analysis, electric charge loading is interpreted as negative electric charge or negative charge density. The element must lie in global XY plane and Y axis must be the axis of symmetry for axisymmetric models. The axisymmetric structure must be modeled in +X quadrant.

3.5 CONTACT ELEMENTS

3.5.1 CONTA174

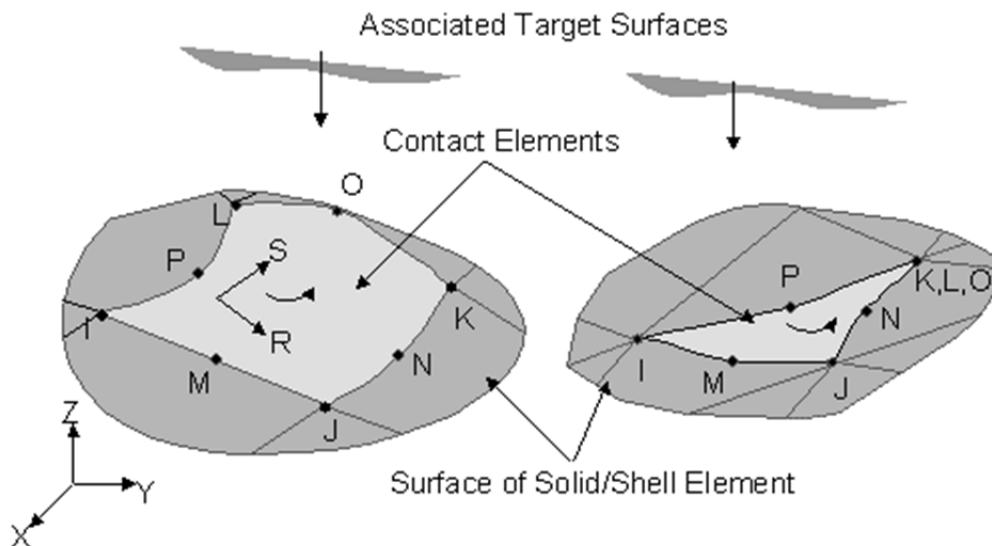


Figure 3.3: CONTA174 Element Geometry

CONTA174 has been used as a surface to surface contact element to model the contact surface for generating the contact pair in our research. CONTA173 which is 3-D 4-Node Surface-to-Surface Contact element could also be used. But the accuracy wouldn't be the same as CONTA 174 due to the lower number of nodes. CONTA174 is used to represent contact and sliding between 3-D target surfaces with element TARGE170 and a deformable surface which is defined by this element. The element is applicable to 3-D structural and coupled field contact analyses. This element is located on the surfaces of 3-D solid or shell elements with midside nodes e.g. SOLID 227. It has the same geometric characteristics as the solid or shell element face with which it is connected. Contact occurs when the element surface penetrates one of the target segment elements TARGE170 on a specified target surface. The element is defined by eight nodes I, J, K, L, M, N, O, P (the underlying solid or shell element has midside nodes). It can degenerate to a six node element depending on the shape of the underlying solid or shell elements. The positive normal is given by the right-hand rule going around the nodes of the element and is identical to the external normal direction of the underlying solid or shell element surface. For shell elements, the same nodal ordering between shell and contact elements defines upper surface contact; otherwise, it represents bottom surface contact. The target surfaces must always be on its outward normal direction. Damping, coefficient of friction and emissivity are the required material properties. This element includes special features nonlinear, large deflection and 'element birth and death'.

Table 3.6: Real Constants for CONTA174

Target circle radius	Contact cohesion
Superelement thickness	Thermal contact conductance
Normal penalty stiffness factor	Frictional heating factor
Penetration tolerance factor	Stefan-Boltzmann constant
Upper limit of initial allowable penetration	Radiation view factor
Lower limit of initial allowable penetration	Heat distribution weighing factor
Initial contact closure	Electric contact conductance
Pinball region	Joule dissipation weight factor
Maximum friction stress	Static/dynamic ratio
Contact surface offset	Exponential decay factor
Contact opening stiffness	Allowable elastic slip
Target penalty stiffness	Target edge extension factor
Maximum allowable tensile contact pressure	

KEYOPT options and degrees of freedoms are listed in Table 3.7.

Table 3.7: KEYOPT Options for CONTA174 Element

<p>KEYOPT (1) Degree of freedom 0:UX, UY, UZ 1: UX, UY, UZ, TEMP 2: TEMP 3: UX, UY, UZ, TEMP, VOLT 4: TEMP, VOLT 5: UX, UY, UZ, VOLT 6:VOLT 7:MAG</p>	<p>KEYOPT (5) Automated adjustment 0:no automatic adjustment 1:close gap with automatic adjustment 2:reduce penetration with no adjustment 3:closegap/reduce penetration with no auto. 4: Auto ICONT</p>	<p>KEYOPT (10) Contact stiffness update 0:each load step 1:each sub step 2:each iteration 3: each load step for individual element 4: each sub step for individual element 5:each iteration for Individual element.</p>
<p>KEYOPT (2) Contact algorithm 0: Augmented Lagrangian 1: Penalty function 2: Multipoint constraints 3: Lagrange multiplier on contact normal and penalty on tangent 4:Pure Lagrange multiplier on contact normal and tangent</p>	<p>KEYOPT (7) Element level time incrementation control 0:no control 1:automatic bisection of increment 2: change in contact predictions made to maintain reasonable load increment.</p>	<p>KEYOPT (11) Beam / Shell thickness effect 0:exclude 1:include</p>
<p>KEYOPT (3) Stress state (with superelement) 0:use with h elements 1:axisymmetric 2:plane stress/strain 3:plane stress + thickness</p>	<p>KEYOPT (8) Asymmetric contact selection 1:no action 2:Ansys automatically selects</p>	<p>KEYOPT (12) Behavior of contact 0:standard 1:rough 2:no separation allow sliding 3:bonded 4:no separation always 5:bonded always 6:bonded initial contact</p>
<p>KEYOPT (4) Location of contact detection 0: on gauss point 1:on nodal point 2: on nodal point-normal to target surface</p>	<p>KEYOPT (9) Effect of initial Penetration or gap 0:include both 1:exclude both 2:includeboth with ramped effect 3:include offset only 4: include offset only</p>	

Element output summary

The output data for CONTA174 element consists of underlying solid/shell, or beam element number, contact status, current penetration or gap status, contact pressure, contact stress, contact stiffness, coefficient of friction, convection coefficient, penetration tolerance, conductance coefficient, radiation coefficient, temperatures, heat flux, frictional energy dissipation, contact current and charge density, contact power, voltage on contact nodes, voltage on associated target, current, charge per contact element.

CONTA174 assumptions

The 3-D contact element must coincide with the external surface of the underlying solid or shell element. This element is nonlinear and requires a full Newton iterative solution, regardless of whether large or small deflections are specified. The normal contact stiffness factor (FKN) must not be so large as to cause numerical instability. You can use this element in nonlinear static or nonlinear full transient analyses, modal analyses, eigenvalue buckling analyses and harmonic analyses. For these analysis types, the program assumes that the initial status of the element does not change. This element allows birth and death and will follow the birth and death status of the underlying solid, shell, beam or target elements.

CONTA174 restrictions

It does not support material properties of coefficient of friction, and damping. Element birth and death special feature is not allowed.

3.5.2 TARGE170

TARGE170 has been used as a surface to surface contact element to model the target surface for generating the contact pair in our research. TARGET 169 could also be used

instead. The reason for not using it is not only because it is a 2D element but also it doesn't have the UZ DOF in which we are interested in case of our work. TARGET170 is used to represent various 3-D target surfaces for the associated contact elements (CONTA173, CONTA174, and CONTA175). The contact elements themselves overlay the solid elements describing the boundary of a deformable body and are potentially in contact with the target surface, defined by TARGET170. This target surface is discretized by a set of target segment elements (TARGET170) and is paired with its associated contact surface via a shared real constant set. Any translational or rotational displacement, forces, moments, temperature, voltage, and magnetic potential on the target segment element can be imposed. For rigid target surfaces, these elements can easily model complex target shapes. For flexible targets, these elements will overlay the solid elements describing the boundary of the deformable target body.

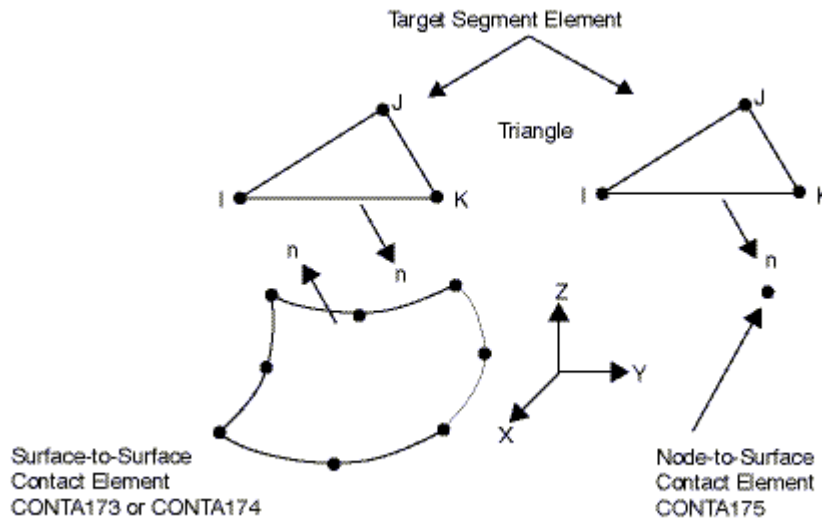


Figure 3.4: TARGET170 Element Geometry

The target surface can either be rigid or deformable. For modeling rigid-flexible contact, the rigid surface must be represented by a target surface. For flexible-flexible contact,

one of the deformable surfaces must be overlaid by a target surface. Each target surface can be associated with only one contact surface, and vice-versa. However, several contact elements could make up the contact surface and thus come in contact with the same target surface.

Considerations for Rigid Target Surfaces

Each target segment of a rigid surface is a single element with a specific shape, or segment type. The segment types are defined by several nodes and a target shape code, which are described in Fig. 3.7. The segment radii are defined by real constants R1 and R2, and the segment location is determined by the nodes.

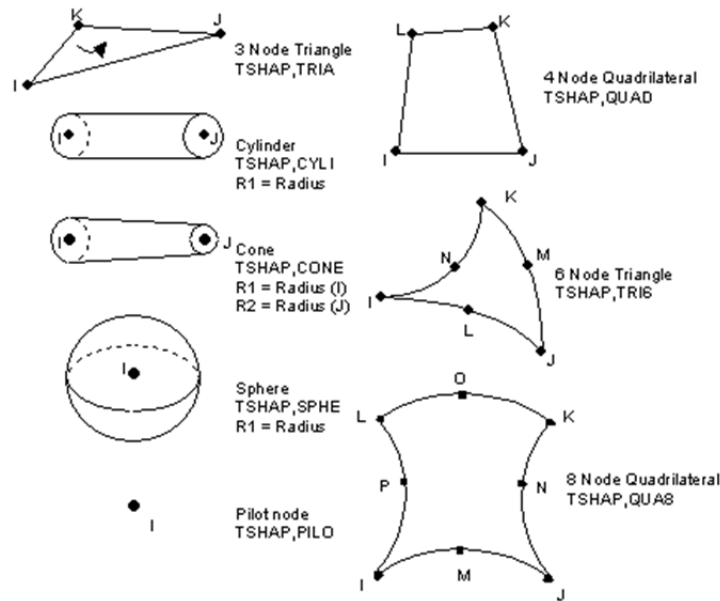


Figure 3.5: TARGE170 3D Segment Types

Element Input data

3 node Triangle

UX, UY, UZ, TEMP, VOLT, MAG degrees of freedom and real constants R1 and R2

4 node quadrilateral

UX, UY, UZ, TEMP, VOLT, MAG degrees of freedom and no real constants R1 and R2 are needed.

6 node triangle (4 and 6 are midside nodes)

UX, UY, UZ, TEMP, VOLT, MAG degrees of freedom + No real constants R1 and R2

8 node quadrilateral (5 and 8 are midside nodes): UX, UY, UZ, TEMP, VOLT, MAG degrees of freedom and no real constants R1 and R2 needed

Cylinder (1 and 2 are axial end points)

UX, UY, UZ, TEMP, VOLT, MAG degrees of freedom

R1 is radius of the cylinder and R2 is not required.

Cone (1 and 2 are axial end points): UX, UY, UZ, TEMP, VOLT, MAG DOF.

R1 is radius at node1 and R2 is radius at node2.

Sphere center point (UX, UY, and UZ): TEMP, VOLT and MAG

R1 is radius of the sphere and R2 is not required.

Pilot node: UX, UY, UZ, ROTX, ROTY, ROTZ, TEMP, VOLT, MAG degrees of freedom and real constants R1 and R2.

TARGE170 Input Summary

It is defined by nodes I, J, K, L, M, N, O, P (J - P are not required for all segment types)

Real Constants R1, R2 and the other real constants are defined through the associated CONTA173, CONTA174, or CONTA175 elements.

Material properties: Body loads and surface loads are not required for this element.

Special Features

Nonlinear and “birth and death”.

Element output data

Element output data includes element numbers, their respective nodes, target surface number, segment shape type and corresponding numbers.

Table 3.8: TARGE170 KEYOPT Options

<p>KEYOPT (1) Element order 0: Low order elements 1: High order elements</p>	<p>KEYOPT (4) DOF set to be constrained, used only for a surface-based constraint n- Enter a six digit value that represents the DOF set to be constrained. The first to sixth digits represent ROTZ, ROTY, ROTX, UZ, UY, UX, respectively. No 1 indicates active degree of freedom and 0 indicates non active degree of freedom.</p>
<p>KEYOPT (2) Boundary conditions for rigid target nodes 0: Automatically constrained by ANSYS 1: Specified by user</p>	<p>KEYOPT (5) Constraint type used when only KEYOPT (2) for contact element = 2. 0: Automatic constraint type detection (default) 1: Solid-solid constraint 2: Shell-shell constraint 3: Shell-solid constraint 4: Shell-solid constraint</p>
<p>KEYOPT (3) Behavior of thermal contact surface 0: Based on contact status 1: Treated as free-surface</p>	

Assumptions and Restrictions

Generally speaking, it is not allowed to change real constants R1 or R2, either between load steps or during restart stages. Otherwise ANSYS assumes the radii of the primitive segments vary between the load steps. When using direct generation, the real constants for cylinders, cones, and spheres may be defined before the input of the element nodes. No external forces can be applied on target nodes except on a pilot node. To ensure the

correct behavior, all boundary conditions should be applied to a pilot node. If a pilot node is specified for a target surface, ANSYS will ignore the boundary conditions on any nodes of the target surface except for the pilot nodes. For each pilot node, ANSYS automatically defines an internal node and an internal constraint equation. The rotational DOF of the pilot node is connected to the translational DOF of the internal node by the internal constraint equation. Constraint equations or coupling cannot be used on pilot nodes.

3.6 STRUCTURAL ELEMENTS

SHELL63

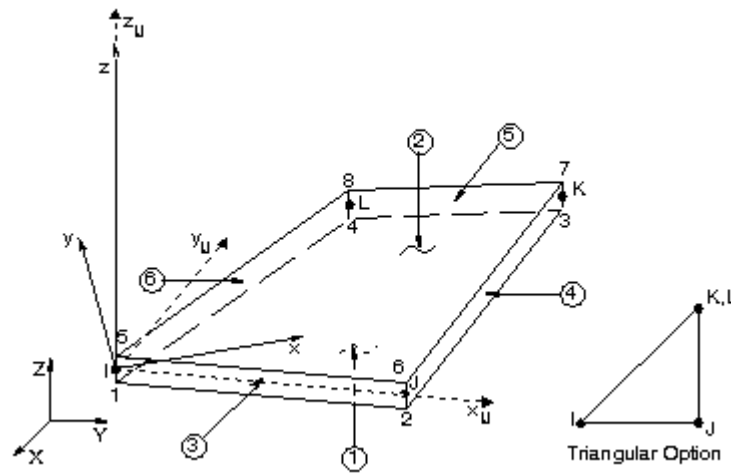


Figure 3.6: SHELL63 Element Geometry

x_{IJ} is x axis if elemental coordinate system is not provided and x is element x axis if the elemental coordinate system is provided.

SHELL63 has been used to model the structures in our research work. SHELL61 could also be used instead. But since it is a 2-D Axisymmetric - Harmonic Structural Shell element has nodes only half of SHELL63 so it is not used in this case. SHELL63 is a Structural 3-D Elastic Shell element and has both bending and membrane capabilities [18]. Both in-plane and normal loads are permitted. Stress stiffening and large deflection

capabilities are included for this element. The thickness is assumed to vary smoothly over the area of the element, with the thickness input at the four nodes. If the element has a constant thickness, only thickness of node I need be input. If the thickness is not constant, the thickness at each node needs to be input. It is defined by four nodes I, J, K and L. The element has six degrees of freedom at each node three translations in the nodal UX, UY, and UZ directions and rotations about the nodal ROTX, ROTY, and ROTZ. Modulus of elasticity, Poison's ratio, coefficient of thermal expansion, density and damping are the required material properties for SHELL63.

Surface Loads: Pressure can be applied on each individual face of the element. SHELL63 has six faces viz. face 1 (I-J-K-L) (bottom, in +Z direction), face 2 (I-J-K-L) (top, in -Z direction), face 3 (J-I), face 4 (K-J), face 5 (L-K), face 6 (I-L).

Table 3.9: SHELL63 Real Constants

Name	Description
TK(I)	Shell thickness at node I
TK(J)	Shell thickness at node J
TK(K)	Shell thickness at node K
TK(L)	Shell thickness at node L
EFS	Elastic foundation stiffness
THETA	Element X-axis rotation
RMI	Bending moment of inertia ratio
CTOP	Distance from mid surface to top
CBOT	Distance from mid surface to bottom
ADMSUA	Added mass/unit area

Special Features: Stress stiffening, large deflection and element birth and death are the special features available for SHELL63 element.

Output data

The element stress directions are parallel to the element coordinate system. The stress output of SHELL63 element is as shown in the Fig. 3.7 below.

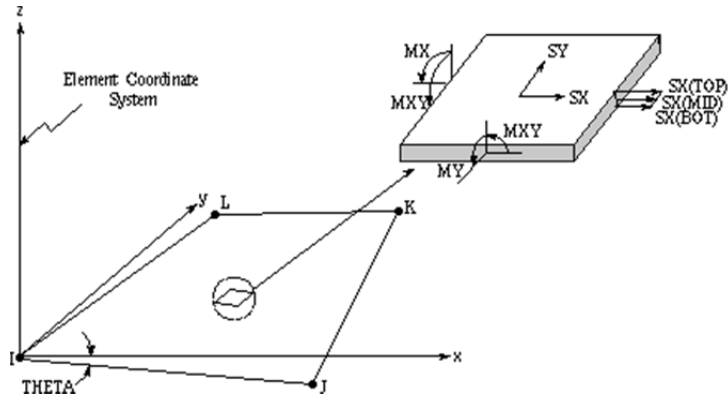


FIGURE 3.7: Stress Output of SHELL63

Table 3.10: KEYOPT OPTIONS for SHELL63

<p>KEYOPT (1) Element stiffness 0: Bending and membrane stiffness 1: Membrane stiffness only 2: Bending stiffness only</p>	<p>KEYOPT(7) Mass matrix 0: Consistent mass matrix 1: Reduced mass matrix</p>
<p>KEYOPT (2) Stress stiffening option 0: Use only the main tangent stiffness matrix when large deflection is ON. 1: Use the consistent tangent stiffness matrix when large deflection is ON. 2: Use to turn off consistent tangent stiffness matrix.</p>	<p>KEYOPT(8) Stress stiffness matrix 0: "Nearly" consistent stress stiffness matrix (default) 1: Reduced stress stiffness matrix</p>
<p>KEYOPT(3) 0: Include extra displacement shapes 1: Suppress extra displacement shapes 2: Include extra displacement shapes</p>	<p>KEYOPT(9) Element coordinate system defined 0: No user subroutine to define element coordinate system. 4: Element x-axis located by user subroutine.</p>
<p>KEYOPT(5) Extra stress output 0: Basic element printout 1: Nodal stress printout</p>	<p>KEYOPT (11) Specify data storage 0: No user subroutine to define element coordinate system 2: Store data for TOP, BOTTOM, and MID surfaces.</p>
<p>KEYOPT(6) Pressure loading 0: Reduced pressure loading 1: Consistent pressure loading</p>	

The element output data includes combined membrane and bending stresses. Membrane stresses in a plate or beam are the normal stresses perpendicular to the surface of the plate or beam and bending stresses are negligibly small. Also, principle stresses, stress intensity, equivalent stress, equivalent strain are calculated.

Assumptions

Either zero area elements or zero thickness elements i.e. elements tapering down to a zero thickness at any corner are not allowed. The applied transverse thermal gradient is assumed to vary linearly through the thickness and vary bilinearly over the shell surface. If the lumped mass matrix formulation is specified, the effect of the implied offsets on the mass matrix is ignored for warped SHELL63 elements.

SHELL63 restriction: The damping material property is not allowed. The only special features allowed are stress stiffening and large deflection. KEYOPT (2) and KEYOPT (9) can only be set to 0 which is by default.

CHAPTER IV

ANALYSES FORMULATION

Multiphysics simulation of PVDF sensor is carried out by a combination of analysis types. The objective of this simulation is to get the nodal complex displacements and voltages when a single point random excitation force is applied away from the support on the beam, plate and cylindrical shell to which PVDF sensor is bonded. Three types of analyses which are used to achieve the required objective of the multiphysics sensor simulation are mode frequency analysis, spectrum analysis and harmonic analysis respectively. Mode frequency analysis is a coupled field analysis where structural and electric fields are coupled by using the direct matrix coupling method [20]. The convergence limits for the current are set in this step since the coupled field analysis requires an iterative solution. The modes are extracted and expanded with elemental solution. This analysis results in natural frequencies and mode shapes of the structure when subjected to free vibration. Also, it gives the voltage developed at the sensor nodes at each frequency and the behavior of the output charge can be animated for each mode in ANSYS. The response spectrum can then be specified in a spectrum analysis to calculate the overall response of a structure. It gives one sigma displacement results to determine one sigma peak displacement when power spectral density (PSD) loading is used. The detail information about PSD loading and one sigma peak displacement with formulation

is presented later in this chapter. Any sustained cyclic load will produce a sustained cyclic response (a harmonic response) in a structural system. Harmonic response analysis is carried out to predict the sustained dynamic behavior of the structure, thus enabling to verify whether or not designed structures will successfully overcome resonance, fatigue, and other harmful effects of forced vibrations. Harmonic response analysis is a technique used to determine the steady-state response of a linear structure to the loads that vary sinusoidally (harmonically) with time. The idea is to calculate the structure's response at several frequencies and obtain a graph of some response quantity (usually displacements) versus frequency. "Peak" responses are then identified on the graph and stresses are reviewed at those peak frequencies. ANSYS writes output of the harmonic frequency analysis in complex form for each frequency in the binary file. The piezoelectric analysis formulation is discussed in the beginning of this chapter before going forward because it is required in the analyses that follows. The three types of analyses that are stated above are described in details at the later part of the chapter.

4.1 PIEZOELECTRIC ANALYSIS

Piezoelectric analysis is the coupling of structural and electric fields, which is a natural property of materials such as quartz and ceramics [20]. Applying a voltage to a piezoelectric material creates a displacement, and applying force to the piezoelectric material generates a voltage. The purpose of piezoelectric analysis is to get results of either output voltage developed due to force applied or to get displacement results due to the applied voltage to the piezoelectric material. Piezoelectric analysis is used in ANSYS multiphysics for designing micro electromechanical systems. Possible piezoelectric analysis types available in ANSYS Multiphysics are static, mode frequency analysis, prestressed modal, harmonic, prestressed harmonic and transient analysis. Some of the elements available for piezoelectric analysis in ANSYS are listed in Table 4.1. Piezoelectric analysis uses the direct method of coupling in multiphysics simulation. The coupling is achieved by the matrix method. The piezoelectric material constitutive properties are permittivity matrix $[\epsilon_r]$, piezoelectric matrix (in the stress form $[e]$ or in the strain $[d]$ form) and elastic coefficient matrix. Elastic coefficient matrix must be in either stiffness matrix form $[c]$ or in the flexibility form i.e. compliance matrix $[S]$.

Table 4.1: ANSYS Elements for Piezoelectric Analysis

PLANE13	coupled-field quadrilateral solid
PLANE223	coupled-field brick
SOLID5	coupled-field tetrahedron
SOLID98	coupled-field 8-node quadrilateral
SOLID226	coupled-field 20-node brick
SOLID227	coupled-field 10-node tetrahedron

4.1.1 Dielectric Relative Permittivity Matrix $[\epsilon_r]$

A measure of the ability of a material to resist the formation of an electric field within the material is called as dielectric constant or permittivity. Relative permittivity can be expressed as the ratio of the electric permittivity in the medium to the free space permittivity which is given by $\epsilon_0 = 8.85e^{-12} F/m$. Relative permittivity values represent the diagonal terms of the permittivity matrix. The permittivity values can be specified either at constant stress or constant strain. ANSYS internally converts the permittivity values at constant strain using piezoelectric stress or strain matrices. Eq. (4.1) gives the IEEE and ANSYS notations for the permittivity matrix.

$$[\epsilon_r] = \begin{bmatrix} \epsilon_{11} & 0 & 0 \\ 0 & \epsilon_{22} & 0 \\ 0 & 0 & \epsilon_{33} \end{bmatrix} \quad (4.1)$$

4.1.2 Piezoelectric matrix

The piezoelectric matrix is defined either in $[e]$ form (piezoelectric stress matrix) or in $[d]$ form (piezoelectric strain matrix). The $[e]$ matrix is typically associated with the input of the anisotropic elasticity in the form of the stiffness matrix $[c]$, while the $[d]$ matrix is associated with the compliance matrix $[S]$. IEEE notations for $[e]$ and $[d]$ matrices for 3D cases has dimensions 3×6 but ANSYS uses 6×3 dimensions because of the different terminology for piezoelectric constitutive relationships are defined. ANSYS constitutive matrix notations follow IEEE standard notations for the piezoelectric constitutive relationships. IEEE and ANSYS constitutive relationships in the stress-charge form are given by Eqs. (4.2) & (4.3)

$$\text{IEEE } \{T\} = [c]\{S\} - [e]^T \{E\} \quad \text{Vs ANSYS } \{T\} = [c]\{S\} - [e]\{E\} \quad (4.2)$$

$$\text{IEEE } \{D\} = [e]\{S\} + [\epsilon]\{E\} \quad \text{Vs ANSYS } \{D\} = [e]^T \{S\} + [\epsilon]\{E\} \quad (4.3)$$

where, $\{D\}$ is the charge displacement vector and $\{T\}$ is the stress vector. ANSYS calculates the charge developed or the displacements using these relationships.

IEEE piezoelectric matrix in stress form

$$[e] = \begin{bmatrix} e_{11} & e_{12} & e_{13} \\ e_{21} & e_{22} & e_{23} \\ e_{31} & e_{32} & e_{33} \\ e_{41} & e_{42} & e_{43} \\ e_{51} & e_{52} & e_{53} \\ e_{61} & e_{62} & e_{63} \end{bmatrix} \text{ for 3D models \& } [e] = \begin{bmatrix} e_{11} & e_{12} \\ e_{21} & e_{22} \\ e_{31} & e_{32} \\ e_{41} & e_{42} \end{bmatrix} \text{ for 2D models.} \quad (4.4)$$

IEEE piezoelectric matrix in strain form

$$[d] = \begin{bmatrix} d_{11} & d_{12} & d_{13} \\ d_{21} & d_{22} & d_{23} \\ d_{31} & d_{32} & d_{33} \\ d_{41} & d_{42} & d_{43} \\ d_{51} & d_{52} & d_{53} \\ d_{61} & d_{62} & d_{63} \end{bmatrix} \text{ for 3D models and } [d] = \begin{bmatrix} d_{11} & d_{12} \\ d_{21} & d_{22} \\ d_{31} & d_{32} \\ d_{41} & d_{42} \end{bmatrix} \text{ for 2D models.} \quad (4.5)$$

The order used for the piezoelectric matrix is x, y, z, yz, xz, xy, based on IEEE standards for most published piezoelectric materials, while the ANSYS input order is x, y, z, xy, yz, xz. So in order to transform IEEE matrix into ANSYS matrix, row data for the shear terms is switched as shown below in Eq. (4.6).

Converting IEEE format into ANSYS format give resulting matrices are as under.

$$[e] = \begin{bmatrix} e_{11} & e_{12} & e_{13} \\ e_{21} & e_{22} & e_{23} \\ e_{31} & e_{32} & e_{33} \\ e_{61} & e_{62} & e_{63} \\ e_{41} & e_{42} & e_{43} \\ e_{51} & e_{52} & e_{53} \end{bmatrix} \quad \text{and} \quad [d] = \begin{bmatrix} d_{11} & d_{12} & d_{13} \\ d_{21} & d_{22} & d_{23} \\ d_{31} & d_{32} & d_{33} \\ d_{61} & d_{62} & d_{63} \\ d_{41} & d_{42} & d_{43} \\ d_{51} & d_{52} & d_{53} \end{bmatrix} \quad (4.6)$$

4.1.3 Elastic coefficient matrix

Elastic coefficient matrix is symmetric matrix and it has dimensions 6×6 for 3D models and 4×4 for 2D models. It can be specified in the stiffness form $[c]$ or in the flexibility form $[S]$ or compliance matrix.

$$[c] = \begin{bmatrix} c_{11} & c_{21} & c_{31} & c_{41} & c_{51} & c_{61} \\ c_{21} & c_{22} & c_{32} & c_{42} & c_{52} & c_{62} \\ c_{31} & c_{32} & c_{33} & c_{43} & c_{53} & c_{63} \\ c_{41} & c_{42} & c_{43} & c_{44} & c_{54} & c_{64} \\ c_{51} & c_{52} & c_{53} & c_{54} & c_{55} & c_{65} \\ c_{61} & c_{62} & c_{63} & c_{64} & c_{65} & c_{66} \end{bmatrix} \quad (4.7)$$

$$[S] = \begin{bmatrix} S_{11} & S_{21} & S_{31} & S_{41} & S_{51} & S_{61} \\ S_{21} & S_{22} & S_{32} & S_{42} & S_{52} & S_{62} \\ S_{31} & S_{32} & S_{33} & S_{43} & S_{53} & S_{63} \\ S_{41} & S_{42} & S_{43} & S_{44} & S_{54} & S_{64} \\ S_{51} & S_{52} & S_{53} & S_{54} & S_{55} & S_{65} \\ S_{61} & S_{62} & S_{63} & S_{64} & S_{65} & S_{66} \end{bmatrix} \quad (4.8)$$

Eqns. (4.7) and (4.8) gives the IEEE format of $[c]$ and $[S]$ matrices which need to be transformed into ANSYS format, same as in case of piezoelectric matrix transformation.

The ANSYS $[c]$ and $[S]$ are symmetric and are given as under.

where, $[K]$ is structural stiffness matrix, $\{u\}$ is nodal displacement vector and $[M]$ is mass matrix. For linear systems having free vibrations, the displacements are in the harmonic form as

$$\{u\} = \{\phi\}_i \cos \omega_i t \quad (4.11)$$

where, $\{\phi\}_i$ is an eigenvector representing the mode shape of the i^{th} natural frequency and ω_i is the i^{th} natural circular frequency (radians per unit time) and t is the time.

Substituting Eqs. (4.11) into (4.10) gives Eq. (4.12).

$$(-\omega_i^2[M] + [K])\{\phi_i\} = \{0\} \quad (4.12)$$

This equality is satisfied if either $\{\phi_i\}$ is zero or if the determinant of $[-\omega_i^2[M] + [K]]$ is zero. The first option is the trivial one and, therefore, is not of interest. Thus, the second one gives the solution as $|[K] - [M]\omega^2| = 0$ which gives the n values for ω_n^2 and eigenvectors $\{\phi_i\}_n$ which satisfies the Eq. (4.12). ANSYS output consists of natural frequencies f^n rather than natural circular frequencies ω_i .

$$f^n = \frac{\omega_n}{2\pi} \quad (4.13)$$

Higher order frequencies can be found by eliminating the largest eigenvalue from the characteristic equation. To find the eigenvector $\{\phi_i\}$, the previous eigenvector $\{\phi_{i-1}\}$ is normalized with respect to $[M]$ such that

$$\{\phi_{i-1}\}^T [M] \{\phi_{i-1}\} = 1 \quad (4.14)$$

4.3 SPECTRUM ANALYSIS

The spectrum is a graph of spectral value versus frequency that captures the intensity and frequency content of time-history loads [20]. Three types of spectra are available for a spectrum analysis which are classified as under

1. Response spectrum
 - Single point response spectrum
 - Multipoint response spectrum
2. Dynamic design analysis method
3. Power spectral density method.

4.3.1 RESPONSE SPECTRUM

A response spectrum represents the response of single degree of freedom systems to a time-history loading function. It is a graph of response versus frequency, where the response might be displacement, velocity, acceleration, or force. Two types of response spectrum analysis possible as stated above.

4.3.2 DYNAMIC DESIGN ANALYSIS METHOD (DDAM)

The Dynamic Design Analysis Method (DDAM) is a technique used to evaluate the shock resistance of shipboard equipment. This technique is essentially a response spectrum analysis in which the spectrum is obtained from a series of empirical equations and shock design tables provided in the U.S. Naval Research Laboratory.

4.3.3 POWER SPECTRAL DENSITY (PSD) APPROACH

Power spectral density (PSD) is a statistical measure defined as the limiting mean-square value of a random variable. It is used in random vibration analyses in which the

instantaneous magnitudes of the response can be specified only by probability distribution functions that show the probability of the magnitude taking a particular value. A PSD is a statistical measure of the response of a structure to random dynamic loading conditions. It is a graph of the PSD value versus frequency, where the PSD may be a displacement PSD, velocity PSD, acceleration PSD, or force PSD. Mathematically, the area under a PSD-versus-frequency curve is equal to the variance. Similar to response spectrum analysis, a random vibration analysis may be single-point or multi-point. In a single-point random vibration analysis, one PSD spectrum is specified at a set of point in the model. In a multi-point random vibration analysis different PSD spectra are specified at different points in the model.

Response spectrum and DDAM analyses are deterministic analyses since both the input to the analyses and output from the analyses are actual maximum values. Random vibration analysis, on the other hand, is indeterministic or probabilistic in nature because both input and output quantities represent only the probability that they take on certain values. The spectrum analysis must be preceded by a mode-frequency analysis and if mode combinations are needed, the required modes must also be expanded in modal analysis. The methods of the spectrum analyses available are the response spectrum method, dynamic design analysis method, random vibration method as mentioned above. This simulation uses single point random vibration response, the formulation for this method is presented in detail.

4.3.4 SINGLE POINT RESPONSE RANDOM VIBRATION ANALYSIS

This analysis is preceded by the modal analysis and after modal solution is obtained modes are expanded to obtain spectral solution. In the next step modes are combined in a single step to obtain the response. This method allows both base excitation and the excitation away from the support i.e. forced random excitation at the single point away from the support.

4.3.5 RANDOM VIBRATION METHOD FORMULATION

The random vibration method allows multiple power spectral density (PSD) inputs in which these inputs can be correlated, non-correlated or partially correlated [20]. The procedure is based on computing statistics of each modal response and then combining them. It is based on the assumption that the excitations are stationary random processes. For partially correlated nodal and base excitations, the complete equations of motions are segregated into the free and the restrained (support) DOF as

$$\begin{bmatrix} [M_{ff}] & [M_{fr}] \\ [M_{rf}] & [M_{rr}] \end{bmatrix} \begin{Bmatrix} \ddot{\{u_f\}} \\ \ddot{\{u_r\}} \end{Bmatrix} + \begin{bmatrix} [C_{ff}] & [C_{fr}] \\ [C_{rf}] & [C_{rr}] \end{bmatrix} \begin{Bmatrix} \dot{\{u_f\}} \\ \dot{\{u_r\}} \end{Bmatrix} + \begin{bmatrix} [K_{ff}] & [K_{fr}] \\ [K_{rf}] & [K_{rr}] \end{bmatrix} \begin{Bmatrix} \{u_f\} \\ \{u_r\} \end{Bmatrix} = \begin{Bmatrix} \{F\} \\ \{0\} \end{Bmatrix} \quad (4.16)$$

where, u_f are the free DOF and u_r are the restrained DOF that are excited by random loading, $\{F\}$ is the nodal force excitation activated by a nonzero value of force which can be other than unity, allowing for scaling of the participation factors. The free displacements can be decomposed into pseudo-static and dynamic parts as in Eq. (4.17)

$$\{u_f\} = \{u_s\} + \{u_D\} \quad (4.17)$$

The pseudo-static displacements may be obtained from Eq. (4.16) by excluding the first two terms on the left-hand side of the equation and by replacing $\{u_f\}$ by $\{u_s\}$.

$$\{u_s\} = -[K_{ff}]^{-1}[K_{fr}]\{u_r\} = [A]\{u_r\} \quad (4.18)$$

in which $[A]$ is $-[K_{ff}]^{-1}[K_{fr}]$. Physically, the elements along the i^{th} column of $[A]$ are the pseudo-static displacements due to a unit displacement of the support DOFs excited by i^{th} the base PSD. Substituting Eqns. (4.17) & (4.18) into (4.16) gives Eq. (4.19).

$$[M_{ff}]\{u_D''\} + [C_{ff}]\{u_D'\} + [K_{ff}]\{u_D\} \approx [F] - ([M_{ff}][A] + [M_{fr}])\{u_r\} \quad (4.19)$$

The second term on the right-hand side of the above equation represents the equivalent forces due to support excitations. Using the mode superposition analysis gives the Eq. (4.20)

$$\{u_d(t)\} = [\phi]\{y(t)\} \quad (4.20)$$

The above equations are decoupled yielding Eq. (4.21)

$$y_j + 2\xi_j \omega_j \dot{y}_j + \omega_j^2 y_j = G_j \text{ where } i = 1, 2, 3, 4, \dots, n \quad (4.21)$$

where, n is the number of modes chosen for the evaluation, y_j is the generalized displacement, ω_j and ξ_j are the natural circular frequency and damping ratio respectively. The modal loads G_j are defined by modal participation factors in Eqn. (4.22)

$$G_j = \{\tau_j\}^T \{u_r''\} + \gamma_j \quad (4.22)$$

where, the modal participation factors corresponding to support excitation and nodal excitation are given by Eqns. (4.23) and (4.24) respectively.

$$\{\Gamma_j\} = -([M_{ff}][A] + [M_{fr}])^T \{\phi_j\} \quad (4.23)$$

$$\{\gamma_j\} = \{\phi_j\}^T \{F\} \quad (4.24)$$

4.3.6 RESPONSE POWER SPECTRAL DENSITIES AND MEAN

SQUARE RESPONSE

Using the theory of random vibrations, the response PSD's can be computed from the input PSD's with the help of transfer functions for single DOF systems $H(\omega)$ and by using mode superposition techniques. The response PSD's for i^{th} DOF are given by the Dynamic part, Pseudo part and Covariance part as expressed below.

Dynamic part

$$S_{d_i}(\omega) = \sum_{j=1}^n \sum_{k=1}^n \phi_{ij} \phi_{ik} \left(\sum_{l=1}^{r_1} \sum_{m=1}^{r_1} \gamma_{lj} \gamma_{mk} H_j^*(\omega) H_k(\omega) \bar{S}_{lm}(\omega) + \sum_{l=1}^{r_2} \sum_{m=1}^{r_2} \Gamma_{lj} \Gamma_{mk} H_j^*(\omega) H_k(\omega) \hat{S}_{lm}(\omega) \right)$$

Pseudo part

$$S_{si}(\omega) = \sum_{l=1}^{r_2} \sum_{m=1}^{r_2} A_{il} A_{im} \left(\frac{1}{\omega^4} \hat{S}_{lm}(\omega) \right)$$

Covariance part

$$S_{sdi}(\omega) = \sum_{j=1}^n \sum_{l=1}^{r_2} \sum_{m=1}^{r_2} \phi_{ij} A_{il} \left(-\frac{1}{\omega^2} \Gamma_{mj} H_j(\omega) \hat{S}_{lm}(\omega) \right)$$

where, n is the number of mode shapes chosen for evaluation and r_1 and r_2 are the numbers of nodal (away from support) and base PSD tables, respectively. The transfer functions for the single degree of freedom system can be computed in different forms depending on the type of the input and type of the response desired. The forms of the transfer functions for the displacement as an output are listed below for different inputs in Eq. (4.25) and (4.26).

- Force or acceleration as an input.

$$H_j(\omega) = \frac{1}{\omega_j^2 - \omega^2 + i(2\xi_i \omega_j \omega)} \quad (4.25)$$

- Velocity

$$H_j(\omega) = \frac{1}{\omega_j^2 - \omega^2 + i(2\xi_i \omega_j \omega)} \quad (4.26)$$

where, ω = forcing frequency and ω_j = natural circular frequency for the j^{th} mode and $i = \sqrt{-1}$. Also, random vibration analysis can be used to show that the absolute value of the mean square response of the i^{th} free displacement can be computed as in Eq. (4.27)

$$\sigma_{fi}^2 = \sigma_{di}^2 + \sigma_{si}^2 + 2C_v(U_{si}, U_{di}) \quad (4.27)$$

where, Re denotes the real part of the argument σ_{di} is the variance of the i^{th} relative (dynamic) free displacements and $C_v(U_{si}, U_{di})$ is the covariance between static and dynamic displacements. Finally one sigma displacement is calculated by using PSD random vibration analysis. The graph of unit standard deviation of the displacements against frequency for each frequency can be plotted using ANSYS POST26 post processor.

4.4 HARMONIC RESPONSE ANALYSIS

Harmonic response analysis is used to solve for the time dependent equations of motion for linear structures under steady state vibration [20]. In harmonic analysis, applied loads and displacements vary sinusoidally at the same known frequency but not necessarily in phase, there might be a phase lag between them. Damping is provided in the structure to cause a phase shift. Phase shift is a phenomenon in which displacements and loads have different phase angles.

4.4.1 FORMULATION

Consider the general equation of motion for a structural system with damping.

$$[M]\{\ddot{u}\} + [c]\{\dot{u}\} + [K]\{u\} = \{F^a\} \quad (4.28)$$

where, $[M]$ is structural mass matrix, $[c]$ is structural damping matrix, $[K]$ is structural stiffness matrix, $\{\ddot{u}\}$ is nodal acceleration vector, $\{\dot{u}\}$ is nodal velocity vector, $\{u\}$ is nodal displacement vector and $\{F^a\}$ is applied load vector. The displacements may be defined by Eq. (4.29).

$$\{u\} = \{u_{\max} e^{i\phi}\} e^{i\Omega t} \quad (4.29)$$

where, u_{\max} is the maximum displacement, i is $\sqrt{-1}$, Ω is imposed circular frequency in (radians/time), ϕ is the displacement phase shift. The u_{\max} and ϕ may be different at each degree of freedom and hence the complex notation allows compact and efficient description of the solution for Eq. (4.29) and it can be rewritten as under.

$$\{u\} = \{u_{\max} (\cos \phi + i \sin \phi)\} e^{i\Omega t} \text{ or } \{u\} = (\{U_1\} + i\{U_2\}) e^{i\Omega t} \quad (4.30)$$

where, $\{U_1\} = \{u_{\max} \cos \phi\}$ which is real displacement vector and $\{U_2\} = \{u_{\max} \sin \phi\}$ is the imaginary displacement vector component.

Also, the force vector can be described analogously to the displacement as under.

$$\{F\} = \{F_{\max} e^{i\psi}\} e^{i\Omega t} \text{ or } \{F\} = \{F_{\max} (\cos \psi + i \sin \psi)\} e^{i\Omega t} \quad (4.31)$$

$$\text{or } \{F\} = (\{F_1\} + i\{F_2\}) e^{i\Omega t} \quad (4.32)$$

where, F_{\max} is the force amplitude and ψ is force phase shift

$$\{F_1\} = \{F_{\max} \cos \psi\} \text{ is real force vector}$$

$\{F_2\} = \{F_{\max} \sin \psi\}$ is imaginary force vector

Substituting Eqns. (4.30) and (4.32) into Eq. (4.28) we get Eq. (4.33).

$$(-\Omega^2[M] + i\Omega[c] + [K])(\{U_1\} + i\{U_2\})e^{i\Omega t} = (\{F_1\} + i\{F_2\})e^{i\Omega t} \quad (4.33)$$

Canceling term $e^{i\Omega t}$ from both sides gives Eq. (4.34).

$$(-\Omega^2[M] + i\Omega[c] + [K])(\{U_1\} + i\{U_2\}) = (\{F_1\} + i\{F_2\}) \quad (4.34)$$

4.4.2 COMPLEX DISPLACEMENT OUTPUT

The complex displacement output at each degree of freedom may be given in one of two forms as

- In the complex form the real part and the imaginary part.
- In the form of amplitude and phase angle at each degree of freedom.

Nodal and Reaction Load Computation

Inertia, damping and static loads on the nodes of each element are computed as in Eq. (4.35).

$$\begin{aligned} \{F_1^m\}_e &= \Omega^2[M_e]\{U_1\}_e \\ \{F_2^m\}_e &= \Omega^2[M_e]\{U_2\}_e \end{aligned} \quad (4.35)$$

where, $\{F_1^m\}_e$, $\{F_2^m\}_e$ are real and imaginary part of vector of element inertia forces, $\{U_1\}_e$, $\{U_2\}_e$ are real and imaginary part of the element displacement vectors and $[M_e]$ is element mass matrix.

The real and imaginary damping loads part of the element output is computed by Eq. (4.36) as shown below.

$$\{F_1^c\}_e = -\Omega[C_e]\{U_2\}_e \text{ and } \{F_2^c\}_e = \Omega[C_e]\{U_1\}_e \quad (4.36)$$

where, $\{F_1^c\}_e$ is a vector of element damping forces (real part), $\{F_2^c\}_e$ is vector of element damping forces (imaginary part) and $[C_e]$ is element damping matrix. The real static load is computed the same way as in a static analysis using the real part of the displacement solution $\{U_1\}_e$. The imaginary static load is computed also the same way, using the imaginary part $\{U_2\}_e$. The nodal reaction loads are computed as the sum of all three types of loads (inertia, damping, and static) over all elements connected to a given fixed displacement node. There are three available methods for the solution of harmonic response analysis which are listed below.

- Full solution method.
- Reduced solution method
- Mode superposition method – used in this sensor simulation

4.4.3 MODE SUPERPOSITION METHOD

The mode superposition method uses the natural frequencies and mode shapes to characterize the dynamic response of a structure to transient or steady harmonic excitations. The equation of motion can be expressed as Eq. (4.37).

$$[M]\{\ddot{u}\} + [c]\{\dot{u}\} + [K]\{u\} = \{F\} \quad (4.37)$$

$$\{F\} = \{F^{nd}\} + s\{F^s\}$$

where, $\{F^{nd}\}$ are time varying nodal forces, $\{F^s\}$ are load vectors from the modal analysis and s is load vector scale factor. A set of modal coordinates y_i is defined as

$$\{u\} = \sum_{i=1}^N \{\phi_i\} y_i \quad (4.38)$$

Where, $\{\phi_i\}$ is the mode shape of mode i and n is the number of modes to be used in harmonic analysis. The inverse relationship does exist for the case where all the displacements are known, but not when only some are known. Substituting Eq. (4.38) into Eq. (4.37).

$$[M] \sum_{i=1}^N \{\phi_i\} \ddot{y}_i + [C] \sum_{i=1}^N \{\phi_i\} \dot{y}_i + [K] \sum_{i=1}^N \{\phi_i\} y_i = \{F\} \quad (4.39)$$

Premultiplying by a typical mode shape $\{\phi_j\}^T$ gives Eq. (4.40).

$$\{\phi_j\}^T [M] \sum_{i=1}^N \{\phi_i\} \ddot{y}_i + \{\phi_j\}^T [C] \sum_{i=1}^N \{\phi_i\} \dot{y}_i + \{\phi_j\}^T [K] \sum_{i=1}^N \{\phi_i\} y_i = \{\phi_j\}^T \{F\} \quad (4.40)$$

The orthogonal condition of the natural modes states that

$$\{\phi_j\}^T [M] \{\phi_i\} = 0 \text{ if } i \neq j$$

$$\{\phi_j\}^T [K] \{\phi_i\} = 0 \text{ if } i \neq j$$

In mode superposition method only Rayleigh or constant damping is allowed so that

$$\{\phi_j\}^T [C] \{\phi_i\} = 0 \text{ if } i \neq j$$

Applying these conditions into Eq. (4.40) gives us Eq. (4.41)

$$\{\phi_j\}^T [M] \{\phi_j\} \ddot{y}_j + \{\phi_j\}^T [C] \{\phi_j\} \dot{y}_j + \{\phi_j\}^T \{\phi_j\} [K] y_j = \{\phi_j\}^T \{F\} \quad (4.41)$$

The coefficient of \ddot{y}_j, \dot{y}_j and y_j are derived as under.

Coefficient of \ddot{y}_j : By the normality condition in Eq. (4.14)

$$\{\phi_j\}^T [M] \{\phi_j\} = 1 \quad (4.42)$$

Coefficient of \dot{y}_j : The damping term is based on treating the modal coordinate as a single degree of freedom system.

$$\{\phi_j\}^T [C] \{\phi_j\} = C_j \phi_j^2 \quad (4.43)$$

$$\{\phi_j\}^T [M] \{\phi_j\} = M_j \phi_j^2 = 1 \quad (4.44)$$

$$\text{From Eq. (4.44) } \phi_j = \frac{1}{\sqrt{M_j}} \quad (4.45)$$

And critical damping constant $C_j = 2\xi_j \sqrt{K_j M_j}$

Where, ξ_j is fraction of critical damping for mode j and ω_j is the natural circular

frequency of the mode j which can be stated as $\omega_j = \sqrt{\frac{K_j}{M_j}}$.

Combining Eqns. (4.44) and (4.43) with Eq. (4.48) gives Eq. (4.46)

$$\{\phi_j\}^T [C] \{\phi_j\} = 2\xi_j \sqrt{K_j M_j} \left(\frac{1}{\sqrt{M_j}} \right)^2 = 2\xi_j \omega_j \quad (4.46)$$

Coefficient of y_j

$[K] \{\phi_j\} = \omega_j^2 [M] \{\phi_j\}$ from Eq. (4.20) and premultiplying by $\{\phi_j\}^T$ gives Eq. (4.47).

$$[K] \{\phi_j\} \{\phi_j\}^T = \omega_j^2 [M] \{\phi_j\} \{\phi_j\}^T \quad (4.47)$$

Substituting Eq. (4.48) for the mass term

$$[K] \{\phi_j\} \{\phi_j\}^T = \omega_j^2$$

For convenient notations let $f_j = \{\phi_j\}^T \{F\}$

From this assumption the equation of motion of the modal coordinates can be written as in Eq. (4.48).

$$\ddot{y}_j + 2\omega_j \xi_j \dot{y}_j + \omega_j^2 y_j = f_j \quad (4.48)$$

Where, y_j is modal coordinate, ω_j is natural circular frequency of mode j , ξ_j is fraction of critical damping for mode j and f_j is force in modal coordinates. The displacement y_j must have the similar form as f_j .

$y_j = y_{jc} e^{i\Omega t}$ where, y_{jc} is complex amplitude of the modal coordinate for mode j .

$$-\omega_j^2 y_{jc} e^{i\Omega t} + 2\omega_j \xi_j (i\Omega y_{jc} e^{i\Omega t}) + \omega_j^2 y_{jc} e^{i\Omega t} = f_{jc} e^{i\Omega t}$$

Collecting coefficients of y_{jc} and dividing by $e^{i\Omega t}$

$$(-\Omega^2 + i2\omega_j \Omega \xi_j + \omega_j^2) y_{jc} = f_{jc}$$

$$y_{jc} = \frac{f_{jc}}{(-\Omega^2 + i2\omega_j \Omega \xi_j + \omega_j^2)} \quad (4.49)$$

The contribution from each mode is give by Eq. (4.50)

$$\{C_j\} = \{\phi_j\} y_{jc} \quad (4.50)$$

Where, $\{C_j\}$ is the contribution of mode j and $\{\phi_j\}$ is the mode shape for mode j .

The complex displacements output is calculated using Eq. (4.51).

$$\{u_c\} = \sum_1^N \{C_j\} \quad (4.51)$$

where, $\{u_c\}$ is the vector of complex displacements.

4.4.4 FREQUENCY SPACING AND FREQUENCY RESPONSE CURVE

In harmonic response analysis, the imposed frequencies that involve the most kinetic energy are those near the natural frequencies of the structure. The automatic frequency spacing provides an approximate method of choosing suitable imposed frequencies. The nearness of the imposed frequencies to the natural frequencies depends on damping, because the resonance peaks narrow when the damping is reduced. In our research the

frequency range we set was from 0 to 1600 Hz as we were mostly interested in that range. We had 100 steps but the range was not divided evenly. So we didn't get the records after each 160 Hz since it was not equally distributed. Instead we got the records in the default set values. Generally the frequency response curve obtained from this method must show resonance peaks and imposed frequencies chosen by this method which are computed from Eq. (4.52).

$$\Omega_{-j}^i = \frac{\omega_i}{a_{ij}}, \Omega_{+j}^i = \omega_i a_{ij}, a_{ij} = 1 + (\xi_i)^b \text{ and } b = \frac{2(N-j)}{N-1} \quad (4.52)$$

where, ξ is modal damping, N is integer ranging from 2 to 10 and $j = 1, 2, 3, \dots, 2N$.

The response of the structure is plotted against the frequency in ANSYS POST26 time history postprocessor which is shown in Fig. 4.1.

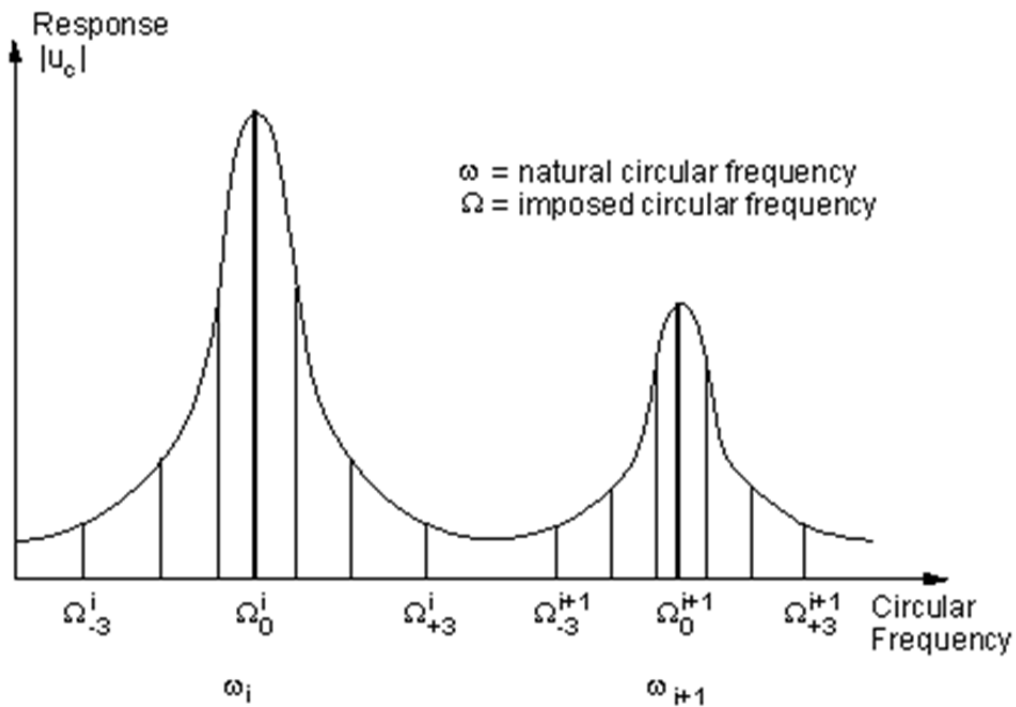


Figure 4.1: Harmonic Frequency Response Plot

CHAPTER V
PVDF CONSTITUTIVE PROPERTY
5.1 PIEZOELECTRICITY

5.1.1 INTRODUCTION

The piezoelectric effect was first discovered by Curie brothers in 1880 while studying the relationship between pyroelectric phenomenon and crystal symmetry [21]. They showed that crystals of tourmaline, quartz, topaz, cane sugar, and Rochelle salt (sodium potassium tartrate tetrahydrate) generate electrical polarization from mechanical stress. Quartz and Rochelle salt exhibited the most piezoelectricity.^[22] Twenty natural crystal classes exhibit direct piezoelectricity. Although most of the relationships between piezoelectricity and crystal structure were established by Curie brothers, Woldemar Voigt in 1894 took the relationship a step further. By combining the elements of symmetry of elastic tensors and of electric vectors with geometrical symmetry elements of the crystals, he explained and detailed 32 crystal classes in which piezoelectric effect could exist. Converse piezoelectricity was mathematically deduced from fundamental thermodynamic principles by Lippmann in 1881. The Curie brothers immediately confirmed the existence of the “converse effect” and established quantitative proof of the complete reversibility of

electro-elasto-mechanical deformations in piezoelectric crystals. The discovery that, the ceramic substance, barium titanate can be made piezoelectric by Polling, in 1947, was followed by the detection of the same effect in lead zirconate titanate (PZT) referred as a piezoelectric ceramic material and used for many applications.

5.1.2 MECHANISM

Piezoelectricity is a coupling between a material's mechanical and electrical behaviors. In short, when a piezoelectric material is squeezed, an electric charge collects on its surface. Conversely, when a piezoelectric material is subjected to a voltage drop, it mechanically deforms. Many crystalline materials exhibit piezoelectric behavior. A few materials exhibit the phenomenon strongly enough to be used in applications that take advantage of their properties. On a nanoscopic scale, piezoelectricity results from a nonuniform charge distribution within a crystal's unit cells. When such a crystal is mechanically deformed, the positive and negative charge centers displace by differing amounts. So while the overall crystal remains electrically neutral, the difference in charge center displacements results in an electric polarization within the crystal. Electric polarization due to mechanical input is perceived as piezoelectricity. Because the charges inside the crystal are separated, the applied voltage affects different points within the crystal differently, resulting in the distortion. The bending forces generated by converse piezoelectricity are extremely high, of the order of tens of millions of pounds (tens of meganewtons), and usually cannot be constrained. The only reason the force is usually not noticed is because it causes a displacement of the order of one billionth of an inch i.e. in the order of few nanometres.

5.1.3 APPLICATIONS

High voltage sources

- Direct piezoelectricity of some substances like quartz, generates thousands of volts known as high-voltage differentials.
- In an electric lighter, pressing the button squeezes piezoelectric crystal, and the high voltage is used to create a spark.

Sensors

- Piezoelectric elements are used in electronic drum pads to detect the impact of the drummer's sticks.
- To detect sound, e.g. piezoelectric microphones in which sound waves bend the piezoelectric material, creating a changing voltage.

Actuators

- Piezoelectric elements are used in the generation of sonar waves.
- Loudspeaker in which voltages are converted to mechanical movement of a piezoelectric polymer film.
- Piezoelectric motor: piezoelectric elements apply a directional force to an axle, causing it to rotate. Due to the extremely small distances involved, the piezo motor is viewed as a high-precision replacement for the stepper motor.

Frequency standards

- Quartz clocks employ a tuning fork made from quartz that uses a combination of both direct and converse piezoelectricity to generate a regularly timed series of electrical pulses that is used to mark time.

5.2 PolyVinylidene Fluoride (PVDF)

Some of the research work from 1970 has been reviewed in the past [23-26]. The electromechanical coupling of PVDF is lower than that of piezoceramic, but since the foil thickness can be as small as 10 micrometers the vibration mass is extremely small. PVDF also has greater damping than ceramics, and the resulting dynamic characteristics allow very short pulses to be generated. This means that it is possible to measure shorter ranges using PVDF than is possible with piezoceramic transducers.

5.2.1 STRUCTURE OF PVDF

PVDF is a semi crystalline polymer commercially available as powder, pellets or semi-transparent films. It has a melting temperature of approximately 170 °C and has reasonable melt viscosity suitable for melt processing without the need for processing aids, stabilizers or additives. The polymer can also be solution processed due to its solubility in common polar solvents (NMP, DMAc for example). The glass transition temperature is typically around -40 °C so that at room temperature the polymer is flexible with good mechanical properties. It consists of long chain of molecules with CH₂CF₂ as a repeating unit. The chemical structure of the PVDF is as shown in Fig. 5.1.

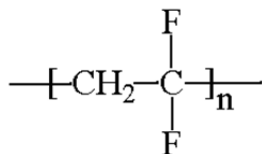


Figure 5.1: Structure of PVDF

PVDF can be obtained in crystalline form as well as in amorphous form. Presently four crystalline forms of PVDF are known as *I, II, III* and *II_p* or β, α, γ and $\alpha_p(\delta)$. The different crystal forms may be obtained from the melt or from solutions. PVDF films used for the sensors are often uniaxially or biaxially stretched. They are poled under tension to improve their mechanical and electrical properties since the molecular chains are oriented as a result of this. Commercially available PVDF film consists usually of the antipolar form *II* material. In order to make this material piezoelectric it has to go through different processes e.g. stretching annealing, thermal or corona polling and evaporation of electrodes etc. Because fluorine is so much more electronegative than carbon, the fluorine atoms will pull electrons away from the carbon atoms to which they are attached. This means the $-\text{CF}_2-$ groups in the chain will be very polar with a partial negative charge on the fluorine atoms and a partial positive charge on the carbon atoms. So when they're placed in an electrical field, they align. This causes the polymer sample to deform and all those $-\text{CF}_2-$ groups trying to align, produce what is known as polarization.

5.2.2 PVDF CONSTITUTIVE RELATIONSHIPS AND PHYSICAL PROPERTIES

Piezoelectricity is described mathematically within a material's constitutive equation, which defines how the piezoelectric material's stress T , strain S , charge-density displacement D , and electric field E interact. The piezoelectric constitutive relationships in the strain-charge form are given by Eqs. (5.1) and (5.2).

$$D = d \cdot T + \epsilon^T \cdot E \quad (5.1)$$

$$S = s^E \cdot T + d \cdot E \quad (5.2)$$

PVDF constitutive relationships in stress-charge form are given by (5.3) and (5.4).

$$T = c^E \cdot S - e^T \cdot E \quad (5.3)$$

$$D = e \cdot S + \epsilon \cdot E \quad (5.4)$$

where, T is the stress component, S is the strain component and E is the electric field component. In order to measure the electric displacement D or the strain S , both electric field intensity E and the stress T need to be specified. Mechanical and electrical boundary conditions must be specified when defining any physical quantity for PVDF. The relationship between the mechanical and electrical behavior of piezoelectric material is expressed in terms of their piezoelectric coefficients. The piezoelectric strain charge coefficient can be expressed as in Eq. (5.5).

$$d = \frac{D}{T^E} = \frac{S}{E^T} \quad (5.5)$$

where, D is the induced electric displacement or charge density, T is the applied stress, S is the induced strain, E is the applied electric intensity and the superscripts E and T represents the boundary condition that maintains the constant electric field and constant stress field respectively. The relationship between the mechanical and electrical behavior of piezoelectric material is expressed in terms of their piezoelectric coefficients such as piezoelectric strain/charge constant d and or piezoelectric strain/voltage constant g .

$$g = \frac{E}{T^D} \quad (5.6)$$

The relationship between strain/charge constant d and strain/voltage constant g is given by Eq. (4.7).

$$d = g \cdot \epsilon^T \quad (5.7)$$

The piezoelectric parameter which relates the stored mechanical energy to the total stored energy within a piezoelectric material is the electromechanical coupling coefficient k which can be expressed as in Eq. (5.8).

$$k^2 = gdc^E \quad (5.8)$$

Where, c^E is the elastic modulus matrix, also called as elastic stiffness matrix of the material. The d constant value for the PVDF is considerably smaller and g constant value is higher than the other piezoelectric materials such as PZT, Quartz etc. Since in actuator or transducer applications the strain is proportional to the d constant and the field, the maximum strain achievable with PVDF actuator is ten times larger than that of the ceramic systems. Generally, the higher the value of g constant, the better it is to use that material for sensor or receiver. This strongly suggests that it is better to use PVDF as a sensor than an actuator. However one drawback of the PVDF is its relatively poor electrical stability which is due to the stress relaxation, or simply relaxation, which is defined as a material's stress response to an applied constant strain input. This makes long term measurements of weak signals somewhat problematic. Also the service temperature of PVDF is limited to $80^\circ C$. In summary, PVDF differs from the conventional piezoelectric materials and has some advantages such as flexibility, ruggedness, softness, lightness, and relatively low acoustic impedance. PVDF thus offers a good alternative in many applications. More specifically, since PVDF is available in the form of thin films of large sheets, it is not expensive to produce and easy to cut or shape into complex configurations and can be integrated into existing structures as a distributed or integrated sensor/ actuator.

5.3 PVDF constitutive matrices

The compliance matrix $[S]$ and stiffness matrix $[c]$ for PVDF in IEEE notation can be written in the form of Young's modulus and Poison's Ratio as under.

$$[C] = \begin{bmatrix} \lambda + 2\mu & \lambda & \lambda & 0 & 0 & 0 \\ \lambda & \lambda + 2\mu & \lambda & 0 & 0 & 0 \\ \lambda & \lambda & \lambda + 2\mu & 0 & 0 & 0 \\ 0 & 0 & 0 & \mu & 0 & 0 \\ 0 & 0 & 0 & 0 & \mu & 0 \\ 0 & 0 & 0 & 0 & 0 & \mu \end{bmatrix} \quad (5.9)$$

$$[S] = \begin{bmatrix} 1/Y & -\nu/Y & -\nu/Y & 0 & 0 & 0 \\ -\nu/Y & 1/Y & -\nu/Y & 0 & 0 & 0 \\ -\nu/Y & -\nu/Y & 1/Y & 0 & 0 & 0 \\ 0 & 0 & 0 & 2(1+\nu)/Y & 0 & 0 \\ 0 & 0 & 0 & 0 & 2(1+\nu)/Y & 0 \\ 0 & 0 & 0 & 0 & 0 & 2(1+\nu)/Y \end{bmatrix} \quad (5.10)$$

where, $\lambda = \nu Y / [(1 + \nu)(1 - 2\nu)]$ and $\mu = Y / [2(1 + \nu)]$.

Table 5.1: Physical Constants for the PVDF Film

Parameter	Value	Units
Thickness, h_s	50	μm
Mass density, ρ	1.8	Kg/m^3
Young Modulus, E	2.5E9	N/m^2
Strain/charge constants, d_{31}	6E-12	C/N
Strain/charge constants, d_{32}	-15.0E-12	C/N
Relative permittivity, ep_{33}	1700	F/m
Poison's Ratio ν	0.34	

The constitutive matrices used by the 2-D model are adjusted to orient the PVDF polarization direction along the Y axis for axisymmetric models. Using the PVDF properties listed in Table 5.1, the above two matrices for the PVDF can be calculated and rewritten in Eqs. (5.11) and (5.12).

$$[c] = \begin{bmatrix} 3.848 & 1.982 & 1.982 & 0 & 0 & 0 \\ 1.982 & 3.848 & 1.982 & 0 & 0 & 0 \\ 1.982 & 1.982 & 3.848 & 0 & 0 & 0 \\ 0 & 0 & 0 & 0.9328 & 0 & 0 \\ 0 & 0 & 0 & 0 & 0.9328 & 0 \\ 0 & 0 & 0 & 0 & 0 & 0.9328 \end{bmatrix} e^9 N/m^2 \quad (5.11)$$

$$[S] = \begin{bmatrix} 4 & -1.36 & -1.36 & 0 & 0 & 0 \\ -1.36 & 4 & -1.36 & 0 & 0 & 0 \\ -1.36 & -1.36 & 4 & 0 & 0 & 0 \\ 0 & 0 & 0 & 10.72 & 0 & 0 \\ 0 & 0 & 0 & 0 & 10.72 & 0 \\ 0 & 0 & 0 & 0 & 0 & 10.72 \end{bmatrix} e^{-10} m^2/N \quad (5.12)$$

By using the piezoelectric strain coefficients and permittivity value for the PVDF the strain matrix $[d]$ and dielectric permittivity matrix $[e]$ in IEEE notations can be written as under in Eqs. (5.13) and (5.14). The IEEE standards are maintained in constitutive relationships which ANSYS uses to calculate results. The ANSYS actually use $[d]^T$ or $[e]^T$ as strain matrix and stress matrix respectively while calculations.

$$[d] = \begin{bmatrix} 0 & 0 & 0 & 0 & 0 & 0 \\ 6 & -15 & 6 & 0 & 0 & 0 \\ 0 & 0 & 0 & 0 & 0 & 0 \end{bmatrix} e^{-12} C/N \quad (5.13)$$

$$[e] = \begin{bmatrix} 1e^{14} & 0 & 0 \\ 0 & 1700 & 0 \\ 0 & 0 & 1e^{14} \end{bmatrix} F/m \quad (5.14)$$

CHAPTER VI
MULTIPHYSICS MODELING & SIMULATION AND
EXPERIMENTAL RESULTS

This chapter summarizes the multiphysics modeling and simulation technique in stepwise manner. ANSYS elements, analyses formulations are described in Chapter III and Chapter IV respectively. The process is carried out using ANSYS parametric design language (APDL) which is an important tool in multiphysics modeling is briefly described. Multiphysics modeling technique for the structure of sensor bonded to the structures & contact generation technique for bonding the sensor on the structures are presented too for both generic and shaped piezoelectric films. Techniques for creating the structure, specifying material properties, and specifying boundary conditions are also specified. Along with random vibration analysis technique, the procedure for processing ANSYS displacements results in MATLAB is discussed. It also describes the process of providing a way to calculate the output charge of a thin piezoelectric film bonded to different structures. The experimental setups, procedures and results for all the structures along with the comments are described at the end of this chapter before conclusion & future scope.

6.1 ANSYS Parametric Design Language (APDL)

ANSYS Parametric Design Language is a scripting language that can be used to automate common tasks or to build FEA model in terms of parameters or variables. APDL also includes a wide range of other features such as repeating a command, macros, if-then-else branching, do-loops, and scalar, vector and matrix operations. While APDL is the foundation for sophisticated features such as design optimization and adaptive meshing, it also offers many conveniences that can be used in day-to-day analyses. APDL can be widely used in variety of applications in advanced multiphysics analyses. All the commands for APDL are taken from Multiphysics Analysis Guide [16]. APDL can be used to define any variables or arrays which are used in the parametric function for modeling. Also in APDL, controlling of the output by writing output file and applying time varying load is possible by looping. Thus APDL plays an important role in ANSYS multiphysics.

6.2 Multiphysics Modeling

Sensor Modeling

The shape of the sensor strip is based on parametric equation which can be modeled using ANSYS APDL code. The sensor shape is a parametric function of two variables x and y . Eq. (6.1) is used to plot the sensor area in MATLAB.

$$F(x) = k(x^2 - lx) \quad (6.1)$$

The reduction factor α is calculated to fit the sensor in desired beam width. MATLAB code for plotting sensor area is as under where b is the width of the beam, hb is beam

thickness, h_s is sensor thickness, e_{31} is piezoelectric stress charge coefficient and L is the length of the beam. α is calculated in Matlab, which comes to be 0.2667.

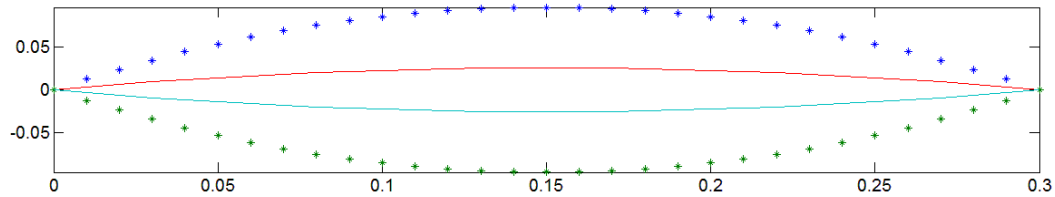


Figure 6.1: Sensor Shape MATLAB Plot [Solid Line(Desired Shape) Star(Actual Shape)]

Using the APDL code in APPENDIX A the sensor area created in ANSYS required for this simulation. APDL code follows stepwise general procedure for creation of the sensor volume.

1. Assigning of the required variables in the parametric equation.
2. Define the array for data storage.
3. Define a separate array parameter for each loop.
4. Define the parametric equation in loop.
5. Creation of the KEYPOINTS in a coordinate system using parametric equation.
6. Line creation using created adjacent KEYPOINTS using a loop.
7. Repeat the procedure using separate loop for each curve if required.
8. Merge all the KEYPOINTS created using APDL code.
9. Arbitrary area creation by selecting different loops created by lines.

Using Boolean operation, the sensor area is extruded to create a sensor volume having desired thickness which is $50\mu m$ thin PVDF sensor used for this simulation.

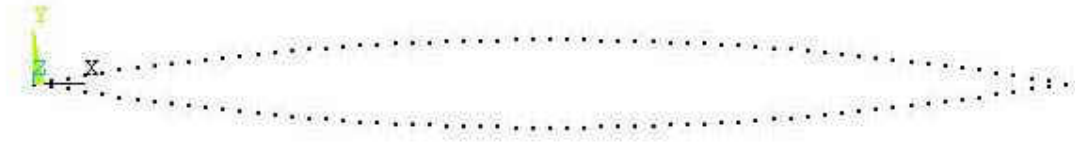


Figure 6.2: Keypoint Creation Using APDL Code



Figure 6.3: Line Plot Using APDL Code

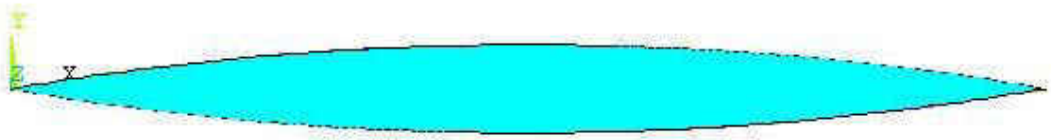


Figure 6.4: Sensor Area Creation in ANSYS

This sensor area is then extruded using Boolean operation to create a sensor volume as shown in Fig. 6.5.

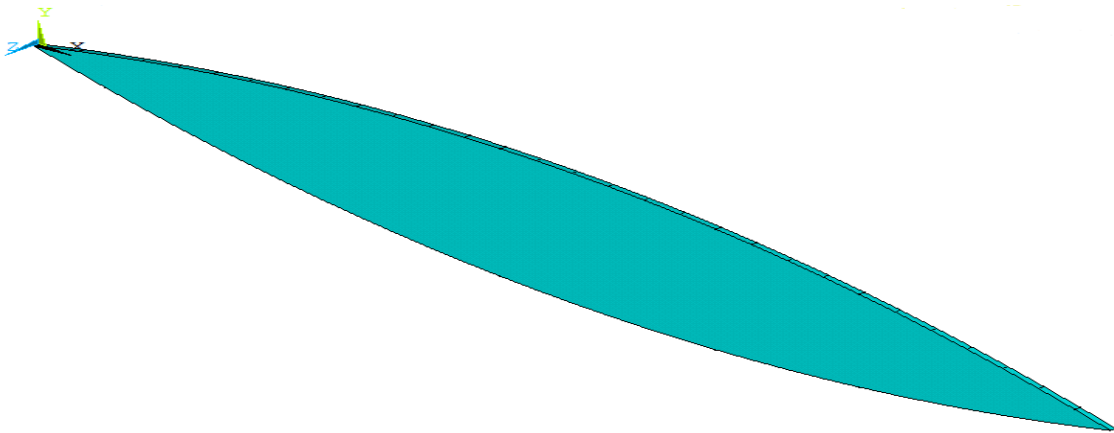


Figure 6.5: 50 μm Thick Sensor Volume

Sensor Material Properties

Sensor Material: PolyVinylidene Fluoride (PVDF)

PVDF constitutive matrices from Eqs. (5.12), (5.13) and (5.14) and Density ρ from Table 6.1 are entered as Material 1 properties.

Sensor Element Type and Meshing

SOLID 227 element with piezoelectric option is selected to mesh sensor volume. Due to complex shape of the sensor strip, sensor volume is free meshed as shown by Fig. 6.6. For uniform meshing the global size of the element is set to 10 in size control menu.

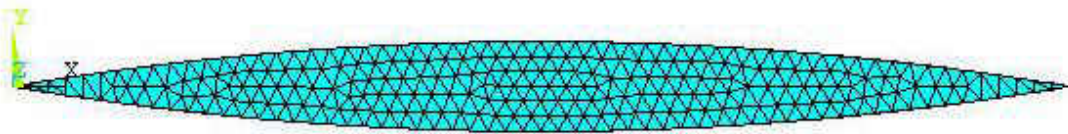


Figure 6.6: Meshed Sensor Volume

The next step in multiphysics modeling is modeling of aluminum beam below the sensor which is described as under.

Beam Area Modeling and Material Properties

Beam area is created below the sensor volume. Material properties and physical constants for aluminum beam are entered according to Table 6.1 as Material 2.

Table 6.1: Geometrical and Material Properties for Aluminum Beam

Parameter	Value	Units
Length, L_x	0.3	m
Width, L_y	0.0508	m
Thickness, h_b	0.003175	m
Mass density, ρ	2700	Kg / m^3
Young's modulus, E	70E9	N / m^2
Poisson ratio, ν	0.33	-

Beam Element Type and Meshing

SHELL63 element as described in Chapter III is selected for aluminum beam. Real constant set for beam element for thickness is entered. Beam area is meshed with 30 elements along the length and 10 elements along the width which is shown by Fig. 6.7 below.

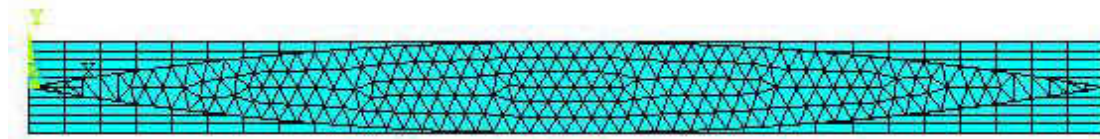


Figure 6.7: Meshed Aluminum Beam and Sensor Volume

After meshing of beam and sensor the contact is generated between bottom area of the sensor volume and beam area by following ANSYS GUI contact generation procedure which is briefly described in next step.

6.3 Contact Generation

Contact problems are highly nonlinear and require significant computer resources to solve. It is important to understand the physics of the problem and take the time to set up FEA model to run as efficiently as possible. Contact problems present two significant difficulties. First, we generally do not know the regions of contact until running the problem. Depending on the loads, material, boundary conditions, and other factors, surfaces can come into and go out of contact with each other in a largely unpredictable and abrupt manner. Second, most contact problems need to account for friction. There are several friction laws and models to choose from, and all are nonlinear. Frictional response can be chaotic, making solution convergence difficult. In addition to these two difficulties, many contact problems must also address multi-field effects, such as the

conductance of heat, electrical currents, and magnetic flux in the areas of contact. If we neglect friction in FEA model, and the interaction between the bodies is always bonded, may be able to use the internal multipoint constraint (MPC) feature (available for certain contact elements) to model various types of contact assemblies and surface-based constraints. By this method, the program builds MPC equations internally based on the contact kinematics. This method can be used to create shell-solid contact assembly in which the contact surface pastes onto shell element faces and the target surfaces paste onto solid element faces. The 3-D shell-solid assembly provides a transition from a shell element region to a solid element region. This approach is useful when local modeling requires a full three-dimensional model with a relatively fine mesh, but other parts of the structure can be represented by shell elements. No alignment is required between the solid element mesh and the shell element mesh.

ANSYS automatically creates an internal set of force-distributed constraints between nodes on the shell edges and nodes on the solid surface. The program uses the pinball region (PINB), initial adjustment zone (ICONT), and influence distance (FTOLN) to determine which nodes on the shell edge will be constrained with which nodes on the solid surface. Each shell node acts as the master node, and associated solid nodes act as slave nodes. For the “bonded always” option, any shell node that lies inside the pinball region (PINB) will be included in the constraint if an intersection with the target surface is detected in the contact normal direction. This holds true at the beginning of deformation, as well as during the deformation process. A relatively small PINB value may be used to prevent any false contact. The default for PINB is 0.25 (25% of the contact depth) for small deformation analysis, and 0.5 (50% of the contact depth) for

large deformation analysis. The shell-solid assembly is usually used for the case where the solid mesh is fine with respect to the shell thickness. The shell-solid interface should be located in a region of the structure where shell theory is valid for an approximation.

In this multiphysics simulation always bonded, flexible and surface to surface contact is created between SHELL63 elements on the beam area and SOLID227 elements on the bottom area of the sensor volume. Beam area is selected as a target surface and sensor bottom area is selected as a contact surface for this SHELL-SOLID contact assembly. A contact pair selected automatically by ANSYS program, which includes CONTA174 element and TARGE170 element as described in Chapter III. While creating a contact pair Material 3 is created as a contact material. Fig. 6.8 shows SHELL- SOLID contact assembly. The contact type selection and contact generation plays a vital role in any multiphysics simulation. We have written commands in the ANSYS command prompt for creating the contact pair.

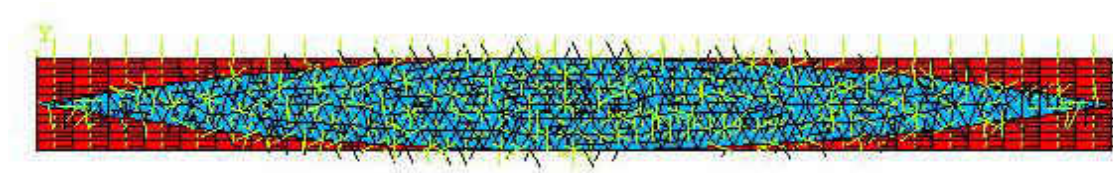


Figure 6.8: Shell-Solid Bonded Contact Assembly

Boundary Conditions

To satisfy cantilevered boundary conditions for the beam the left side of the beam area are constrained in all degrees of freedom (ALL DOF's). Fig 6.9 shows boundary conditions on FEA model.

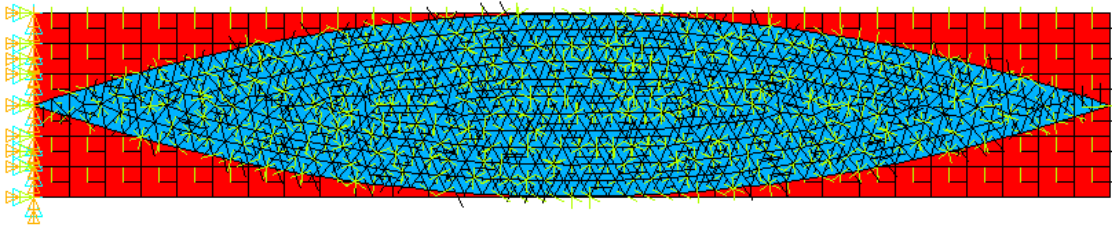


Figure 6.9: Cantilevered Aluminum Beam with Bonded Sensor

6.4 Multiphysics Simulation

To achieve the objective of the research PSD single point random vibration analysis is carried out in specific analyses sequence to study the dynamic frequency response of the structure to the displacement of the beam, plate, cylindrical shell and the sensor output charge. The sequence of the consecutive analyses types used for this simulation includes Mode Frequency Analysis, PSD Spectrum Analysis and Harmonic analysis. These analyses types and their formulations are briefly presented in Chapter IV.

6.4.1 Mode Frequency Analysis

It is free vibration analysis which gives the natural frequencies and mode shapes of the structure. It is usually done before PSD spectrum analysis. For nonlinearity and achieving solution convergence, the convergence limits are set in this coupled field mode frequency analysis by CNVTOL command for electric charge. Also, the behavior of the output charge developed due to piezoelectric effect can be animated for each mode of vibration.

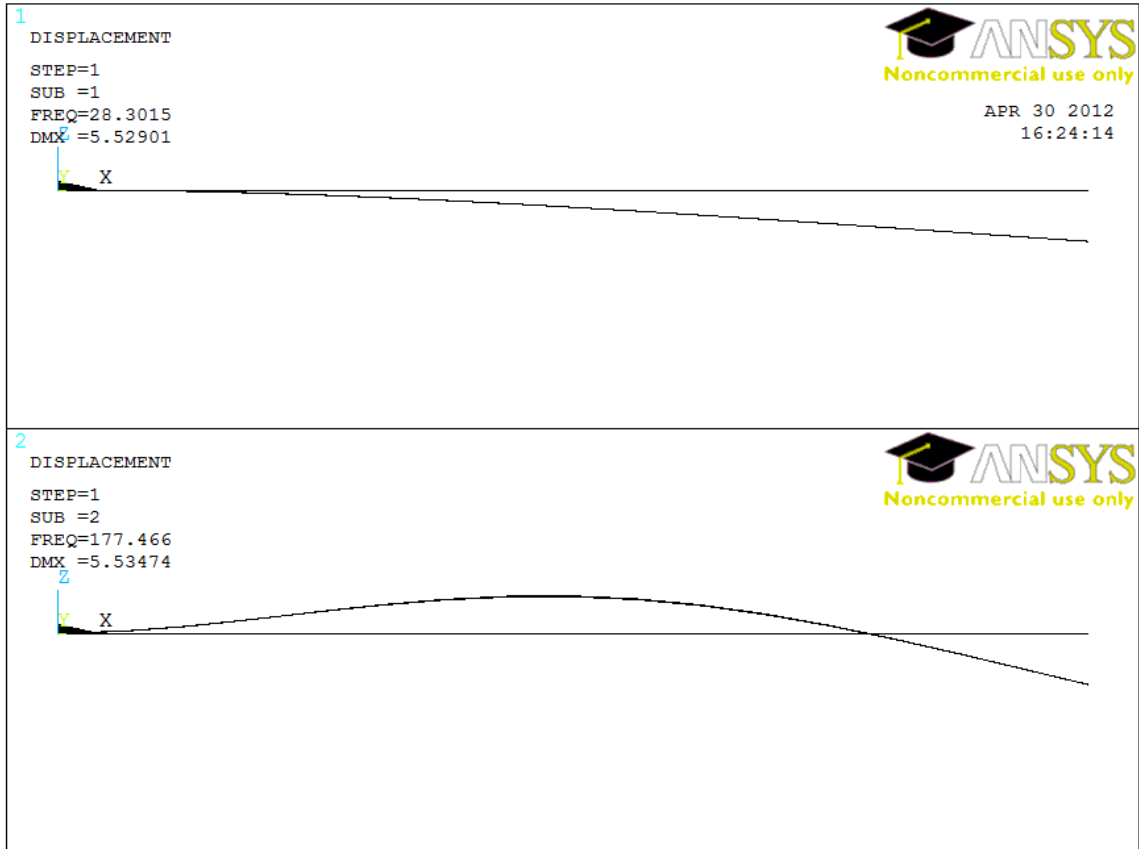


Figure 6.10: First Two Mode Shapes of the Bonded Structure

The first two natural frequencies and Mode shapes of the FEA structure are shown in Fig. 6.10 having 28.3015 Hz and 177.466 Hz as first and second natural frequencies respectively. In mode frequency analysis, first 6 modes are extracted and expanded with element stress calculations option ON. The modes are given in the table below.

Table 6.2: The Value of the First 6 Modes in ANSYS

Mode number	Value (Hz)
1	28.301
2	177.47
3	333.23
4	442.53
5	499.58
6	986.64

6.4.2 Single Point PSD spectrum Random Vibration Analysis

After modal analysis reentering into the solution menu and selecting Spectrum analysis type gives the probable nodal displacement results due to the single point force applied on the bottom of the beam. Modes are combined to achieve the desired results using power spectral density mode combination method in this analysis. First 6 significant modes are selected to calculate element stresses. A force of 600N is applied on the node of the structures acting upwards in our case. A different value for the force could also be applied as it was a single point random excitation. Also, this analysis is used to calculate one sigma peak displacement results.

6.4.3 Harmonic Response Analysis

Harmonic Response Analysis is carried out after the Spectrum Analysis to calculate the harmonic response of the structure to a single point randomly varying force. The damping of 0.02 is set for harmonic analysis to introduce the phase shift. The mode superposition method sums factored mode shapes obtained from a modal analysis to calculate the harmonic response. Also, frequency response of the structure, transfer functions can be plotted using ANSYS POSTPROCESSOR26. ANSYS writes all the results of the harmonic analysis in binary file *.rfrq in complex format. This binary file contains all the complex displacement data and complex voltage data for all the nodes for each frequency. ANSYS code which is used to run this simulation is attached as an APPENDIX A in this dissertation.

As after each analysis an ANSYS output binary file named reduced complex displacement file which is also known as *.rfrq file is automatically created in the default drive of the computer where the program was run. This information can be imported in Matlab, which requires this data to be in text (ASCII) form. It is possible to recall it by using the ANSYS DUMP command as it converts the binary data into ASCII data. The nodal displacements are listed in ascending node order and then in ascending frequency. The ANSYS DUMP command is found in the GUI under Main Menu> List> Files> Binary Files, while choosing All Records to be listed and Entire Record of output per record. The file 'file.rfrq' is selected, creating the 'DUMP.txt' file. This file contains all the complex displacement for the beam for each node at each frequency. This is then used in MATLAB for further processing.

6.5 Graphs, Results & Figures

6.5.1 Procedure

The results we got in this section fits our objective as we took all the necessary steps one after another to reach our goal. First the structures were modeled using ANSYS, and the simulation was performed to find the displacement field. A series of analyses were carried out in a specific sequence in order to study the dynamic frequency response of the structures. The sequence of the analyses was Mode Frequency Analysis, Single Point PSD Spectrum Analysis, and Harmonic Response Analysis. Mode Frequency analysis was used for natural frequency and mode shape determination. In this analysis, the first few modes were expanded and extracted within a specified frequency range, then were written to the results file. The next step after mode frequency analysis was to perform a

spectrum analysis. The spectrum analysis was preceded by a mode-frequency analysis, because a structure's mode shapes and frequencies must be available to calculate the spectrum solution. Also, by performing the spectrum solution before mode expansion, only the significant modes that contributed to the final solution were expanded. In this step the results of a modal analysis were used with a known spectrum to calculate displacements in the model. The spectrum was a graph of spectral values versus frequency that captured the intensity and frequency content of time-history loads. In our case the value was displacement. The model was excited with a force and the modal responses were combined using power spectral density mode combination method. Lastly, a displacement solution output is written to the results file from the PSD analysis. The third analysis was harmonic response using the mode superposition method option which summed factored mode shapes to calculate the harmonic response. In a structural system, any sustained cyclic load produces a sustained cyclic or harmonic response. Harmonic response analysis gave the ability to predict the sustained dynamic behavior of structures, thus gave the ability to verify whether or not the design was successful to overcome resonance, fatigue, and other harmful effects of forced vibrations. It calculated only the steady-state, forced vibrations of a structure. The transient vibrations, which occurred at the beginning of the excitation, were not accounted in this analysis. This analysis calculated the response of the structure to cyclic loads over a frequency range and obtained a graph of displacements versus frequency. The harmonic output option to print complex displacements as real and imaginary components was turned on, whereas the cluster option was turned off for uniform spacing of frequency solutions. The results were written in ANSYS output binary file in *.rfrq format. Those binary files contained

all the displacement data for all the nodes at each frequency interval. Then the ANSYS displacement results are read in MATLAB for further processing to calculate the output charge of the sensor.

Two things were calculated using MATLAB to plot the graphs. One was the charge which was for the sensors and the other thing was the displacement which was for the metallic structures. Usually a number of sets of records were obtained in each case. The frequency range was not distributed among the exact equal intervals. Fourteen different components were found for each node. We were interested with the third and fourth or the fifth or sixth components which were the real and imaginary parts of the displacements in the Y and Z direction respectively depending on the direction of the applied force & we were also interested in the thirteenth and fourteenth components which were respectively the real and imaginary parts of the voltages. For calculating the charge first all the real parts of the voltage for a specific record were summed. Then all the imaginary parts of the voltage for that record were also added. Hence with these two components one complex number was got. Finally, the absolute value of that complex number was the charge with respect to that particular frequency of that record. In the other hand for calculating displacement, instead of adding the displacements of all nodes any random node of the structure was selected. Then a complex number was made with the real and imaginary part of the displacement of that node. And finally the absolute value of that complex number was the displacement of that node with respect to that particular frequency of that record. The MATLAB processing of the ANSYS data results in the final plots are shown below.

6.5.2 Comments on the results

The results for beam that is plotted in figure 6.11 and figure 6.14 indicates that sensor output captures the behavior of the structures for both the generic and shaped case as far as the modes are concerned. But in case of plate results which are plotted in figure 6.12 and in figure 6.15 gives a little bit of inaccuracy. One reason for this was meshing. If we could have used finer mesh the results would have been more accurate. At first we used a coarse mesh and then kept making it finer. We have noticed after running several computations that by increasing the number of nodes, the precision of the results can be increased as the resolution increases which decreases the amount of errors in numeric computing. We have observed the change in the results as the sensor was capturing the results more correctly. But since in case of plate as the number of nodes were already too high, so it was not possible to keep increasing it after a certain point as ANSYS was not able to mesh it. We can describe the shell results which are plotted in figure 6.13 and 6.16 by the same explanation as the plate results. The frequency range we used was from 0 to 1600 Hz for all the above cases as we were concerned about the first few modes. So we can summarize that the proposed method can be applied to calculate the output charge of films attached to complex structures or structures with complex boundary conditions. This can also be applied in cases where close form equations cannot be derived and the only data available are discrete or experimental. Moreover, in sensor design applications where the film is often shaped so that its output charge corresponds to a specific structural dynamic property, the proposed method greatly simplifies the design process.

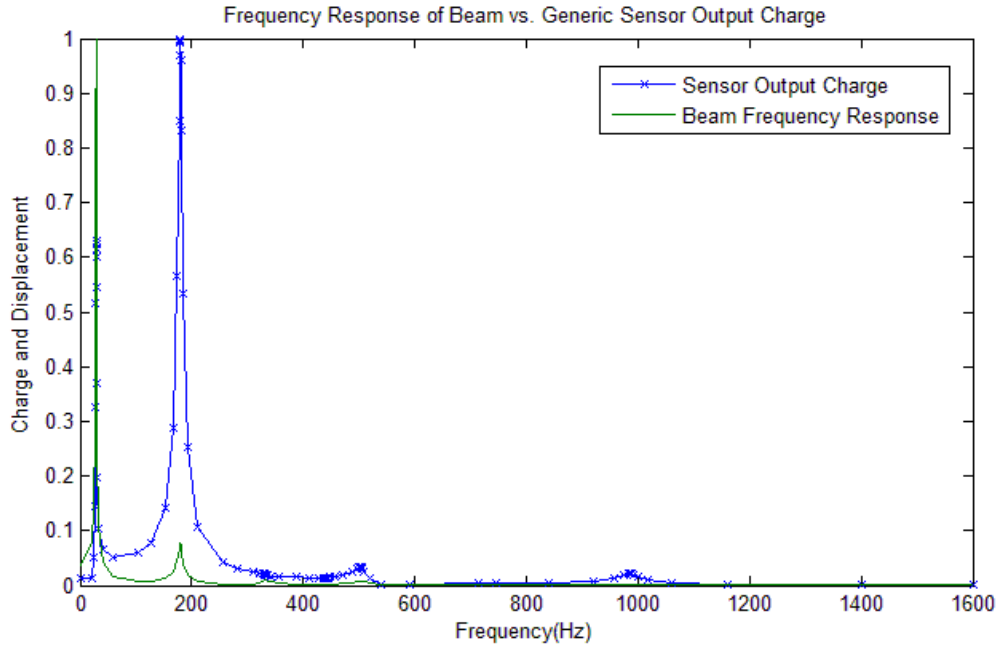


Figure 6.11: Frequency Response of Beam vs. Generic Sensor Output Charge

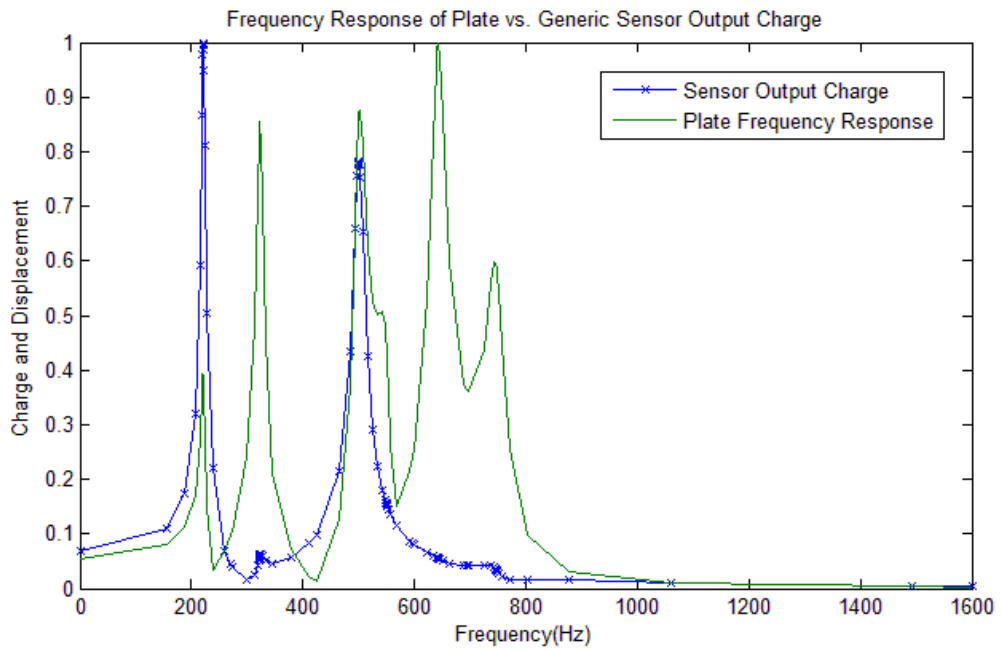


Figure 6.12: Frequency Response of Plate vs. Generic Sensor Output Charge

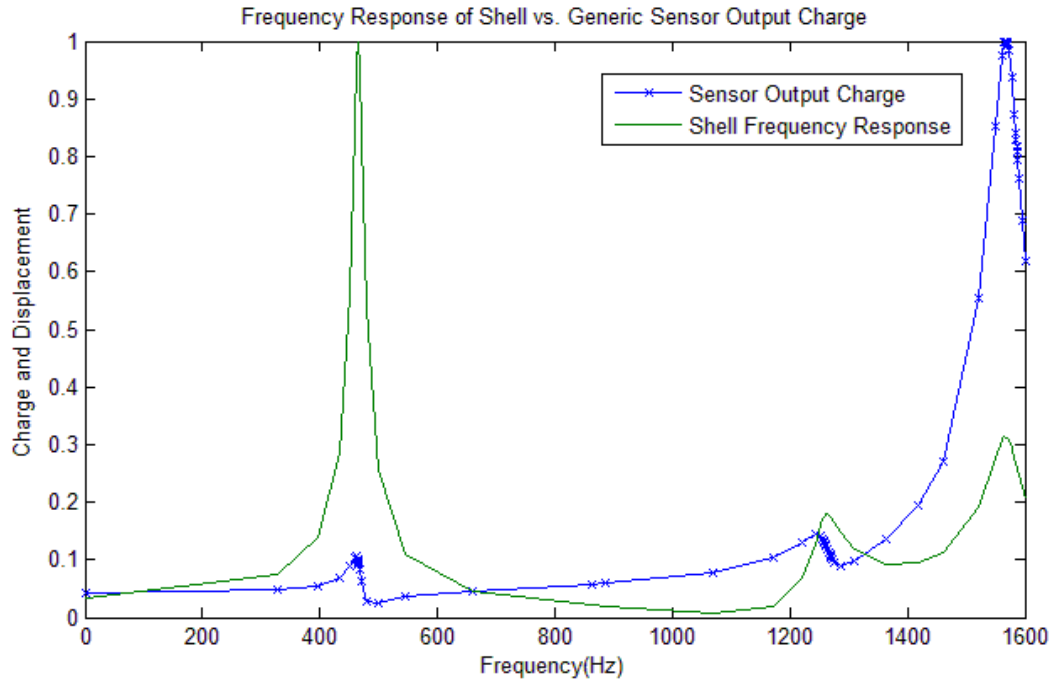


Figure 6.13: Frequency Response of Shell vs. Generic Sensor Output Charge

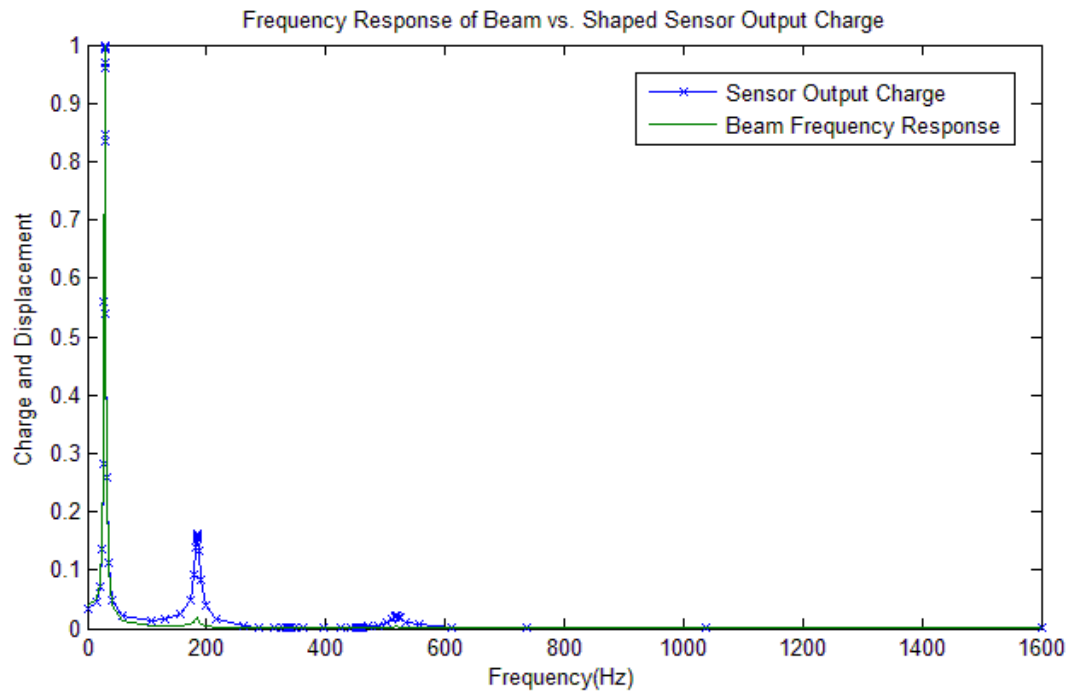


Figure 6.14: Frequency Response of Beam vs. Shaped Sensor Output Charge

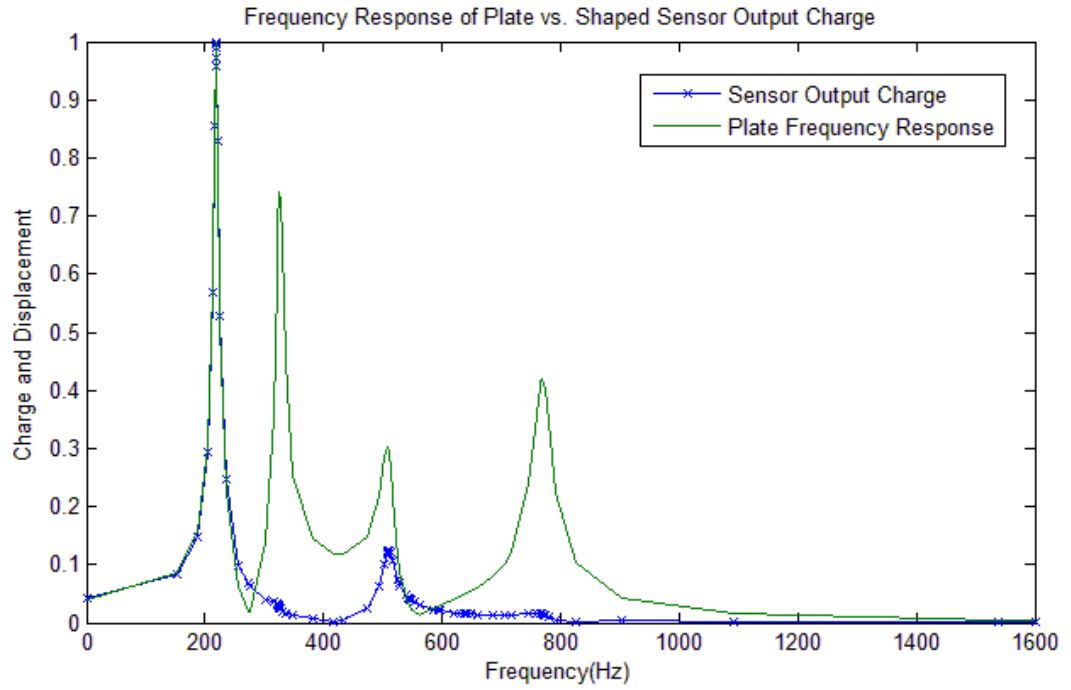


Figure 6.15: Frequency Response of Plate vs. Shaped Sensor Output Charge

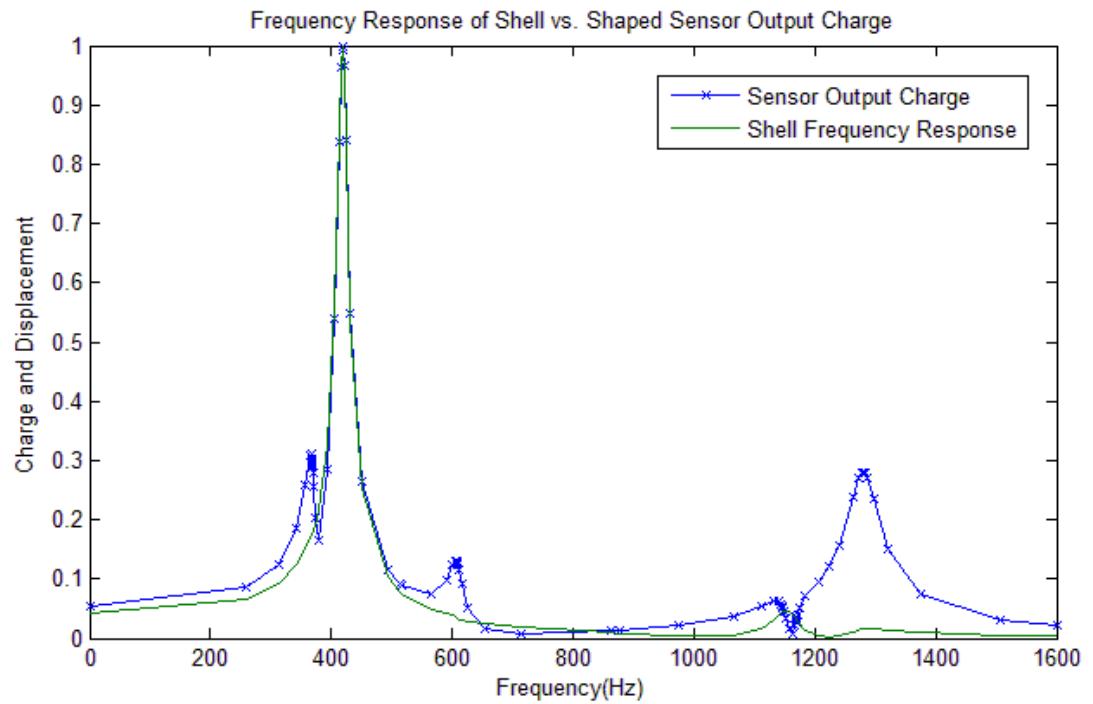


Figure 6.16: Frequency Response of Shell vs. Shaped Sensor Output Charge

6.6 Experimental Setup, Procedures & Results

6.6.1 Experimental Setup

In our case the beam was cantilevered. The length of the beam was 0.3 meter, the width was 0.0508 m and the thickness was 0.00317 meter. We can see in figure 6.17 that the beam was mounted between two circular metallic discs and tightened through nuts and bolts. To get the experimental results different equipment were introduced in our case. We can see from figure 6.18 and figure 6.21 that a Dynamic Signal Analyzer (DSA) Agilent 35670A has been used. An amplifier was connected with the source of the DSA through wiring. This connected the DSA source with the input of an amplifier. A shaker was connected with the output of the amplifier. A force gauge was placed on the top of the shaker.



Figure 6.17: Side View of the Cantilevered Beam Setup



Figure 6.18: The Experimental Setup for the Beam with Sensor on Top

For all the cases the height of the shaker along with the force gauge was manipulated in such a way that the tip of the force gauge just touched the structure. This was a very tricky adjustment because if there was no contact between the force gauge and the structure the measurement would have been wrong. Also if the proximity was in such a way that the structures couldn't vibrate properly after striking by the force gauge the measurement would have given error in the result. An accelerometer was put on the structures which was a PCB Piezotronics Inc. Model U353B03. Both the force gauge and the accelerometer was connected with PCB outputs. When the sensors were bonded with the structures, accelerometers were used for the measurement. For getting the results for PVDF we cut the sensor in such a way that there was an extended portion of the sensor which was directly connected to the PCB through wiring. We have used two sided glues to put the sensors on the structures. One side of the glue was stuck with the structure and the other side of the glue was stuck with sensor. The input of the PCBs were connected with the DSA through the channels. After all the connections have been made we started the whole setup to get the results. In our case the plate was all end fixed. The length of the plate was 0.6 meter, the width was 0.3 m and the thickness was 0.00317 meter. We can see from figure 6.19 that the plate was placed on a metallic platform and was fixed through screws.



Figure 6.19: The Experimental Setup for the All End Fixed Plate



Figure 6.20: Top View of the Experimental Setup of the Cantilevered Pipe

We were having difficulty when we tried to run the experiments for the shell as we didn't had any specific setup for that. But after thinking about it in different ways we ended up

getting a good solution of our problem. As we can see from figure 6.20 and figure 6.21 that we have used the beam setup for the shell experiment. But we used an aluminum block, drilled a hole inside it with the same diameter as of the outside diameter of our shell. After making the hole in the center of the block we cut the block in half in two identical pieces. Then we put the shell between the pieces and mounted the whole thing between the circular metallic disc. We tightened the entire thing afterwards.



Figure 6.21: The Experimental Setup for the Pipe with Sensor on Top

6.6.2 Procedures

The purpose of the experiments were to determine the frequency response of the structures with the sensors attached to them. We have got the natural frequencies of the first few modes of the structures and produced amplitude & phase versus frequency plots.

To get the frequency response we put the DSA in FRF mode:

- 1) To initialize the analyzer we did the following steps.

Press [**Preset**] [DO PRESET].
Press [**Active Trace**] [A B]
Press [Avg ON OFF] to highlight ON
Press [Number of Avg] type 25 [Enter]
Press [**Meas Data**] [FREQ RESP 2/1].

2) We have connected the device-under-test (DUT) as shown in the illustration below.

3) To specify the measurement parameters we did the following steps.

Press [**Freq**] [START] <number> <unit>
Press [STOP] <number> <unit>.

4) To configure the display we did the following steps.

Press [**Trace Coord**] [X-AXIS LIN LOG] to highlight LIN.
Press [Freq] [Span] [1.6 KHz]
Press [**Active Trace**] [B].
Press [**Trace Coord**] [PHASE].
Press [**Active Trace**] [A B].
Press [**Scale**],
Press [AUTOSCALE ON OFF] to highlight ON.

5) To measure the device under test we did the following steps.

Press [Random Noise]
Press [Level]
Select [1 Vpk]
Press [**Source**] on
Press [Amp]
Press [**Avg.**]
Press [Avg. on],
Press [Marker]
Press [Next left peak]
Press [Next right peak]

In this stage we were able to read the peak values. In our case the peak values were the natural frequencies of the structures. We wrote all the peak values for our record. To get these results in the computer we connected a computer with our setup and did the following steps.

6) Press [**Basic**]
Press Instrument Basic
Press [**Utilities**]
Press Memory Size
Select 9000
Press Secure
Press Perform Secure

Press [**Active Trace**] [A B]
 Press [**Save/Recall**]
 Press [Save Data]
 Press [Format ASCII]
 Press [Save Trace]
 Press [Into file] type the file name
 Press [Enter]
 Press Refresh List
 Press Transfer Files To PC

After this step we have got the folders that were created in our computer which consisted files that we used in MATLAB to draw the figures. We have used four files for each cases. All of them were text files. Two of them consisted the whole frequency range from 0 to 1600 Hz. Another one consisted all the amplitude values within the frequency range and the other one consisted all the phase values within the frequency range. First the files were opened and then they were read in MATLAB. After that they were transferred from the output files to MATLAB arrays to plot the graphs. We have kept frequencies in the x axis and kept corresponding amplitude & phase values in the y axis respectively for our drawing. The whole procedure was same for both the measurements of the accelerometer and the PVDF since they have produced the same type and amount of files.

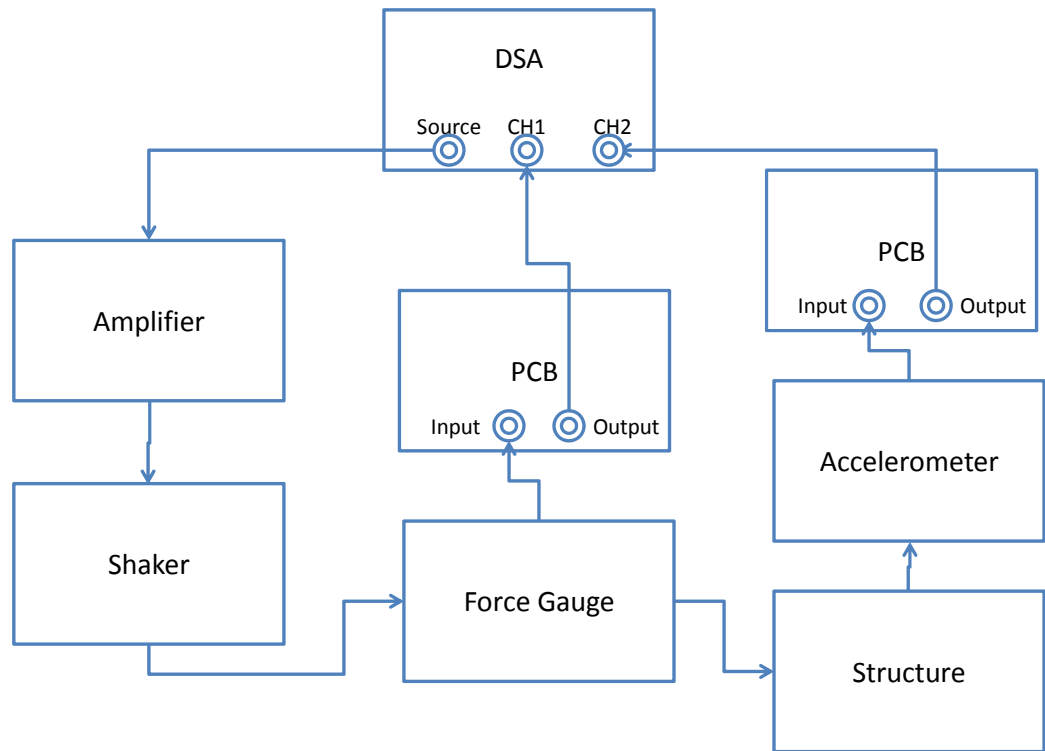


Figure 6.22: The Block Diagram for Getting the Results with Accelerometer

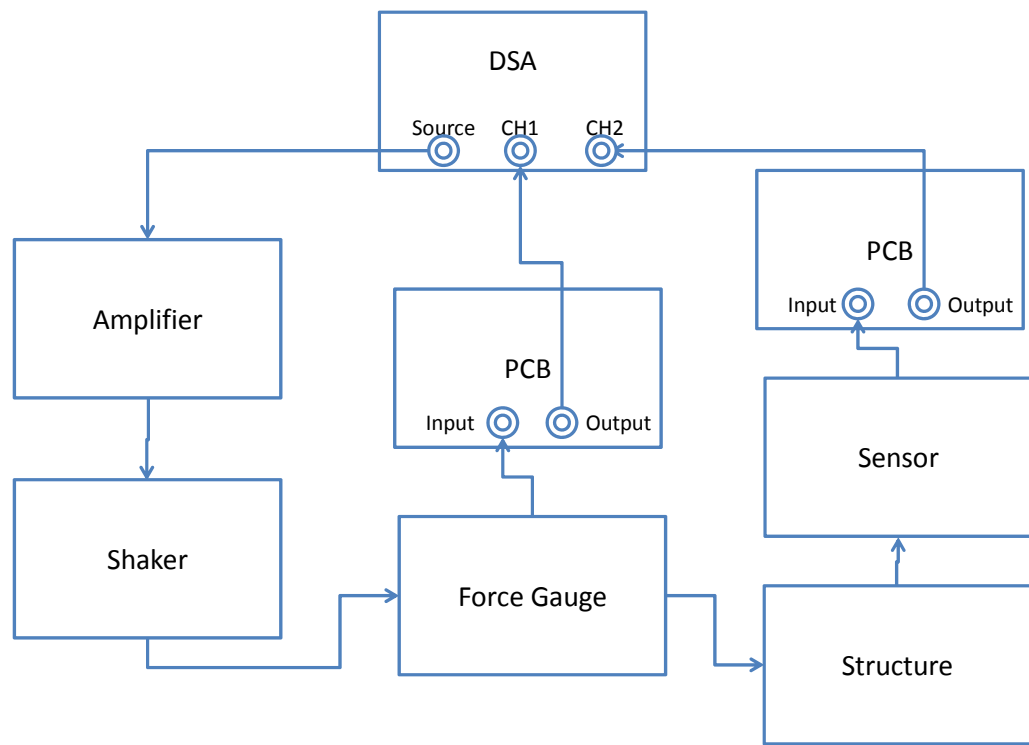


Figure 6.23: The Block Diagram for Getting the Results with PVDF

6.6.3 Results

Comments on the results

We did the measurement and recorded the results for single point for all the structures since the results were almost the same with respect to the position of the accelerometer. There was no specific points for putting the accelerometer. For both the beam and the shell we put the accelerometer in a position near the clamped end and for the plate we put the accelerometer almost in the middle of it. There were reasons that occurred the error in the results. One reason was the sensors were very difficult to put on the top surface of the structures. It was one of the most challenging things to do. Usually it needs a great amount of expertise to do it perfectly. The misplacement of the sensor on the structures had a great influence which resulted inaccuracy of the results. As we can see from figure 6.24 through figure 6.27 that the precision of the results reduced due to the shift of the sensor along the length of the structures that exhibited both phase and magnitude errors [32]. Since there were some air bubbles trapped between the sensor and the structure so it had an impact on the results too. One more reason for error in our result is we commonly assume that there is no air friction if the objects are not moving fast. In reality even though that friction is small but not equal to zero. Moreover, inaccuracy of the measuring equipment involved was an additional source of error. Another reason for the error was due to the limitations and simplifications of the experimental procedures. Uncontrolled changes to the environment such as small changes of the temperature and the humidity in the lab was a possible source of error too.

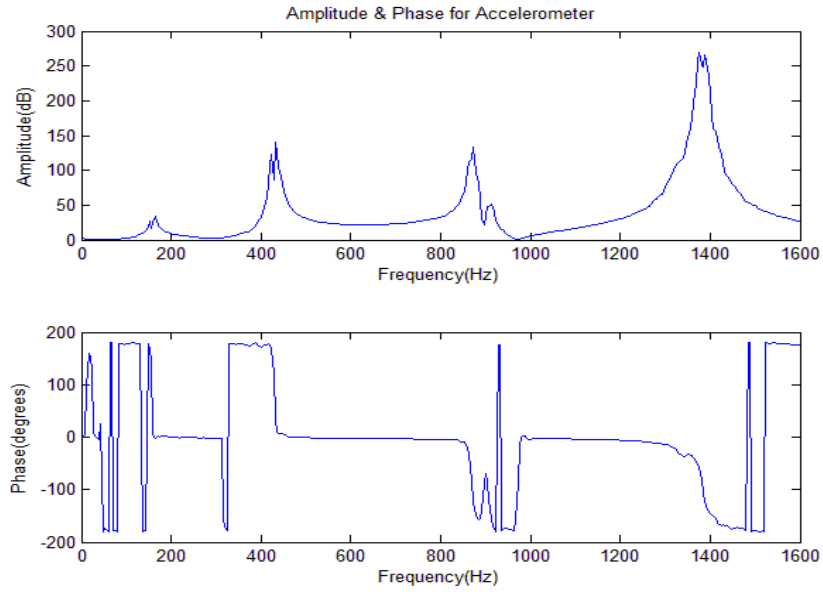


Figure 6.24: Accelerometer Reading for the Cantilevered Beam with Sensor on Top

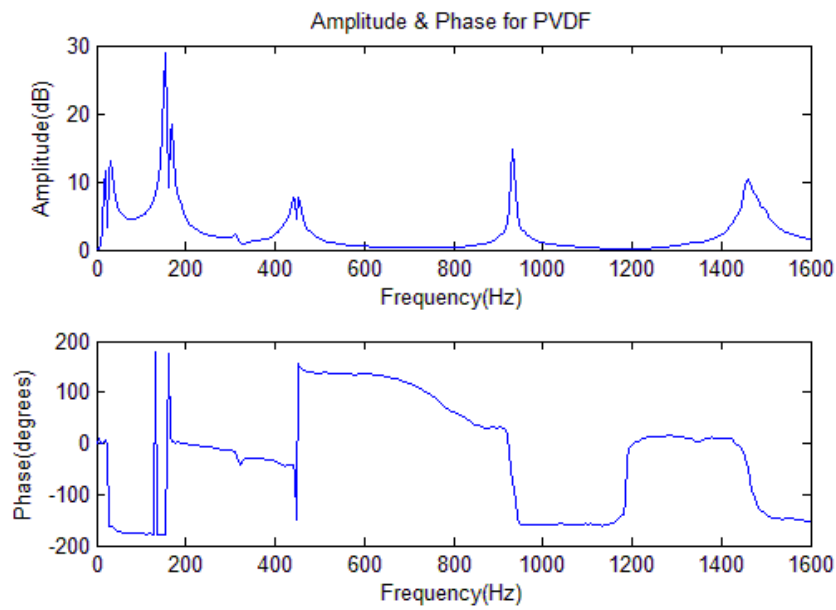


Figure 6.25: PVDF Reading for the Cantilevered Beam with Sensor Bonded on Top

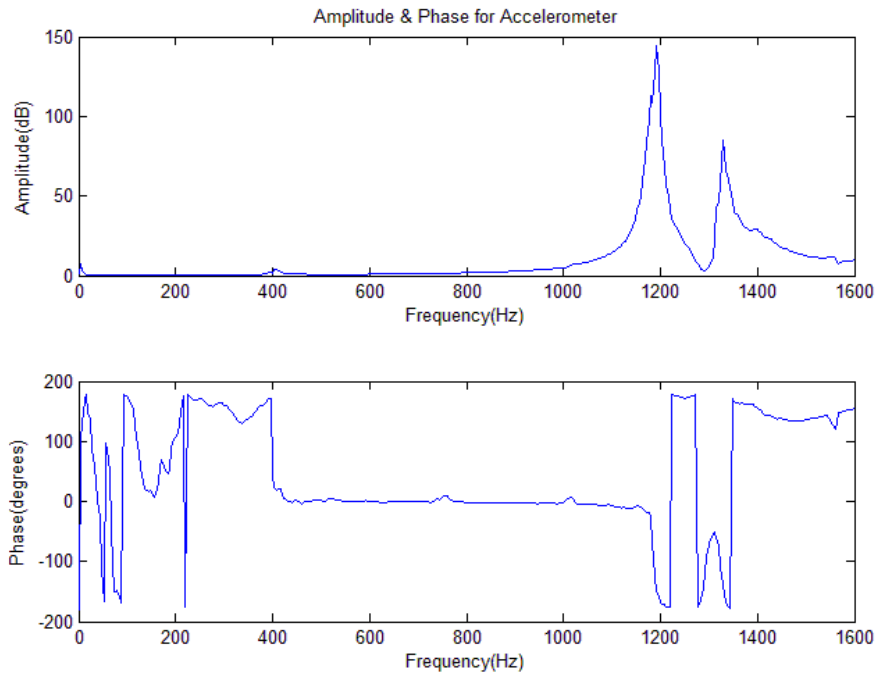


Figure 6.26: Accelerometer Reading for the Cantilevered Shell with Sensor on Top

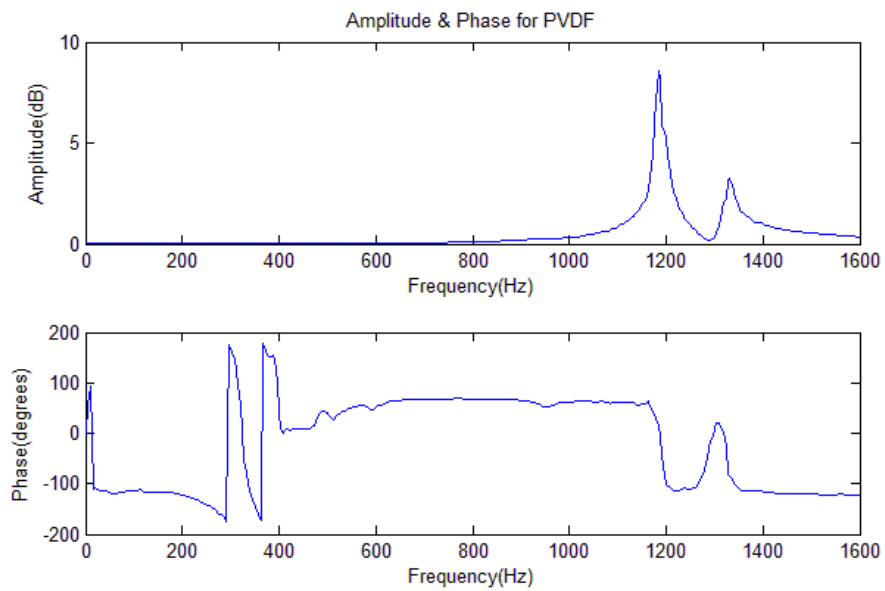


Figure 6.27: PVDF Reading for the Cantilevered Shell with Sensor Bonded on Top

6.7 Conclusion & Future Scope

This project is a perfect combination of computational, theoretical and experimental works. It is an excellent blend as both 2D and 3D structures are incorporated here. Our work shows that finite element method (ANSYS) along with MATLAB can be used in order to measure the frequency response of the structures and to calculate the output charge of the thin piezoelectric film bonded to different structures. In our case, we have applied this method for beam, plate and cylindrical shell for both the generic and shaped piezoelectric film. This method can also be used in the cases where the required input variables such as film shape and vibration profile of structures are in discontinuous form. Hence, experimentally obtained input variables can be used with the above described method to calculate the piezoelectric film output charge and in this manner a sensor can be designed for desired output. Even though the results that we got from the experiments were not exactly the same and there was an amount of error present but they were pretty consistent with the ANSYS results. We tried to run our experiments as accurately as possible but there were always chances of inaccuracies that existed. Some of them were inherent in nature so it was almost impossible for us to skip them. Due to the time constraints and the lack of significant amount of literature the theoretical analysis for all the structures were not possible but it could be an ideal project for another graduate student to continue work in the future. Another obvious step after the simulation of the structures and finding the output charge of their sensors would be to develop an actuator and use it in the same control system as the sensor. But performing an experiment afterwards is necessary for the verification of the findings. It is also possible to extend the applied method to more complex structures such as arches.

APPENDICES

APPENDIX A

ANSYS INPUT LOG FILE FOR MULTIPHYSICS SIMULATION

ANSYS APDL CODE FOR SENSOR SHAPE CREATION

```
/PREP7
```

```
hb=0.003175
```

```
hs=50e-6
```

```
e31=1.861
```

```
b=0.0508
```

```
k=-b/(2*(hb+hs)*e31)
```

```
*DIM,Y,ARRAY,10000
```

```
L=0.3
```

```
I=1
```

```
*DO,x,0,L,0.01
```

```
Y(I)=0.2667*(k*(x*x-L*x))
```

```
K,I,x,Y(I),0,
```

```
I=I+1
```

```
*ENDDO
```

```
var1 =0.3/0.01
```

```
*DO,I,1, var1, 1
```

```
LSTR, I, I+1
```

```

*ENDDO

*DIM,YY,ARRAY,10000

LL=0.3

II=32

*Do,xx,LL,0,-0.01

YY(II)=-0.2667*(k*(xx*xx-LL*xx))

K,II,xx,YY(II),0,

II=II+1

*ENDDO

var2 =30+0.3/.01

*Do,II,31,var2+1, 1

LSTR, II, II+1

*ENDDO

```

**ANSYS INPUT LOG FILE FOR MULTIPHYSICS SIMULATION FOR BEAM
TOTALLY COVERED WITH SENSOR**

```

/PREP7
!*
! SENSOR PROPERTIES

MPTEMP,,,,,,,,
MPTEMP,1,0
MPDATA,DENS,1,,1.8
TB,PIEZ,1,,1
TBMODIF,1,1,
TBMODIF,1,2,
TBMODIF,1,3,6e-12
TBMODIF,2,1,
TBMODIF,2,2,
TBMODIF,2,3,-15e-12

```

TBMODIF,3,1,
 TBMODIF,3,2,
 TBMODIF,3,3,6e-12
 TBMODIF,4,1,
 TBMODIF,4,2,
 TBMODIF,4,3,
 TBMODIF,5,1,
 TBMODIF,5,2,
 TBMODIF,5,3,
 TBMODIF,6,1,
 TBMODIF,6,2,
 TBMODIF,6,3,
 TB,ANEL,1,1,21,1
 TBTEMP,0
 TBDATA,,4e-10,-1.36e-10,-1.36e-10,0,0,0
 TBDATA,,4e-10,-1.36e-10,0,0,0,4e-10
 TBDATA,,0,0,0,10.72e-10,0,0
 TBDATA,,10.72e-10,0,10.72e-10,,
 MPTEMP,,,,,,,,
 MPTEMP,1,0
 MPDATA,PERX,1,,1e14
 MPDATA,PERY,1,,1e14
 MPDATA,PERZ,1,,1700

 /NOPR
 /PMETH,OFF,1
 KEYW,PR_SET,1
 KEYW,PR_STRUC,1
 KEYW,PR_THERM,0
 KEYW,PR_FLUID,0
 KEYW,PR_ELMAG,1
 KEYW,MAGNOD,0
 KEYW,MAGEDG,0
 KEYW,MAGHFE,0
 KEYW,MAGELC,1
 KEYW,PR_MULTI,1
 KEYW,PR_CFD,0
 /GO
 !/COM,
 !/COM,Preferences for GUI filtering have been set to display:
 !/COM, Structural
 !/COM, Electric
 ET,1,SOLID227,1001
 KEYOPT,1,1,1001
 /prep7
 *SET,hb,0.00315

```

*SET,hs,50e-6
*SET,e31,1.861
*SET,b,0.0508
*SET,L,0.3048
RECTNG,,0.3048,-0.0254,0.0254,

! DEFINE SENSOR AREA AND THICKNESS
LSEL,ALL
AL,ALL
VOFFST,1,50e-6, ,

! MESH SENSOR
ESIZE,0.01,0,
MSHKEY,0
MSHAPE,0,3d
VSEL,ALL
VMESH,ALL

ET,2,SHELL63
R,1,hb
MPTEMP,,,,,,,,
MPTEMP,1,0
MPDATA,EX,2,,70e9
MPDATA,PRXY,2,,0.33
MPDATA,DENS,2,,2700
RECTNG,,0.3048,-0.0254,0.0254,
!MESH BEAM
TYPE,2
MAT,2
REAL,1
ESYS,0
SECNUM,
ESIZE,0.01,0,
MSHKEY,0
MSHAPE,0,3d
ASEL,A,AREA,,7
AMESH,7

!/COM, CONTACT PAIR CREATION - START
CM,_NODECM,NODE
CM,_ELEMCM,ELEM
CM,_KPCM,KP
CM,_LINECM,LINE
CM,_AREACM,AREA
CM,_VOLUCM,VOLU
!/GSAV,cwz,gsav,,temp

```


MP,MU,3,
MAT,3
MP,EMIS,3,7.88860905221e-031
R,3
REAL,3
ET,3,170
ET,4,CONTA 174
R,3,,1.0,0.1,0,
RMORE,,,1.0E20,0.0,1.0,
RMORE,0.0,0,1.0,,1.0,0.5
RMORE,0,1.0,1.0,0.0,,1.0
KEYOPT,4,1,5
KEYOPT,4,2,0
KEYOPT,4,4,0
KEYOPT,4,5,0
KEYOPT,4,7,0
KEYOPT,4,8,0
KEYOPT,4,9,0
KEYOPT,4,10,1
KEYOPT,4,11,0
KEYOPT,4,12,0

KEYOPT,3,5,0

! Generate the target surface
ASEL,S,,,7
CM,_TARGET,AREA
TYPE,3
NSLA,S,1
ESLN,S,0
ESURF,ALL
CMSEL,S,_ELEMCM
! Generate the contact surface
ASEL,S,,,1
CM,_CONTACT,AREA
TYPE,4
NSLA,S,1
ESLN,S,0
ESURF,ALL
*SET,_REALID,3
ALLSEL
ESEL,ALL
ESEL,S,TYPE,,3
ESEL,A,TYPE,,4
ESEL,R,REAL,,3
!/PSYMB,ESYS,1

```
! /PNUM,TYPE,1
! /NUM,1
! EPLOTT
ESEL,ALL
ESEL,S,TYPE,,3
ESEL,A,TYPE,,4
ESEL,R,REAL,,3
CMSEL,A,_NODECM
CMDEL,_NODECM
CMSEL,A,_ELEMCM
CMDEL,_ELEMCM
CMSEL,S,_KPCM
CMDEL,_KPCM
CMSEL,S,_LINECM
CMDEL,_LINECM
CMSEL,S,_AREACM
CMDEL,_AREACM
CMSEL,S,_VOLUCM
CMDEL,_VOLUCM
! /GRES,cwz,gsav
CMDEL,_TARGET
CMDEL,_CONTACT
! /COM, CONTACT PAIR CREATION - END
! /MREP,EPLOTT
! EPLOTT
FINISH
```

```
/SOL
FLST,2,2,4,ORDE,2
FITEM,2,4
FITEM,2,9
DL,P51X, ,ALL,
FLST,2,2,4,ORDE,2
FITEM,2,12
FITEM,2,16
DL,P51X, ,ALL,
```

```
/SOLU
ANTYPE,2
MSAVE,0
MODOPT,LANB,6
EQSLV,SPAR
MXPAND,6, , ,1
LUMPM,0
PSTRES,0
MODOPT,LANB,6,0,1600, ,OFF
```

CNVTOL,AMPS,1,1.E-8
SOLVE
FINISH

/POST1
SET,LIST
/SOLU
ANTYPE,SPECTR ! DEFINE ANALYSIS TYPE
SPOPT,PSD,6,ON ! USE FIRST 6 MODES, CALC ELEM. STRESSES
PSDUNIT,1,FORCE ! DEFINE TYPE OF PSD AS A FORCE SPECTRUM
DMPRAT,0.0005
F,2800,FZ,-600
PSDFRQ,1,1,1.0,1600.0
PSDVAL,1,1.0,1.0 ! IN N**2/HZ
PFACT,1,NODE
PSDRES,DISP,REL
PSDCOM
SOLVE
FINISH

/POST1
SET,3,1 ! ONE SIGMA DISPLACEMENT SOLUTION RESULTS
/VIEW,1,2,3,4
PLNSOL,U,Z
PRNSOL,U,Z
FINISH

/SOLUTION
ANTYPE,HARMIC ! REDEFINE ANALYSIS TYPE AND SOLVE AGAIN
HROPT,MSUP ! USING MODE SUPERPOSITION HARMONIC
 ANALYSIS
HROUT,OFF,ON ! PRINT AMPLITUDE & PHASE, CLUSTER
 FREQUENCIES
KBC,1
HARFRQ,1,1600
DMPRAT,0.02
NSUBSTEP,100
SOLVE
FINISH

/POST26
FILE,,rfrq
PRCPLX,1
NSOL,2,2800,U,Z
PSDDAT,6,1,1.0,80,1.0
PSDTYP,2

PSDCAL,7,2
PSDPRT
PRVAR,2,7
*GET,P,VARI,7,EXTREM,VMAX
*status,parm

ANSYS INPUT LOG FILE FOR MULTIPHYSICS SIMULATION FOR PLATE

TOTALLY COVERED WITH SENSOR

/PREP7
!*

! SENSOR PROPERTIES

MPTEMP,,,,,,,,
MPTEMP,1,0
MPDATA,DENS,1,,1.8
TB,PIEZ,1,,1
TBMODIF,1,1,
TBMODIF,1,2,
TBMODIF,1,3,6e-12
TBMODIF,2,1,
TBMODIF,2,2,
TBMODIF,2,3,-15e-12
TBMODIF,3,1,
TBMODIF,3,2,
TBMODIF,3,3,6e-12
TBMODIF,4,1,
TBMODIF,4,2,
TBMODIF,4,3,
TBMODIF,5,1,
TBMODIF,5,2,
TBMODIF,5,3,
TBMODIF,6,1,
TBMODIF,6,2,
TBMODIF,6,3,
TB,ANEL,1,1,21,1
TBTEMP,0
TBDATA,,4e-10,-1.36e-10,-1.36e-10,0,0,0
TBDATA,,4e-10,-1.36e-10,0,0,0,4e-10
TBDATA,,0,0,0,10.72e-10,0,0
TBDATA,,10.72e-10,0,10.72e-10,,
MPTEMP,,,,,,,,
MPTEMP,1,0

MPDATA,PERX,1,,1e14
MPDATA,PERY,1,,1e14
MPDATA,PERZ,1,,1700

/NOPR
/PMETH,OFF,1
KEYW,PR_SET,1
KEYW,PR_STRUC,1
KEYW,PR_THERM,0
KEYW,PR_FLUID,0
KEYW,PR_ELMAG,1
KEYW,MAGNOD,0
KEYW,MAGEDG,0
KEYW,MAGHFE,0
KEYW,MAGELC,1
KEYW,PR_MULTI,1
KEYW,PR_CFD,0
/GO
!/COM,
!/COM,Preferences for GUI filtering have been set to display:
!/COM, Structural
!/COM, Electric

ET,1,SOLID227,1001
KEYOPT,1,1,1001
/prep7
*SET,hb,0.004762
*SET,hs,50e-6
*SET,e31,1.861
*SET,b,0.381
*SET,L,0.6096
RECTNG,,0.6096,-0.1905,0.1905,

! DEFINE SENSOR AREA AND THICKNESS
LSEL,ALL
AL,ALL
VOFFST,1,50e-6, ,

! MESH SENSOR
ESIZE,0.02,0,
MSHKEY,0
MSHAPE,0,3d
VSEL,ALL
VMESH,ALL

ET,2,SHELL63

```

R,1,hb
MPTEMP,,,,,,,,
MPTEMP,1,0
MPDATA,EX,2,,70e9
MPDATA,PRXY,2,,0.33
MPDATA,DENS,2,,2700
RECTNG,,0.6096,-0.1905,0.1905,
!MESH BEAM
TYPE,2
MAT,2
REAL,1
ESYS,0
SECNUM,
ESIZE,0.01,0,
MSHKEY,0
MSHAPE,0,3d
ASEL,A,AREA,,7
AMESH,7

!/COM, CONTACT PAIR CREATION - START
CM,_NODECM,NODE
CM,_ELEMCM,ELEM
CM,_KPCM,KP
CM,_LINECM,LINE
CM,_AREACM,AREA
CM,_VOLUCM,VOLU
!/GSAV,cwz,gsav,,temp
MP,MU,3,
MAT,3
MP,EMIS,3,7.88860905221e-031
R,3
REAL,3
ET,3,170
ET,4,CONTA 174
R,3,,,1.0,0.1,0,
RMORE,,,1.0E20,0.0,1.0,
RMORE,0.0,0,1.0,,1.0,0.5
RMORE,0,1.0,1.0,0.0,,1.0
KEYOPT,4,1,5
KEYOPT,4,2,0
KEYOPT,4,4,0
KEYOPT,4,5,0
KEYOPT,4,7,0
KEYOPT,4,8,0
KEYOPT,4,9,0
KEYOPT,4,10,1

```

KEYOPT,4,11,0
KEYOPT,4,12,0

KEYOPT,3,5,0

! Generate the target surface
ASEL,S,,,7
CM,_TARGET,AREA
TYPE,3
NSLA,S,1
ESLN,S,0
ESURF,ALL
CMSEL,S,_ELEMCM
! Generate the contact surface
ASEL,S,,,1
CM,_CONTACT,AREA
TYPE,4
NSLA,S,1
ESLN,S,0
ESURF,ALL
*SET,_REALID,3
ALLSEL
ESEL,ALL
ESEL,S,TYPE,,3
ESEL,A,TYPE,,4
ESEL,R,REAL,,3
!/PSYMB,ESYS,1
!/PNUM,TYPE,1
!/NUM,1
! EPLOTT
ESEL,ALL
ESEL,S,TYPE,,3
ESEL,A,TYPE,,4
ESEL,R,REAL,,3
CMSEL,A,_NODECM
CMDEL,_NODECM
CMSEL,A,_ELEMCM
CMDEL,_ELEMCM
CMSEL,S,_KPCM
CMDEL,_KPCM
CMSEL,S,_LINECM
CMDEL,_LINECM
CMSEL,S,_AREACM
CMDEL,_AREACM
CMSEL,S,_VOLUCM
CMDEL,_VOLUCM

```
! /GRES,cwz,gsav
CMDEL,_TARGET
CMDEL,_CONTACT
! /COM, CONTACT PAIR CREATION - END
! /MREP,EPLOTT
! EPLOTT
FINISH
```

```
/SOL
```

```
FLST,2,2,4,ORDE,2
FITEM,2,9
FITEM,2,10
DL,P51X, ,ALL,
FLST,2,2,4,ORDE,2
FITEM,2,11
FITEM,2,12
DL,P51X, ,ALL,
FLST,2,2,4,ORDE,2
FITEM,2,13
FITEM,2,14
DL,P51X, ,ALL,
FLST,2,2,4,ORDE,2
FITEM,2,15
FITEM,2,16
DL,P51X, ,ALL,
```

```
/SOLU
ANTYPE,2
MSAVE,0
MODOPT,LANB,6
EQSLV,SPAR
MXPAND,6, , ,1
LUMPM,0
PSTRES,0
MODOPT,LANB,6,0,1600, ,OFF
CNVTOL,AMPS,1,1.E-8
SOLVE
FINISH
```

```
/POST1
SET,LIST
```

```
/SOLU
```

```
ANTYPE,SPECTR
SPOPT,PSD,10,ON
PSDUNIT,1,FORCE
```

```
! DEFINE ANALYSIS TYPE
! USE FIRST 6 MODES, CALC ELEM. STRESSES
! DEFINE TYPE OF PSD AS A FORCE SPECTRUM
```



```

DMPRAT,0.0005
F,11000,FZ,-600
PSDFRQ,1,1,1.0,1600
PSDVAL,1,1.0,1.0      ! IN N**2/HZ
PFACT,1,NODE
PSDRES,DISP,REL
PSDCOM
SOLVE
FINISH

/POST1
SET,3,1                ! ONE SIGMA DISPLACEMENT SOLUTION RESULTS
/VIEW,1,2,3,4
PLNSOL,U,Z
PRNSOL,U,Z
FINISH

/SOLUTION
ANTYPE,HARMIC         ! REDEFINE ANALYSIS TYPE AND SOLVE AGAIN
HROPT,MSUP           ! USING MODE SUPERPOSITION HARMONIC
ANALYSIS
HROUT,OFF,ON         ! PRINT AMPLITUDE & PHASE, CLUSTER
FREQUENCIES
KBC,1
HARFRQ,1,1600
DMPRAT,0.02
NSUBSTEP,100
SOLVE
FINISH

/POST26
FILE,,rfrq
PRCPLX,1
NSOL,2,11000,U,Z
PSDDAT,10,1,1.0,80,1.0
PSDTYP,2
PSDCAL,7,2
PSDPRT
PRVAR,2,7
*GET,P,VARI,7,EXTREM,VMAX
*status,parm

```

**ANSYS INPUT LOG FILE FOR MULTIPHYSICS SIMULATION FOR
CYLINDRICAL PIPE TOTALLY COVERED WITH SENSOR**

/PREP7

!*

! SENSOR PROPERTIES

**MPTEMP,,,,,,,,
MPTEMP,1,0
MPDATA,DENS,1,,1.8
TB,PIEZ,1,,1
TBMODIF,1,1,
TBMODIF,1,2,
TBMODIF,1,3,6e-12
TBMODIF,2,1,
TBMODIF,2,2,
TBMODIF,2,3,-15e-12
TBMODIF,3,1,
TBMODIF,3,2,
TBMODIF,3,3,6e-12
TBMODIF,4,1,
TBMODIF,4,2,
TBMODIF,4,3,
TBMODIF,5,1,
TBMODIF,5,2,
TBMODIF,5,3,
TBMODIF,6,1,
TBMODIF,6,2,
TBMODIF,6,3,
TB,ANEL,1,1,21,1
TBTEMP,0
TBDATA,,4e-10,-1.36e-10,-1.36e-10,0,0,0
TBDATA,,4e-10,-1.36e-10,0,0,0,4e-10
TBDATA,,0,0,0,10.72e-10,0,0
TBDATA,,10.72e-10,0,10.72e-10,,
MPTEMP,,,,,,,,
MPTEMP,1,0
MPDATA,PERX,1,,1e14
MPDATA,PERY,1,,1e14
MPDATA,PERZ,1,,1700**

/NOPR

/PMETH,OFF,1

```
KEYW,PR_SET,1
KEYW,PR_STRUC,1
KEYW,PR_THERM,0
KEYW,PR_FLUID,0
KEYW,PR_ELMAG,1
KEYW,MAGNOD,0
KEYW,MAGEDG,0
KEYW,MAGHFE,0
KEYW,MAGELC,1
KEYW,PR_MULTI,1
KEYW,PR_CFD,0
/GO
!/COM,
!/COM,Preferences for GUI filtering have been set to display:
!/COM, Structural
!/COM, Electric
```

```
ET,1,SOLID227,101
KEYOPT,1,1,1001
/prep7
*SET,hb,0.000889
*SET,hs,50e-6
*SET,e31,1.861
CYL4,0,0,0.022225,0,0.022275,360,0.3048
```

```
! MESH SENSOR
ESIZE,0.0067,,
MSHKEY,0
MSHAPE,0,3D
VSEL,ALL
VMESH,ALL
```

```
ET,2,SHELL63
R,1,0.000889
MPTEMP,,,,,,,,
MPTEMP,1,0
MPDATA,EX,2,,70e9
MPDATA,PRXY,2,,0.33
MPDATA,DENS,2,,2700
```

```
CYL4,0,0,0.022225,0,,360,0.3048
VDELE,2,2,0,0,
ADELE,7,8,1,0,
```

```
!MESH BEAM
```

TYPE,2
MAT,2
REAL,1
ESYS,0
SECNUM,
ESIZE,0.005,0,
MSHKEY,0
MSHAPE,0,3d
ASEL,A,AREA,,9,10,1,0
AMESH,ALL,

!/COM, CONTACT PAIR CREATION - START

CM,_NODECM,NODE
CM,_ELEMCM,ELEM
CM,_KPCM,KP
CM,_LINECM,LINE
CM,_AREACM,AREA
CM,_VOLUCM,VOLU
!/GSAV,cwz,gsav,,temp
MP,MU,3,
MAT,3
MP,EMIS,3,7.88860905221e-031
R,3
REAL,3
ET,3,170
ET,4,CONTA 174
R,3,,,1.0,0.1,0,
RMORE,,,1.0E20,0.0,1.0,
RMORE,0.0,0,1.0,,1.0,0.5
RMORE,0,1.0,1.0,0.0,,1.0
KEYOPT,4,1,5
KEYOPT,4,2,0
KEYOPT,4,4,0
KEYOPT,4,5,0
KEYOPT,4,7,0
KEYOPT,4,8,0
KEYOPT,4,9,0
KEYOPT,4,10,1
KEYOPT,4,11,0
KEYOPT,4,12,0

KEYOPT,3,5,0

! Generate the target surface

ASEL,S,,,9,10,1
CM,_TARGET,AREA

```

TYPE,3
NSLA,S,1
ESLN,S,0
ESURF,ALL
CMSEL,S,_ELEMCM
! Generate the contact surface
ASEL,S,,,5,6,1
CM,_CONTACT,AREA
TYPE,4
NSLA,S,1
ESLN,S,0
ESURF,ALL
*SET,_REALID,3
ALLSEL
ESEL,ALL
ESEL,S,TYPE,,3
ESEL,A,TYPE,,4
ESEL,R,REAL,,3
!/PSYMB,ESYS,1
!/PNUM,TYPE,1
!/NUM,1
! EPLOTT
ESEL,ALL
ESEL,S,TYPE,,3
ESEL,A,TYPE,,4
ESEL,R,REAL,,3
CMSEL,A,_NODECM
CMDEL,_NODECM
CMSEL,A,_ELEMCM
CMDEL,_ELEMCM
CMSEL,S,_KPCM
CMDEL,_KPCM
CMSEL,S,_LINECM
CMDEL,_LINECM
CMSEL,S,_AREACM
CMDEL,_AREACM
CMSEL,S,_VOLUCM
CMDEL,_VOLUCM
!/GRES,cwz,gsav
CMDEL,_TARGET
CMDEL,_CONTACT
!/COM, CONTACT PAIR CREATION - END
!/MREP,EPLOTT
! EPLOTT
FINISH

```

```

/SOL
FLST,2,2,4,ORDE,2
FITEM,2,1
FITEM,2,2
DL,P51X, ,ALL,
FLST,2,2,4,ORDE,2
FITEM,2,3
FITEM,2,4
DL,P51X, ,ALL,
FLST,2,2,4,ORDE,2
FITEM,2,5
FITEM,2,6
DL,P51X, ,ALL,
FLST,2,2,4,ORDE,2
FITEM,2,7
FITEM,2,8
DL,P51X, ,ALL,
FLST,2,2,4,ORDE,2
FITEM,2,21
FITEM,2,22
DL,P51X, ,ALL,
FLST,2,2,4,ORDE,2
FITEM,2,23
FITEM,2,24
DL,P51X, ,ALL,

```

```

/SOLU
ANTYPE,2
MSAVE,0
MODOPT,LANB,6
EQLV,SPAR
MXPAND,6, , ,1
LUMPM,0
PSTRES,0
MODOPT,LANB,6,0,1600, ,OFF
SOLVE
FINISH

```

```

/POST1
SET,LIST
/SOLU

```

```

ANTYPE,SPECTR
SPOPT,PSD,6,ON
PSDUNIT,1,FORCE
DMPRAT,0.0005
F,15000,FY,-600

```

```

! DEFINE ANALYSIS TYPE
! USE FIRST 6 MODES, CALC ELEM. STRESSES
! DEFINE TYPE OF PSD AS A FORCE SPECTRUM

```

```

PSDFRQ,1,1,1.0,1600.0
PSDVAL,1,1.0,1.0      ! IN N**2/HZ
PFACT,1,NODE
PSDRES,DISP,REL
PSDCOM
SOLVE
FINISH
/POST1
SET,3,1                ! ONE SIGMA DISPLACEMENT SOLUTION RESULTS
/VIEW,1,2,3,4
PLNSOL,U,Y
PRNSOL,U,Y
FINISH

/SOLUTION
ANTYPE,HARMIC         ! REDEFINE ANALYSIS TYPE AND SOLVE AGAIN
HROPT,MSUP            ! USING MODE SUPERPOSITION HARMONIC
  ANALYSIS
HROUT,OFF,ON         ! PRINT AMPLITUDE & PHASE, CLUSTER
  FREQUENCIES
KBC,1
HARFRQ,1,1600
DMPRAT,0.02
NSUBSTEP,100
SOLVE
FINISH

/POST26
FILE,,rfrq
PRCPLX,1
NSOL,2,15000,U,Y
PSDDAT,6,1,1.0,80,1.0
PSDTYP,2
PSDCAL,7,2
PSDPRT
PRVAR,2,7
*GET,P,VARI,7,EXTREM,VMAX
*status,parm

```

**ANSYS INPUT LOG FILE FOR MULTIPHYSICS SIMULATION OF BEAM
WITH SHAPED SENSOR**

/PREP7

!*

! SENSOR PROPERTIES

MPTEMP,,,,,,,,

MPTEMP,1,0

MPDATA,DENS,1,,1.8

TB,PIEZ,1,,1

TBMODIF,1,1,

TBMODIF,1,2,

TBMODIF,1,3,6e-12

TBMODIF,2,1,

TBMODIF,2,2,

TBMODIF,2,3,-15e-12

TBMODIF,3,1,

TBMODIF,3,2,

TBMODIF,3,3,6e-12

TBMODIF,4,1,

TBMODIF,4,2,

TBMODIF,4,3,

TBMODIF,5,1,

TBMODIF,5,2,

TBMODIF,5,3,

TBMODIF,6,1,

TBMODIF,6,2,

TBMODIF,6,3,

TB,ANEL,1,1,21,1

TBTEMP,0

TBDATA,,4e-10,-1.36e-10,-1.36e-10,0,0,0

TBDATA,,4e-10,-1.36e-10,0,0,0,4e-10

TBDATA,,0,0,0,10.72e-10,0,0

TBDATA,,10.72e-10,0,10.72e-10,,,

MPTEMP,,,,,,,,

MPTEMP,1,0

MPDATA,PERX,1,,1e14

MPDATA,PERY,1,,1e14

MPDATA,PERZ,1,,1700

/NOPR

/PMETH,OFF,1

KEYW,PR_SET,1


```

KEYW,PR_STRUC,1
KEYW,PR_THERM,0
KEYW,PR_FLUID,0
KEYW,PR_ELMAG,1
KEYW,MAGNOD,0
KEYW,MAGEDG,0
KEYW,MAGHFE,0
KEYW,MAGELC,1
KEYW,PR_MULTI,1
KEYW,PR_CFD,0
/GO
!/COM,
!/COM,Preferences for GUI filtering have been set to display:
!/COM, Structural
!/COM, Electric

```

```

ET,1,SOLID227,1001
KEYOPT,1,1,1001
/prep7
*SET,hb,0.003175
*SET,hs,50e-6
*SET,e31,1.861
*SET,b,0.0508
*SET,k,-b/(2*(hb+hs)*e31)
*DIM,Y,ARRAY,10000
*SET,I,1
*Do,x,0,0.3,0.01
*SET,Y(I),0.2667*k*(x*x-0.3*x)
K,I,x,Y(I),0,
*SET,I,I+1
*ENDDO
*SET,hmt ,0.3/0.01
*Do,I,1, hmt, 1
LSTR, I,I+1
*ENDDO
*DIM,YY,ARRAY,10000
*SET,II,32
*Do,xx,0.3,0,-0.01
*SET,YY(II),-k*0.2667*(xx*xx-0.3*xx)
K,II,xx,YY(II),0,
*SET,II,II+1
*ENDDO
*SET,hmthmt ,30+0.3/0.01
*Do,II,32, hmthmt+1, 1
LSTR, II, II+1
*ENDDO

```

NUMMRG,KP, , ,LOW

! DEFINE SENSOR AREA AND THICKNESS

LSEL,ALL

AL,ALL

VOFFST,1,-50e-6, ,

! MESH SENSOR

ESIZE,0.01,0,

MSHKEY,0

MSHAPE,1,3d

VSEL,ALL

VMESH,ALL

ET,2,SHELL63

R,1,0.003175

MPTEMP,,,,,,,,,

MPTEMP,1,0

MPDATA,EX,2,,70e9

MPDATA,PRXY,2,,0.33

MPDATA,DENS,2,,2700

RECTNG,,0.3,-0.0254,0.0254,

!MESH BEAM

MAT,2

REAL,1

ESYS,0

SECNUM,

ESIZE,0.01,0,

MSHKEY,0

MSHAPE,1,3d

ASEL,A,AREA,,63

AMESH,63

! /COM, CONTACT PAIR CREATION - START

CM,_NODECM,NODE

CM,_ELEMCM,ELEM

CM,_KPCM,KP

CM,_LINECM,LINE

CM,_AREACM,AREA

CM,_VOLUCM,VOLU

! /GSAV,cwz,gsav,,temp

MP,MU,3,

MAT,3

MP,EMIS,3,7.88860905221e-031

R,3

REAL,3

```

ET,3,170
ET,4,CONTA 174
R,3,,,1.0,0.1,0,
RMORE,,,1.0E20,0.0,1.0,
RMORE,0.0,0,1.0,,1.0,0.5
RMORE,0,1.0,1.0,0.0,,1.0
KEYOPT,4,1,5
KEYOPT,4,2,0
KEYOPT,4,4,0
KEYOPT,4,5,0
KEYOPT,4,7,0
KEYOPT,4,8,0
KEYOPT,4,9,0
KEYOPT,4,10,1
KEYOPT,4,11,0
KEYOPT,4,12,0

KEYOPT,3,5,0

! Generate the target surface
ASEL,S,,,63
CM,_TARGET,AREA
TYPE,3
NSLA,S,1
ESLN,S,0
ESURF,ALL
CMSEL,S,_ELEMCM
! Generate the contact surface
ASEL,S,,,1
CM,_CONTACT,AREA
TYPE,4
NSLA,S,1
ESLN,S,0
ESURF,ALL
*SET,_REALID,3
ALLSEL
ESEL,ALL
ESEL,S,TYPE,,3
ESEL,A,TYPE,,4
ESEL,R,REAL,,4
!/PSYMB,ESYS,1
!/PNUM,TYPE,1
!/NUM,1
! EPLOTT
ESEL,ALL
ESEL,S,TYPE,,3

```

```

ESEL,A,TYPE,,4
ESEL,R,REAL,,3
CMSEL,A,_NODECM
CMDEL,_NODECM
CMSEL,A,_ELEMCM
CMDEL,_ELEMCM
CMSEL,S,_KPCM
CMDEL,_KPCM
CMSEL,S,_LINECM
CMDEL,_LINECM
CMSEL,S,_AREACM
CMDEL,_AREACM
CMSEL,S,_VOLUCM
CMDEL,_VOLUCM
!/GRES,cwz,gsav
CMDEL,_TARGET
CMDEL,_CONTACT
!/COM, CONTACT PAIR CREATION - END
!/MREP,EPLOTT
! EPLOTT
FINISH

```

```

/SOL
FLST,2,2,4,ORDE,2
FITEM,2,121
FITEM,2,184
DL,P51X, ,ALL,

```

```

/SOLU
ANTYPE,2
MSAVE,0
MODOPT,LANB,6
EQLV,SPAR
MXPAND,6, , ,1
LUMPM,0
PSTRES,0
MODOPT,LANB,6,0,1600, ,OFF
CNVTOL,AMPS,1,1.E-8
SOLVE
FINISH

```

```

/POST1
SET,LIST
/SOLU

```

```

ANTYPE,SPECTR
SPOPT,PSD,6,ON

```

```

! DEFINE ANALYSIS TYPE
! USE FIRST 6 MODES, CALC ELEM. STRESSES

```

```

PSDUNIT,1,FORCE          ! DEFINE TYPE OF PSD AS A FORCE SPECTRUM
DMPRAT,0.0005
F,6500,FZ,-600
PSDFRQ,1,1,1.0,1600.0
PSDVAL,1,1.0,1.0        ! IN N**2/HZ
PFACT,1,NODE
PSDRES,DISP,REL
PSDCOM
SOLVE
FINISH

/POST1
SET,3,1                  ! ONE SIGMA DISPLACEMENT SOLUTION RESULTS
/VIEW,1,2,3,4
PLNSOL,U,Z
PRNSOL,U,Z
FINISH
/SOLUTION
ANTYPE,HARMIC           ! REDEFINE ANALYSIS TYPE AND SOLVE AGAIN
HROPT,MSUP              ! USING MODE SUPERPOSITION HARMONIC
ANALYSIS
HROUT,OFF,ON           ! PRINT AMPLITUDE & PHASE, CLUSTER
FREQUENCIES
KBC,1
HARFRQ,1,1600
DMPRAT,0.02
NSUBSTEP,100
SOLVE
FINISH

/POST26
FILE,,rfrq
PRCPLX,1
NSOL,2,6500,U,Z
PSDDAT,6,1,1.0,80,1.0
PSDTYP,2
PSDCAL,7,2
PSDPRT
PRVAR,2,7
*GET,P,VARI,7,EXTREM,VMAX
*status,parm

```

**ANSYS INPUT LOG FILE FOR MULTIPHYSICS SIMULATION OF PLATE
WITH SHAPED SENSOR**

```
/PREP7  
!*  
  
! SENSOR PROPERTIES  
MPTEMP,,,,,,,,  
MPTEMP,1,0  
MPDATA,DENS,1,,1.8  
TB,PIEZ,1,,1  
TBMODIF,1,1,  
TBMODIF,1,2,  
TBMODIF,1,3,6e-12  
TBMODIF,2,1,  
TBMODIF,2,2,  
TBMODIF,2,3,-15e-12  
TBMODIF,3,1,  
TBMODIF,3,2,  
TBMODIF,3,3,6e-12  
TBMODIF,4,1,  
TBMODIF,4,2,  
TBMODIF,4,3,  
TBMODIF,5,1,  
TBMODIF,5,2,  
TBMODIF,5,3,  
TBMODIF,6,1,  
TBMODIF,6,2,  
TBMODIF,6,3,  
TB,ANEL,1,1,21,1  
TBTEMP,0  
TBDATA,,4e-10,-1.36e-10,-1.36e-10,0,0,0  
TBDATA,,4e-10,-1.36e-10,0,0,0,4e-10  
TBDATA,,0,0,0,10.72e-10,0,0  
TBDATA,,10.72e-10,0,10.72e-10,,,  
MPTEMP,,,,,,,,  
MPTEMP,1,0  
MPDATA,PERX,1,,1e14  
MPDATA,PERY,1,,1e14  
MPDATA,PERZ,1,,1700  
  
/NOPR  
/PMETH,OFF,1  
KEYW,PR_SET,1
```

```

KEYW,PR_STRUC,1
KEYW,PR_THERM,0
KEYW,PR_FLUID,0
KEYW,PR_ELMAG,1
KEYW,MAGNOD,0
KEYW,MAGEDG,0
KEYW,MAGHFE,0
KEYW,MAGELC,1
KEYW,PR_MULTI,1
KEYW,PR_CFD,0
/GO
!/COM,
!/COM,Preferences for GUI filtering have been set to display:
!/COM, Structural
!/COM, Electric

```

```

ET,1,SOLID227,1001
KEYOPT,1,1,1001
/prep7
*SET,hb,0.004762
*SET,hs,50e-6
*SET,e31,1.861
*SET,b,0.381
*SET,k1,-b/(2*(hb+hs)*e31)
*SET,k,-5
*DIM,Y,ARRAY,10000
*SET,I,1
*Do,x,0,0.6,0.01
*SET,Y(I),0.2636*k*(x*x-0.6*x)
K,I,x,Y(I),0,
*SET,I,I+1
*ENDDO
*SET,hmt ,0.6/0.01
*Do,I,1, hmt, 1
LSTR, I,I+1
*ENDDO
*DIM,YY,ARRAY,10000
*SET,II,62
*Do,xx,0.6,0,-0.01
*SET,YY(II),-k*0.2636*(xx*xx-0.6*xx)
K,II,xx,YY(II),0,
*SET,II,II+1
*ENDDO
*SET,hmthmt ,60+0.6/0.01
*Do,II,62, hmthmt+1, 1
LSTR, II, II+1

```

```

*ENDDO
NUMMRG,KP, , , ,LOW

! DEFINE SENSOR AREA AND THICKNESS
LSEL,ALL
AL,ALL
VOFFST,1,-50e-6, ,

! MESH SENSOR
ESIZE,0.02,0,
MSHKEY,0
MSHAPE,1,3d
VSEL,ALL
VMESH,ALL

ET,2,SHELL63
R,1,hb
MPTEMP,,,,,,,,
MPTEMP,1,0
MPDATA,EX,2,,70e9
MPDATA,PRXY,2,,0.33
MPDATA,DENS,2,,2700
RECTNG,,0.6,-0.1905,0.1905,
!MESH BEAM
MAT,2
REAL,1
ESYS,0
SECNUM,
ESIZE,0.02,0,
MSHKEY,0
MSHAPE,1,3d
ASEL,A,AREA,,123
AMESH,123

! /COM, CONTACT PAIR CREATION - START
CM,_NODECM,NODE
CM,_ELEMCM,ELEM
CM,_KPCM,KP
CM,_LINECM,LINE
CM,_AREACM,AREA
CM,_VOLUCM,VOLU
! /GSAV,cwz,gsav,,temp
MP,MU,3,
MAT,3
MP,EMIS,3,7.88860905221e-031
R,3

```



```

REAL,3
ET,3,170
ET,4,CONTA 174
R,3,,,1.0,0.1,0,
RMORE,,,1.0E20,0.0,1.0,
RMORE,0.0,0,1.0,,1.0,0.5
RMORE,0,1.0,1.0,0.0,,1.0
KEYOPT,4,1,5
KEYOPT,4,2,0
KEYOPT,4,4,0
KEYOPT,4,5,0
KEYOPT,4,7,0
KEYOPT,4,8,0
KEYOPT,4,9,0
KEYOPT,4,10,1
KEYOPT,4,11,0
KEYOPT,4,12,0

KEYOPT,3,5,0

! Generate the target surface
ASEL,S,,,123
CM,_TARGET,AREA
TYPE,3
NSLA,S,1
ESLN,S,0
ESURF,ALL
CMSEL,S,_ELEMCM
! Generate the contact surface
ASEL,S,,,1
CM,_CONTACT,AREA
TYPE,4
NSLA,S,1
ESLN,S,0
ESURF,ALL
*SET,_REALID,3
ALLSEL
ESEL,ALL
ESEL,S,TYPE,,3
ESEL,A,TYPE,,4
ESEL,R,REAL,,4
! /PSYMB,ESYS,1
! /PNUM,TYPE,1
! /NUM,1
! EPLOTT
ESEL,ALL

```

```
ESEL,S,TYPE,,3
ESEL,A,TYPE,,4
ESEL,R,REAL,,3
CMSEL,A,_NODECM
CMDEL,_NODECM
CMSEL,A,_ELEMCM
CMDEL,_ELEMCM
CMSEL,S,_KPCM
CMDEL,_KPCM
CMSEL,S,_LINECM
CMDEL,_LINECM
CMSEL,S,_AREACM
CMDEL,_AREACM
CMSEL,S,_VOLUCM
CMDEL,_VOLUCM
!/GRES,cwz,gsav
CMDEL,_TARGET
CMDEL,_CONTACT
!/COM, CONTACT PAIR CREATION - END
!/MREP,EPLOTT
! EPLOTT
FINISH
```

```
/SOL
FLST,2,2,4,ORDE,2
FITEM,2,361
FITEM,2,362
DL,P51X, ,ALL,
FLST,2,2,4,ORDE,2
FITEM,2,363
FITEM,2,364
DL,P51X, ,ALL,
FLST,2,2,4,ORDE,2
FITEM,2,241
FITEM,2,301
DL,P51X, ,ALL,
```

```
/SOLU
ANTYPE,2
MSAVE,0
MODOPT,LANB,6
EQSLV,SPAR
MXPAND,6, ,1
LUMPM,0
PSTRES,0
MODOPT,LANB,6,0,1600, ,OFF
```

```
CNVTOL,AMPS,1,1.E-8
SOLVE
FINISH
```

```
/POST1
SET,LIST
/SOLU
ANTYPE,SPECTR          ! DEFINE ANALYSIS TYPE
SPOPT,PSD,6,ON         ! USE FIRST 6 MODES, CALC ELEM. STRESSES
PSDUNIT,1,FORCE       ! DEFINE TYPE OF PSD AS A FORCE SPECTRUM
DMPRAT,0.0005
F,13500,FZ,-600
PSDFRQ,1,1,1.0,1600.0
PSDVAL,1,1.0,1.0      ! IN N**2/HZ
PFACT,1,NODE
PSDRES,DISP,REL
PSDCOM
SOLVE
FINISH
```

```
/POST1
SET,3,1                ! ONE SIGMA DISPLACEMENT SOLUTION RESULTS
/VIEW,1,2,3,4
PLNSOL,U,Z
PRNSOL,U,Z
FINISH
```

```
/SOLUTION
ANTYPE,HARMIC          ! REDEFINE ANALYSIS TYPE AND SOLVE AGAIN
HROPT,MSUP             ! USING MODE SUPERPOSITION HARMONIC
ANALYSIS
HROUT,OFF,ON          ! PRINT AMPLITUDE & PHASE, CLUSTER
FREQUENCIES
KBC,1
HARFRQ,1,1600
DMPRAT,0.02
NSUBSTEP,100
SOLVE
FINISH
```

```
/POST26
FILE,,rfrq
PRCPLX,1
NSOL,2,13500,U,Z
PSDDAT,6,1,1.0,80,1.0
PSDTYP,2
PSDCAL,7,2
```

```
PSDPRT
PRVAR,2,7
*GET,P,VARI,7,EXTREM,VMAX
*status,parm
```

ANSYS INPUT LOG FILE FOR MULTIPHYSICS SIMULATION OF CYLINDRICAL PIPE WITH SHAPED SENSOR

```
/PREP7
```

```
!*
```

! SENSOR PROPERTIES

```
MPTEMP,,,,,,,,
MPTEMP,1,0
MPDATA,DENS,1,,1.8
TB,PIEZ,1,,,1
TBMODIF,1,1,
TBMODIF,1,2,
TBMODIF,1,3,6e-12
TBMODIF,2,1,
TBMODIF,2,2,
TBMODIF,2,3,-15e-12
TBMODIF,3,1,
TBMODIF,3,2,
TBMODIF,3,3,6e-12
TBMODIF,4,1,
TBMODIF,4,2,
TBMODIF,4,3,
TBMODIF,5,1,
TBMODIF,5,2,
TBMODIF,5,3,
TBMODIF,6,1,
TBMODIF,6,2,
TBMODIF,6,3,
TB,ANEL,1,1,21,1
TBTEMP,0
TBDATA,,4e-10,-1.36e-10,-1.36e-10,0,0,0
TBDATA,,4e-10,-1.36e-10,0,0,0,4e-10
TBDATA,,0,0,0,10.72e-10,0,0
TBDATA,,10.72e-10,0,10.72e-10,,,
MPTEMP,,,,,,,,
MPTEMP,1,0
MPDATA,PERX,1,,1e14
MPDATA,PERY,1,,1e14
```

MPDATA,PERZ,1,,1700

/NOPR

/PMETH,OFF,1

KEYW,PR_SET,1

KEYW,PR_STRUC,1

KEYW,PR_THERM,0

KEYW,PR_FLUID,0

KEYW,PR_ELMAG,1

KEYW,MAGNOD,0

KEYW,MAGEDG,0

KEYW,MAGHFE,0

KEYW,MAGELC,1

KEYW,PR_MULTI,1

KEYW,PR_CFD,0

/GO

!/COM,

!/COM,Preferences for GUI filtering have been set to display:

!/COM, Structural

!/COM, Electric

ET,1,SOLID227,1001

KEYOPT,1,1,1001

/prep7

*SET,hb,0.00889

*SET,hs,50e-6

*SET,e31,1.861

*SET,b,0.24

SET,k,-b/(2(hb+hs)*e31)

!*SET,LLL,-1.585

*SET,LLL,-3

*DIM,X,ARRAY,10000

*SET,I,1

*Do,Z,0,0.3,0.01

*SET,X(I),0.2636*LLL*(Z*Z-0.3*Z)

K,I,X(I),0,Z,

*SET,I,I+1

*ENDDO

*SET,hmt,0.3/0.01

*Do,I,1,hmt,1

LSTR,I,I+1

*ENDDO

```

*DIM,XX,ARRAY,10000
*SET,II,32

*Do,ZZ,0.3,0,-0.01
*SET,XX(II),-LLL*0.2636*(ZZ*ZZ-0.3*ZZ)
K,II,XX(II),0,ZZ,
*SET,II,II+1
*ENDDO

*SET,hmthmt ,30+0.3/.01
*Do,II,32, hmthmt+1, 1
LSTR, II, II+1
*ENDDO

NUMMRG,KP, , , ,LOW

! DEFINE SENSOR AREA AND THICKNESS
LSEL,ALL
AL,ALL
VOFFST,1,-.1, ,

CYL4,0,0,0.022225,0,0.022275,360,0.3

VINV,1,2

! MESH SENSOR
ESIZE,0.005,0,
MSHKEY,0
MSHAPE,1,3d
VSEL,ALL
VMESH,ALL

ET,2,SHELL63
R,1,0.000889
MPTEMP,,,,,,,,
MPTEMP,1,0
MPDATA,EX,2,,70e9
MPDATA,PRXY,2,,0.33
MPDATA,DENS,2,,2700

CYL4,0,0,0.022225,0,,360,0.3
VDELE,1,1,0,0,
ADELE,1,2,1,0,

!MESH BEAM
TYPE,2

```

MAT,2
REAL,1
ESYS,0
SECNUM,
ESIZE,0.005,0,
MSHKEY,0
MSHAPE,0,3d
ASEL,A,AREA,,1,2,1,0
AMESH,ALL,

!/COM, CONTACT PAIR CREATION - START

CM,_NODECM,NODE
CM,_ELEMCM,ELEM
CM,_KPCM,KP
CM,_LINECM,LINE
CM,_AREACM,AREA
CM,_VOLUCM,VOLU
!/GSAV,cwz,gsav,,temp
MP,MU,3,
MAT,3
MP,EMIS,3,7.88860905221e-031
R,3
REAL,3
ET,3,170
ET,4,CONTA 174
R,3,,,1.0,0.1,0,
RMORE,,,1.0E20,0.0,1.0,
RMORE,0.0,0,1.0,,1.0,0.5
RMORE,0,1.0,1.0,0.0,,1.0
KEYOPT,4,1,5
KEYOPT,4,2,0
KEYOPT,4,4,0
KEYOPT,4,5,0
KEYOPT,4,7,0
KEYOPT,4,8,0
KEYOPT,4,9,0
KEYOPT,4,10,1
KEYOPT,4,11,0
KEYOPT,4,12,0

KEYOPT,3,5,0

! Generate the target surface
ASEL,S,,,3
CM,_TARGET,AREA
TYPE,3

```

NSLA,S,1
ESLN,S,0
ESURF,ALL
CMSEL,S,_ELEMCM
! Generate the contact surface
ASEL,S,,,130
CM,_CONTACT,AREA
TYPE,4
NSLA,S,1
ESLN,S,0
ESURF,ALL
*SET,_REALID,3
ALLSEL
ESEL,ALL
ESEL,S,TYPE,,3
ESEL,A,TYPE,,4
ESEL,R,REAL,,4
!/PSYMB,ESYS,1
!/PNUM,TYPE,1
!/NUM,1
! EPlot
ESEL,ALL
ESEL,S,TYPE,,3
ESEL,A,TYPE,,4
ESEL,R,REAL,,3
CMSEL,A,_NODECM
CMDEL,_NODECM
CMSEL,A,_ELEMCM
CMDEL,_ELEMCM
CMSEL,S,_KPCM
CMDEL,_KPCM
CMSEL,S,_LINECM
CMDEL,_LINECM
CMSEL,S,_AREACM
CMDEL,_AREACM
CMSEL,S,_VOLUCM
CMDEL,_VOLUCM
!/GRES,cwz,gsav
CMDEL,_TARGET
CMDEL,_CONTACT
!/COM, CONTACT PAIR CREATION - END
!/MREP,EPlot
! EPlot
FINISH

/SOL

```



```
FLST,2,2,4,ORDE,2
FITEM,2,1
FITEM,2,2
DL,P51X, ,ALL,
FLST,2,3,4,ORDE,3
FITEM,2,3
FITEM,2,4
FITEM,2,201
DL,P51X, ,ALL,
```

```
/SOLU
ANTYPE,2
MSAVE,0
MODOPT,LANB,6
EQLSV,SPAR
MXPAND,6, , ,1
LUMPM,0
PSTRES,0
MODOPT,LANB,6,0,1600, ,OFF
CNVTOL,AMPS,1,1.E-8
SOLVE
FINISH
```

```
/POST1
SET,LIST
/SOLU
ANTYPE,SPECTR          ! DEFINE ANALYSIS TYPE
SPOPT,PSD,6,ON         ! USE FIRST 6 MODES, CALC ELEM. STRESSES
PSDUNIT,1,FORCE       ! DEFINE TYPE OF PSD AS A FORCE SPECTRUM
DMPRAT,0.0005
F,11000,FY,-600
PSDFRQ,1,1,1.0,1600.0
PSDVAL,1,1.0,1.0      ! IN N**2/HZ
PFACT,1,NODE
PSDRES,DISP,REL
PSDCOM
SOLVE
FINISH
```

```
/POST1
SET,3,1                ! ONE SIGMA DISPLACEMENT SOLUTION RESULTS
/VIEW,1,2,3,4
PLNSOL,U,Y
PRNSOL,U,Y
FINISH
```

```

/SOLUTION
ANTYPE,HARMIC      ! REDEFINE ANALYSIS TYPE AND SOLVE AGAIN
HROPT,MSUP        ! USING MODE SUPERPOSITION HARMONIC
  ANALYSIS
HROUT,OFF,ON      ! PRINT AMPLITUDE & PHASE, CLUSTER
  FREQUENCIES
KBC,1
HARFRQ,1,1600
DMPRAT,0.02
NSUBSTEP,100
SOLVE
FINISH

/POST26
FILE,,rfrq
PRCPLX,1
NSOL,2,11000,U,Y
PSDDAT,6,1,1.0,80,1.0
PSDTYP,2
PSDCAL,7,2
PSDPRT
PRVAR,2,7
*GET,P,VARI,7,EXTREM,VMAX
*status,parm

```

APPENDIX B

*.RFRQ BINARY FILE FORMAT

SET 1: STANDARD ANSYS FILE HEADER

Each of the ANSYS program's binary files contains a standard, 100-integer file header that describes the file contents. The header contains the items listed below, always in the order shown below.

- | | |
|-------------|---|
| Item 1 | The file number |
| Item 2 | The file format. This item has a value of 0 if the file is internal, or 1 if the file is external. |
| Item 3 | The time, in compact form |
| Item 4 | The date, in compact form |
| Item 5 | The units of measurement used. The value of this item is as follows:
· 0 for user-defined units
· 1 for SI units
· 2 for CSG units
· 3 for British units (feet)
· 4 for British units (inches) |
| Item 10 | The ANSYS release level in integer form ("5.4" in character form) |
| Item 11 | The date of the ANSYS release |
| Items 12-14 | The machine identifier in integer form (three four-character strings) |
| Items 15-16 | The Jobname in integer form (two four-character strings) |
| Items 17-18 | The ANSYS product name in integer form (two four-character strings) |
| Item 19 | The ANSYS special version label in integer form (one four-character string) |
| Items 20-22 | The user name in integer form (three four-character strings) |
| Items 23-25 | The machine identifier in integer form (three four-character strings) |
| Item 26 | The system record size |
| Item 27 | The maximum file length |
| Item 28 | The maximum record number |
| Item 29 | The number of processors assigned to this task |
| Items 41-60 | The main analysis title in integer form (20 four-character strings) |
| Items 61-80 | The first subtitle in integer form (20 four-character strings) |

SET 2 - RFRQ FILE HEADER

- Record ID: N/A
- Type: Integer
- Number of Records: 1
- Record Length: 40

fun10	nmrow	nmatrx	nmode	numdof
maxn	wfmax	lenbac	0	ncumit
kan	0	0	0	0
0	0	0	0	0
ptrDOF	ptrDNC	ptrSTF	ptrMAS	ptrDMP
ptrFRQ	ptrDSP	0	0	0
0	0	0	0	0
0	0	0	0	0

where:

- fun10 - unit number (rfrq file is 10)
- nmrow - number of rows/columns in matrices
- nmatrx - number of reduced matrices on file
- nmode - number of modes extracted during modal analysis (or nmrow if reduced method)
- numdof - number of dofs per node
- maxn - maximum node number
- wfmax - maximum wavefront
- lenbac - number of nodes
- 0 - position not used
- ncumit - total number of iterations done during analysis
- kan - analysis type = 6 - reduced harmonic
- 0 - position not used
- 0 - position not used
- 0 - position not used
- 0 - position not used
- 0 - position not used
- 0 - position not used
- 0 - position not used
- 0 - position not used
- 0 - position not used
- ptrDOF - pointer to degree of freedom set used in model
- ptrDNC - pointer to nodal constraints
- ptrSTF - pointer to the reduced stiffness matrix
- ptrMAS - pointer to the reduced mass matrix
- ptrDMP - pointer to the reduced damping matrix or mode shapes
- ptrFRQ - pointer to the frequencies
- ptrDSP - pointer to the calculated displacements
- 0 - position not used
- 0 - position not used
- 0 - position not used

- 0 - position not used
- 0 - position not used
- 0 - position not used
- 0 - position not used
- 0 - position not used
- 0 - position not used
- 0 - position not used
- 0 - position not used
- 0 - position not used
- 0 - position not used

SET 3 - ANALYSIS INFORMATION

Group 1 - Degrees Of Freedom Per Node The following define the degree of freedom reference numbers:

UX = 1	UY = 2	UZ = 3	ROTX= 4
ROTY= 5	ROTZ= 6	AX = 7	AY = 8
AZ = 9	VX =10	VY =11	VZ =12
13-18 are spares	PRES=19	TEMP=20	VOLT=21
MAG =22	ENKE=23	ENDS=24	EMF =25
CURR=26	27-32 are spares		

Group 2 - Nodal Equivalence Table

- Record ID: N/A
- Type: Integer
- Number of Records: 1
- Record Length: lenbac

This table equates the actual node number to the number used for storage. (baclst(i),i=1,lenbac)

Group 3 - Unused Record

- Record ID: N/A
- Type: Double-precision
- Number of Records: 1
- Record Length: 10

The record contents are as follows:

1.0 0.0 0.0 0.0 0.0 0.0
0.0 0.0 0.0 0.0 0.0 0.0

Group 4 - Degree Of Freedom Set Used

- Record ID: DOF
- Type: Integer
- Number of Records: 1
- Record Length: nmrow

The DOFs are calculated as (N-1)*numdof+DOF, where N is the position number of the node in the nodal equivalence table and DOF is the DOF reference number given above. If the analysis uses the reduced method, the original DOF order (see next record) is rearranged so that DOFs having nodal constraints are listed first.

If the analysis uses the mode superposition method (using the reduced mode extraction technique), the DOF order is the same as the original order (see next record).
(l(i),i=1,nmrow)

Group 5 - Original Reduced Set Of Degrees Of Freedom Used

- Record ID: N/A
- Type: Integer
- Number of Records: 1
- Record Length: nmrow+1

The DOFs are calculated as $(N-1)*\text{numdof}+\text{DOF}$, where N is the position number of the node in the nodal equivalence table and DOF is the DOF reference number given above.

If the analysis uses the reduced method, the original DOF order, plus the number of nodal constraints (nbcdsp), is stored. If the analysis uses the mode superposition method (using the reduced mode extraction technique), this record matches the previous record. The nmrow+1 entry will be zero. (lorig(i),i=1,nmrow),nbcds

Group 6 - DOF of Nodal Constraints

- Record ID: DNC
- Type: Integer
- Number of Records: 1
- Record Length: nbcdsp

This record is present only if the analysis uses the reduced method and nbcdsp > 0 (see record at ptrDOF). These numbers are the positions in the previous record of dofs with a nodal constraint. These are nodal constraints only on nodes that also are masters.
(na(i),i=1,nbcdsp)

SET 4 - REDUCED MATRICES DATA

Group 1 - Reduced Stiffness Matrix

- Record ID: STF
- Type: Double-precision
- Number of Records: 1
- Record Length: nbcdsp

Each row of the matrix is stored as a record. The matrix is present only if nmatrix > 0 and analysis is not using mode superposition method (using the subspace mode extraction method). Row order is the same as the DOF order in record at ptrDOF.
(ak(i,j),i=1,nmrow)

Group 2 - Reduced Mass Matrix

- Record ID: MAS
- Type: Double-precision
- Number of Records: nmrow
- Record Length: nmrow

Each row of the matrix is stored as a record. The matrix is present only if nmatrix > 1 and analysis is not using mode superposition method (using the subspace extraction technique). Row order is the same as the DOF order in record at ptrDOF.
(am(i,j),i=1,nmrow)

Group 3 - Reduced Damping Matrix Or Mode Shapes

- Record ID: DMP
- Type: Double-precision
- Number of Records: varies
- Record Length: varies

If the analysis uses the reduced method, each record will be nmrow items in length. The reduced damping matrix is present only if nmatrix > 2. There will be nmrow records of this type stored here. Row order is the same as the DOF order in record at ptrDOF.

If the analysis uses the mode superposition method (using the reduced mode extraction technique), each record will be nmode items in length. These records contain mode shapes (eigenvectors) of the frequencies (eigenvalues) actually used in the harmonic analysis. There will be nmode records of this type stored here, with the first N records containing the mode shapes and the other records containing zeros, where N is the number of modes actually used in the harmonic analysis. Order corresponds to the DOF order given in record at ptrDOF. If the analysis uses the mode superposition method (using the subspace mode extraction technique), this record will not be present. (psi(i,j),i=1,nmrow) (or ac)

Group 4 - Frequencies Extracted From Modal Analysis

- Record ID: FRQ
- Type: Double-precision
- Number of Records: 1
- Record Length: nmrow

This record is present only for analyses using the mode superposition method (using the reduced mode extraction technique). (freq(i),i=1,nmrow)

Set 5 - Calculated Displacements

Located by the PTRDSP variable defined in Set 2.

Set 5 is repeated NCUMIT times.

Group 1 - Calculated Complex Displacements

- Record ID: DSP
- Type: cmp
- Number of Records: ncumit
- Record Length: nmrow+5

The first nmrow entries are the displacements in the same order as the original set of DOFs (see record AFTER ptrDOF). For the last five entries:

Real part

1. frequency for these values
2. load step number
3. cumulative iteration number
4. zero
5. scale factor (zero if the analysis uses the reduced method)

Imaginary part

- frequency increment
- substep number
- zero
- zero
- zero

MATLAB CODE TO PLOT THE SENSOR SHAPE IN ACTUAL DIMENSIONS.

```
b=0.0508;
hb=0.003175;
hs=50e-6;
e31=1.861;
L=0.3;
x=0:0.01:L;
k=-b/(2*(hb+hs)*e31);
y=k*(x.^2-L*x);
alpha=b/(2*max(abs(y)))
plot(x,y,'*','x,-y','*','x,alpha*y,x,-alpha*y)
```

beam.m MATLAB CODE

```
clc
clear all
close all
%
% Data
LoadStep=90;
Wy = fopen('DUMP1.lis','r');
Junk1=fscanf(Wy,'%s',8);
for j=1:110; %LoadStep % Total displrecord
    for i=1:(40485/5-1);% 74630/5 line per record
        WyTmp=fscanf(Wy,'%g',[1 5]);
        Junk2=fscanf(Wy,'%s',2);
        RawData(i,:j)=WyTmp;
    end
    Junk3=fscanf(Wy,'%s',12);
end

a=RawData;
```



```

for k=1:110

    for i=1:8096
        for j=1:5
            b(5*(i-1)+j)=a(i,j,k);
        end
    end

    freq(k)=b(40475);

    for i=1:2891
        for j=1:14
            c(i,j,k)=b((i-1)*14+j);
        end
    end
end

%disp=zeros(5330,2,100);
for k=1:110
    for i=1:2667

        %disp(i,:,k)=[c(i,5,k),c(i,6,k)];
        volt(i,:,k)=[c(i,13,k),c(i,14,k)];
    end
end

for k=1:110
    for i=1:224

        disp(i,:,k)=[c(i+2667,5,k),c(i+2667,6,k)];
        %volt(i,:,k)=[c(i,13,k),c(i,14,k)];
    end
end

for k=1:110
    volt_sum(k,:)=sum(volt(:, :, k));
    charge(k)=abs(complex(volt_sum(k,1),volt_sum(k,2)));

end

for k=1:110
    disp_sum(k,:)=(disp(150, :, k));
    disp_beam(k)=abs(complex(disp_sum(k,1),disp_sum(k,2)));
end

```

```

end

a= charge/max(charge);
b=disp_beam/max(disp_beam);

figure,plot(freq,a,freq,b)
%figure,plot(freq,disp_beam,freq,charge)

%figure,subplot(2,1,1),plot(freq,(charge),freq,(disp_beam))
title('Charge and Displacement vs. Frequency Curve')
legend('Charge','Displacement')
xlabel('Frequency(Hz)')
ylabel('Charge and Displacement')

```

plate.m MATLAB CODE

```

clc
clear all
close all
%
% Data
LoadStep=104;
Wy = fopen('DUMP3.LIS','r');
Junk1=fscanf(Wy,'%s',8);
for j=1:104; %LoadStep % Total displrecord
    for i=1:(155470/5-1);% 96190/5 line per record
        WyTmp=fscanf(Wy,'%g',[1 5]);
        Junk2=fscanf(Wy,'%s',2);
        RawData(i,:,j)=WyTmp;
    end
    Junk3=fscanf(Wy,'%s',9);
end

a=RawData;
for k=1:104

    for i=1:31093
        for j=1:5
            b(5*(i-1)+j)=a(i,j,k);
        end
    end
end

freq(k)=b(155457);

```

```

for i=1:11103
    for j=1:14
        c(i,j,k)=b((i-1)*14+j);
    end
end
end

%disp=zeros(6870,2,98);
for k=1:104
    for i=1:8623

        %disp(i,:,k)=[c(i,5,k),c(i,6,k)];
        volt(i,:,k)=[c(i,13,k),c(i,14,k)];
    end
end

for k=1:104
    for i=1:2480

        disp(i,:,k)=[c(i+8623,5,k),c(i+8623,6,k)];
        %volt(i,:,k)=[c(i,13,k),c(i,14,k)];
    end
end

for k=1:104
    volt_sum(k,:)=sum(volt(:,:,k));
    charge(k)=abs(complex(volt_sum(k,1),volt_sum(k,2)));

end

for k=1:104
    disp_sum(k,:)=(disp(300,:,k));
    disp_plate(k)=abs(complex(disp_sum(k,1),disp_sum(k,2)));

end

a= charge/max(charge);
b=disp_plate/max(disp_plate);

figure,plot(freq,a,freq,b)

```

```
%figure,plot(freq,disp_plate)
```

```
%figure,subplot(2,1,1),plot(freq,(charge),freq,(disp_plate))  
title('Charge and Displacement vs. Frequency Curve')  
legend('Charge','Displacement')  
xlabel('Frequency(Hz)')  
ylabel('Charge and Displacement')
```

Cylindrical Pipe.m Matlab Code

```
clc  
clear all  
close all  
%  
% Data  
LoadStep=71;  
Wy = fopen('DUMP.lis','r');  
Junk1=fscanf(Wy,'%s',8);  
for j=1:71; %LoadStep % Total displrecord  
    for i=1:(218565/5-1);% 77585/5 line per record  
        WyTmp=fscanf(Wy,'%g',[1 5]);  
        Junk2=fscanf(Wy,'%s',2);  
        RawData(i,:j)=WyTmp;  
    end  
    Junk3=fscanf(Wy,'%s',12);  
end  
  
a=RawData;  
  
for k=1:71  
  
    for i=1:43712  
        for j=1:5  
            b(5*(i-1)+j)=a(i,j,k);  
        end  
    end  
  
    freq(k)=b(218555);  
  
    for i=1:15611
```

```

        for j=1:14
            c(i,j,k)=b((i-1)*14+j);
        end
    end
end

%disp=zeros(5546,2,102);
for k=1:71
    for i=1:13875

        %disp(i,:,k)=[c(i,3,k),c(i,4,k)];
        volt(i,:,k)=[c(i,13,k),c(i,14,k)];
    end
end

for k=1:71
    for i=1:1736

        disp(i,:,k)=[c(i+13875,3,k),c(i+13875,4,k)];
        %volt(i,:,k)=[c(i,13,k),c(i,14,k)];
    end
end

for k=1:71
    volt_sum(k,:)=sum(volt(:,:,k));
    charge(k)=abs(complex(volt_sum(k,1),volt_sum(k,2)));

end

for k=1:71
    disp_sum(k,:)=(disp(300,:,k));
    disp_shell(k)=abs(complex(disp_sum(k,1),disp_sum(k,2)));

end

a= charge/max(charge);
b=disp_shell/max(disp_shell);

figure,plot(freq,a,freq,b)
%figure,plot(freq,disp_shell)

%figure,subplot(2,1,1),plot(freq,(charge),freq,(disp_shell))
title('Charge and Displacement vs. Frequency Curve')

```

```

legend('Charge','Displacement')
xlabel('Frequency(Hz)')
ylabel('Charge and Displacement')

```

Shaped Beam.m MATLAB CODE

```

clc
clear all
close all
%
% Data
LoadStep=92;
Wy = fopen('DUMP2.lis','r');
Junk1=fscanf(Wy,'%s',8);
for j=1:92; %LoadStep % Total displrecord
    for i=1:(91700/5-1);% 74630/5 line per record
        WyTmp=fscanf(Wy,'%g',[1 5]);
        Junk2=fscanf(Wy,'%s',2);
        RawData(i,:j)=WyTmp;
    end
    Junk3=fscanf(Wy,'%s',9);
end

a=RawData;
for k=1:92

    for i=1:18339
        for j=1:5
            b(5*(i-1)+j)=a(i,j,k);
        end
    end

freq(k)=b(91687);

    for i=1:6549
        for j=1:14
            c(i,j,k)=b((i-1)*14+j);
        end
    end
end

%disp=zeros(5330,2,100);
for k=1:92

```

```

for i=1:6332

    %disp(i,:,k)=[c(i,5,k),c(i,6,k)];
    volt(i,:,k)=[c(i,13,k),c(i,14,k)];
end
end

for k=1:92
    for i=1:217

        disp(i,:,k)=[c(i+6332,5,k),c(i+6332,6,k)];
        %volt(i,:,k)=[c(i,13,k),c(i,14,k)];
    end
end

for k=1:92
    volt_sum(k,:)=sum(volt(:, :, k));
    charge(k)=abs(complex(volt_sum(k,1),volt_sum(k,2)));

end

for k=1:92
    disp_sum(k,:)=(disp(150, :, k));
    disp_beam(k)=abs(complex(disp_sum(k,1),disp_sum(k,2)));

end

a= charge/max(charge);
b=disp_beam/max(disp_beam);

figure,plot(freq,a,freq,b)
%figure,plot(freq,disp_beam,freq,charge)

%figure,subplot(2,1,1),plot(freq,(charge),freq,(disp_beam))
title('Charge and Displacement vs. Frequency Curve')
legend('Charge','Displacement')
xlabel('Frequency(Hz)')
ylabel('Charge and Displacement')

```

Shaped Plate.m MATLAB CODE

```
clc
clear all
close all
%
% Data
LoadStep=92;
Wy = fopen('DUMP2.lis','r');
Junk1=fscanf(Wy,'%s',8);
for j=1:92; %LoadStep % Total displrecord
    for i=1:(91700/5-1);% 74630/5 line per record
        WyTmp=fscanf(Wy,'%g',[1 5]);
        Junk2=fscanf(Wy,'%s',2);
        RawData(i,:j)=WyTmp;
    end
    Junk3=fscanf(Wy,'%s',9);
end

a=RawData;
for k=1:92

    for i=1:18339
        for j=1:5
            b(5*(i-1)+j)=a(i,j,k);
        end
    end

freq(k)=b(91687);

    for i=1:6549
        for j=1:14
            c(i,j,k)=b((i-1)*14+j);
        end
    end
end
end

%disp=zeros(5330,2,100);
for k=1:92
    for i=1:6332

        %disp(i,:,k)=[c(i,5,k),c(i,6,k)];
        volt(i,:,k)=[c(i,13,k),c(i,14,k)];
    end
end
```



```

end

for k=1:92
    for i=1:217

        disp(i,:,k)=[c(i+6332,5,k),c(i+6332,6,k)];
        %volt(i,:,k)=[c(i,13,k),c(i,14,k)];
    end
end

for k=1:92
    volt_sum(k,:)=sum(volt(:, :,k));
    charge(k)=abs(complex(volt_sum(k,1),volt_sum(k,2)));

end

for k=1:92
    disp_sum(k,:)=(disp(150, :,k));
    disp_beam(k)=abs(complex(disp_sum(k,1),disp_sum(k,2)));

end

a= charge/max(charge);
b=disp_beam/max(disp_beam);

figure,plot(freq,a,freq,b)
%figure,plot(freq,disp_beam,freq,charge)

%figure,subplot(2,1,1),plot(freq,(charge),freq,(disp_beam))
title('Charge and Displacement vs. Frequency Curve')
legend('Charge','Displacement')
xlabel('Frequency(Hz)')
ylabel('Charge and Displacement')

```

Shaped Cylindrical Pipe.m MATLAB CODE

```

clc
clear all
close all
%
% Data
LoadStep=95;
Wy = fopen('DUMP.lis','r');

```

```

Junk1=fscanf(Wy,'%s',8);
for j=1:95; %LoadStep % Total displrecord
    for i=1:(161560/5-1);% 77585/5 line per record
        WyTmp=fscanf(Wy,'%g',[1 5]);
        Junk2=fscanf(Wy,'%s',2);
        RawData(i,:j)=WyTmp;
    end
    Junk3=fscanf(Wy,'%s',9);
end

```

```

a=RawData;

```

```

for k=1:95

    for i=1:32311
        for j=1:5
            b(5*(i-1)+j)=a(i,j,k);
        end
    end
end

```

```

freq(k)=b(161547);

```

```

for i=1:11539
    for j=1:14
        c(i,j,k)=b((i-1)*14+j);
    end
end
end

```

```

%disp=zeros(5546,2,102);
for k=1:95
    for i=1:9831

        %disp(i,:,k)=[c(i,3,k),c(i,4,k)];
        volt(i,:,k)=[c(i,13,k),c(i,14,k)];
    end
end

```

```

for k=1:95
    for i=1:1708

        disp(i,:,k)=[c(i+9831,3,k),c(i+9831,4,k)];
        %volt(i,:,k)=[c(i,13,k),c(i,14,k)];
    end
end

```

```

end

for k=1:95
    volt_sum(k,:)=sum(volt(:,k));
    charge(k)=abs(complex(volt_sum(k,1),volt_sum(k,2)));
end

for k=1:95
    disp_sum(k,:)=(disp(300,:,k));
    disp_shell(k)=abs(complex(disp_sum(k,1),disp_sum(k,2)));
end

a= charge/max(charge);
b=disp_shell/max(disp_shell);

figure,plot(freq,a,freq,b)
%figure,plot(freq,disp_beam,freq,charge)

%figure,subplot(2,1,1),plot(freq,(charge),freq,(disp_shell))
title('Charge and Displacement vs. Frequency Curve')
legend('Charge','Displacement')
xlabel('Frequency(Hz)')
ylabel('Charge and Displacement')

```

Experimental Results for Beam:

```

clc;
clear all;
close all;
%
% Data
%LoadStep=90;

amp = fopen('PVDF_A.TXT','r');
amp_f= fopen('PVDF_A.X','r');
phase = fopen('PVDF_P.TXT','r');
phase_f = fopen('PVDF_P.X','r');

```

```

for j=1:401; %LoadStep % Total displrecord
    %for i=1:(40485/5-1);% 74630/5 line per record
        amp1(j)=fscanf(amp,'%g',[1]);
        amp1_f(j)=fscanf(amp_f,'%g',[1]);
        phase1(j)=fscanf(phase,'%g',[1]);
        phase1_f(j)=fscanf(phase_f,'%g',[1]);

        j;
        %Junk2=fscanf(Wy,'%s',2);
        %RawData(i,:,j)=WyTmp
    %end
    %Junk3=fscanf(Wy,'%s',12);
end

```

```

amp1
amp1_f

```

```

%figure,plot(amp1)
%title('Amplitude for Accelerometer')
%figure,plot(phase1)
%title('Phase for Accelerometer')

```

```

figure,subplot(2,1,1),plot(amp1_f,amp1)
title('Amplitude for PVDF')
xlabel('Frequency(Hz)')
ylabel('Amplitude(dB)')
subplot(2,1,2),plot(phase1_f,phase1)
title('Phase for PVDF')
xlabel('Frequency(Hz)')
ylabel('Phase(degrees)')

```

```

amp = fopen('ACCA.TXT','r');
amp_f= fopen('ACCA.X','r');
phase = fopen('ACCP.TXT','r');
phase_f = fopen('ACCP.X','r');

```

```

%amp = fopen('ACCA.TXT','r');
%phase = fopen('ACCP.TXT','r');

```

```

%Junk1=fscanf(Wy,'%s',8);
for j=1:401; %LoadStep % Total displrecord
    %for i=1:(40485/5-1);% 74630/5 line per record
        amp1(j)=fscanf(amp,'%g',[1]);
        amp1_f(j)=fscanf(amp_f,'%g',[1]);
        phase1(j)=fscanf(phase,'%g',[1]);
        phase1_f(j)=fscanf(phase_f,'%g',[1]);

        j;
        %Junk2=fscanf(Wy,'%s',2);
        %RawData(i,:j)=WyTmp
    %end
    %Junk3=fscanf(Wy,'%s',12);
end

```

```

%figure,plot(amp1)
%title('Amplitude for Accelerometer')
%figure,plot(phase1)
%title('Phase for Accelerometer')

```

```

figure,subplot(2,1,1),plot(amp1_f,amp1)
title('Amplitude for Accelerometer')
xlabel('Frequency(Hz)')
ylabel('Amplitude(dB)')
subplot(2,1,2),plot(phase1_f,phase1)
title('Phase for Accelerometer')
xlabel('Frequency(Hz)')
ylabel('Phase(degrees)')

```

Experimental Results for Pipe:

```

clc;
clear all;
close all;
%
% Data
%LoadStep=90;

amp = fopen('PVDF_A.TXT','r');
amp_f = fopen('PVDF_A.X','r');
phase = fopen('PVDF_P.TXT','r');
phase_f = fopen('PVDF_P.X','r');

```

```

for j=1:401; %LoadStep % Total displrecord
    %for i=1:(40485/5-1);% 74630/5 line per record
        amp1(j)=fscanf(amp,'%g',[1]);
        amp1_f(j)=fscanf(amp_f,'%g',[1]);
        phase1(j)=fscanf(phase,'%g',[1]);
        phase1_f(j)=fscanf(phase_f,'%g',[1]);

        j;
        %Junk2=fscanf(Wy,'%s',2);
        %RawData(i,,:j)=WyTmp
    %end
    %Junk3=fscanf(Wy,'%s',12);
end

```

```

amp1
amp1_f

```

```

%figure,plot(amp1)
%title('Amplitude for Accelerometer')
%figure,plot(phase1)
%title('Phase for Accelerometer')

```

```

figure,subplot(2,1,1),plot(amp1_f,amp1)
title('Amplitude for PVDF')
xlabel('Frequency(Hz)')
ylabel('Amplitude(dB)')
subplot(2,1,2),plot(phase1_f,phase1)
title('Phase for PVDF')
xlabel('Frequency(Hz)')
ylabel('Phase(degrees)')

```

```

amp = fopen('ACCA.TXT','r');
amp_f= fopen('ACCA.X','r');
phase = fopen('ACCP.TXT','r');
phase_f = fopen('ACCP.X','r');

```

```

%amp = fopen('ACCA.TXT','r');
%phase = fopen('ACCP.TXT','r');
%Junk1=fscanf(Wy,'%s',8);
for j=1:401; %LoadStep % Total displrecord
    %for i=1:(40485/5-1);% 74630/5 line per record
        amp1(j)=fscanf(amp,'%g',[1]);
        amp1_f(j)=fscanf(amp_f,'%g',[1]);
        phase1(j)=fscanf(phase,'%g',[1]);
        phase1_f(j)=fscanf(phase_f,'%g',[1]);

        j;
        %Junk2=fscanf(Wy,'%s',2);
        %RawData(i,:j)=WyTmp
    %end
    %Junk3=fscanf(Wy,'%s',12);
end

```

```

%figure,plot(amp1)
%title('Amplitude for Accelerometer')
%figure,plot(phase1)
%title('Phase for Accelerometer')

```

```

figure,subplot(2,1,1),plot(amp1_f,amp1)
title('Amplitude for Accelerometer')
xlabel('Frequency(Hz)')
ylabel('Amplitude(dB)')
subplot(2,1,2),plot(phase1_f,phase1)
title('Phase for Accelerometer')
xlabel('Frequency(Hz)')
ylabel('Phase(degrees)')

```

APPENDIX C HAND CALCULATION

Hand Calculation for the beam

```
function f=myfunc(x)
f=((cos(x)*cosh(x))+1);

clear all;
close all;
clc;
b = 0.0508;
h = 0.00315;
I = (1/12)*(b*h^3);
L= 0.3048;
row = 2700;
A = b*h;
E = 70*10^9;

for(i=1:1:20)
x=fsolve('myfunc1',i)
omega=(x^2)*sqrt((E*I)/(row*A*L^4))
end;
```

Hand Calculation for the plate

```
clear all;
close all;
clc;
m=2;
n=2;
Gx = 1.506;
Gy = Gx;
c = 1.6;           % c= a/b
nu = 0.33;
Hx = 1.248;
Hy = Hx;
```



```

Jx = Hx;
Jy = Jx;
t= 0.004762;
E= 70e9;
g=9.8;
row=2700;
a=0.6096;
D=E*t^3/(12*(1-nu^2));
lamda_square= Gx^4+((Gy^4)*((c)^4))+2*((c)^2)*(nu*Hx*Hy+((1-nu)*Jx*Jy));
lamda=sqrt(lamda_square)*pi^2;
frequency11=lamda/((a^2)*2*pi*sqrt(row*t/D))

```

%%%

```

m=3;
n=2;
Gx =m-0.5 ;
Gy = 1.506;
c = 1.6;           % c= a/b
nu = 0.33;
Hx = ((m-0.5)^2)*(1-(2/((m-0.5)*pi)));
Hy = 1.248;
Jx = ((m-0.5)^2)*(1-(2/((m-0.5)*pi)));
Jy = 1.248;
t= 0.004762;
E= 70e9;
g=9.8;
row=2700;
a=0.6096;
D=E*t^3/(12*(1-nu^2));
lamda_square= Gx^4+((Gy^4)*((c)^4))+2*((c)^2)*(nu*Hx*Hy+((1-nu)*Jx*Jy));
lamda=sqrt(lamda_square)*pi^2;
frequency21=lamda/((a^2)*2*pi*sqrt(row*t/D))

```

%%%

```

m=4;
n=2;
Gx =m-0.5 ;
Gy = 1.506;
c = 1.6;           % c= a/b
nu = 0.33;
Hx = ((m-0.5)^2)*(1-(2/((m-0.5)*pi)));
Hy = 1.248;
Jx = ((m-0.5)^2)*(1-(2/((m-0.5)*pi)));
Jy = 1.248;

```

```

t= 0.004762;
E= 70e9;
g=9.8;
row=2700;
a=0.6096;
D=E*t^3/(12*(1-nu^2));
lamda_square= Gx^4+((Gy^4)*((c)^4))+2*((c)^2)*(nu*Hx*Hy+((1-nu)*Jx*Jy));
lamda=sqrt(lamda_square)*pi^2;
frequency31=lamda/((a^2)*2*pi*sqrt(row*t/D))

```

%%%

```

m=5;
n=2;
Gx =m-0.5 ;
Gy = 1.506;
c = 1.6;           % c= a/b
nu = 0.33;
Hx = ((m-0.5)^2)*(1-(2/((m-0.5)*pi)));
Hy = 1.248;
Jx = ((m-0.5)^2)*(1-(2/((m-0.5)*pi)));
Jy = 1.248;
t= 0.004762;
E= 70e9;
g=9.8;
row=2700;
a=0.6096;
D=E*t^3/(12*(1-nu^2));
lamda_square= Gx^4+((Gy^4)*((c)^4))+2*((c)^2)*(nu*Hx*Hy+((1-nu)*Jx*Jy));
lamda=sqrt(lamda_square)*pi^2;
frequency41=lamda/((a^2)*2*pi*sqrt(row*t/D))

```

%%%

```

m=6;
n=2;
Gx =m-0.5 ;
Gy = 1.506;
c = 1.6;           % c= a/b
nu = 0.33;
Hx = ((m-0.5)^2)*(1-(2/((m-0.5)*pi)));
Hy = 1.248;
Jx = ((m-0.5)^2)*(1-(2/((m-0.5)*pi)));
Jy = 1.248;
t= 0.004762;
E= 70e9;

```

```

g=9.8;
row=2700;
a=0.6096;
D=E*t^3/(12*(1-nu^2));
lamda_square= Gx^4+((Gy^4)*((c)^4))+2*((c)^2)*(nu*Hx*Hy+((1-nu)*Jx*Jy));
lamda=sqrt(lamda_square)*pi^2;
frequency51=lamda/((a^2)*2*pi*sqrt(row*t/D))

```

%%

```

m=2;
n=3;
Gx = 1.506;
Gy = n-0.5;
c = 1.6;           % c= a/b
nu = 0.33;
Hx = 1.248;%((m-0.5)^2)*(1-(2/((m-0.5)*pi)));
Hy = ((n-0.5)^2)*(1-(2/((n-0.5)*pi)));
Jx = Hx;
Jy =((n-0.5)^2)*(1-(2/((n-0.5)*pi)));
lamdasquare= (Gx^4+((Gy^4)*((c)^4))+2*((c)^2)*(nu*Hx*Hy+((1-nu)*Jx*Jy)));
lamda=sqrt(lamdasquare)*pi^2;
frequency12=lamda/((a^2)*2*pi*sqrt(row*t/D))

```

%%

REFERENCES

- [1] Aleksandra M. Vinogradov, V. Hugo Schmidt, George F. Tuthill, Gary W. Bohannon, “Damping and electromechanical energy losses in the piezoelectric polymer PVDF”, *Mechanics of Materials*, Vol. 36, pp. 1007–1016 (2004).
- [2] “Cygnus Research International” The Data Processing Studio.
- [3] Wikipedia the free Encyclopedia.
- [4] Andrzej Odon, “Probe with PVDF Sensor for Energy Measurements of Optical Radiation”, *Measurement Science Review*, Volume 3, Section 3, 2003.
- [5] Rocky R. Reston Captain, USAF AFIT/GE/ENG/88D-41, Thesis entitled as “Robotic tactile sensor fabricated from piezoelectric PVDF films”.
- [6] Rong-Liang Chen and Bor-Tsuen Wang, “The use of polyvinylidene fluoride films as sensors for the experimental modal analysis of structures”, *Smart Mater. Struct.*, Volume 13, pp. 791–799 (2004).
- [7] Satu Kärki, Miika Kiiski, Matti Mäntysalo, Jukka Leikkala, “A PVDF sensor with printed electrodes for normal and shear stress measurements on sole”, XIX IMEKO World Congress, Fundamental and Applied Metrology, September 6-11, 2009, Lisbon, Portugal, ISBN 978-963-88410-0-1 © 2009 IMEKO.
- [8] Eko Supriyanto, Imamul Muttakin, Mohd Hafizul Mohd Fathil, Camallil Omar, “Low Cost PVDF Sensor Casing for Ultrasound Power Measurement”, *Recent researches in circuits, systems and signal processing*, ISBN: 978-1-61804-017-6.
- [9] Chien-Ching Ma, Yu-Hsi Huang and Shan-Ying Pan, “Investigation of the transient behavior of a cantilever beam using PVDF Sensors”, *J. of Sensors*, Volume 12, pp. 2088-2117 (2012).
- [10] Roger Vodicka and Stephen C. Galea, “Use of PVDF strain sensors for health monitoring of bonded composite patches”, *Airframes and Engines Division, Aeronautical and Maritime Research Laboratory, DSTO-TR-0684*.
- [11] Sitthichai Anuphap-udom, Kiranant Ratanathammapan and Tonphong Kaewkongka, “Fabricated PVDF Acoustic Emission Sensor for Lubricated Bearing Monitoring”, *J. of Sci. Res. Chula. Univ.*, Vol. 31, No. 2 (2006).
- [12] John P. Stevenson, Samara L. Firebaugh, Harry K. Charles, Jr., “Biometric Identification from a Floor Based PVDF Sensor Array Using Hidden Markov Models”, *SAS 2007 – Sensors Applications Symposium, Technology Conference San Diego, CA, USA, 06-08 February 2007*.
- [13] Satu Kärki, “Film-type Sensor Materials in Measurement of Physiological Force and Pressure Variables”, *Tampere University of Technology, Publication 849, ISBN 978-952-15-2265-9*.
- [14] J. Dargahi, “A piezoelectric tactile sensor with three sensing elements for robotic, endoscopic and prosthetic applications”, *J. of Sensors and Actuators*, Volume 80, pp. 23–30 (2000).

- [15] Yoshiaki TOKUNAGA , Masatoshi YOSHIMURA ,Koji AIZAWA and Junji HIRAMA, “Amplitude and phase of photo thermal signal in a leaf of plant “schefflera arboricola ” measured by PVDF sensor”, Proceedings of Symposium on Ultrasonic Electronics, Vol. 30, pp. 211-212 (November, 2009).
- [16] ANSYS Inc. Theory Reference – Multiphysics Analysis Guide.
- [17] ANSYS Inc. Theory Reference – Element Characteristics
- [18] ANSYS Element Library
- [19] ANSYS 13.0 Verification Manual – Test Examples
- [20] ANSYS Inc. Theory Reference – Analysis Procedures
- [21] Cady W.G., Piezoelectricity, Vol. 1 Dover, New York, (1964)
- [22] Mason W. P. “Piezoelectricity, Its history and Applications” J. Acoustics. Soc. Am., Vol. 70, No 6, pp. 1561-1566, Dec 1981.
- [23] Berlincourt D. A., D.R. Curran and H. Jafee, “Principles and Methods”, Physical Acoustics Ed. By W.P. Mason, Academic New York, pp. 169-270 (1964).
- [24] Brain K.R., Proc. Phys. Soc. London 36, 81, (1924).
- [25] Fukada E., “Piezoelectricity in Polymers and Biological Materials”, Ultrasonics, Vol. 6, No. 4, pp. 229-234, (1968).
- [26] Kawai H, “Piezoelectricity of PolyVinyleDene Fluoride (PVDF)”, Jap. J. Appl. Phys., Vol. 8, pp. 975-976.
- [27] Mechanical Vibrations (5th Edition) by Singiresu S. Rao.
- [28] G.B. Warburton, “The vibration of rectangular plates”, Proceedings of the Institution of Mechanical Engineers, Vol. **168**, pp. 371-384 (1954).
- [29] A.W.LEISSA, “The free vibration of rectangular plates”, J. of Sound and Vibration, Vol. **31**(3), pp. 257-293 (1973).
- [30] Vibration of Plates by Arthur W. Leissa
- [31] Agilent 35670A Operator’s Guide.
- [32] Marcellin B. Zahui, James W. Kamman, Koorosh Naghshineh “ Theoretical Development and Experimental Validation of Local Volume Displacement Sensors for a Vibrating Beam”, Journal of Vibration and Acoustics, Vol. 123, pp. 110-118, January 2001.
- [33] James W. Kamman, Koorosh Naghshineh “A comparison of open-loop feed forward and closed-loop methods for active noise control using volume velocity minimization”, Journal of Applied Acoustics, Vol. 57, pp. 29-37, (1999).